ADDIS ABABA UNIVERSITY

COLLEGE OF NATURAL SCIENCES

SCHOOL OF EARTH SCIENCES

DEFORMATION, METAMORPHISM AND CHEMICAL STRATIGRAPHY OF NEOPROTEROZOIC ROCKS IN KORARO-GELEBEDA AREA, NORTHERN ETHIOPIA

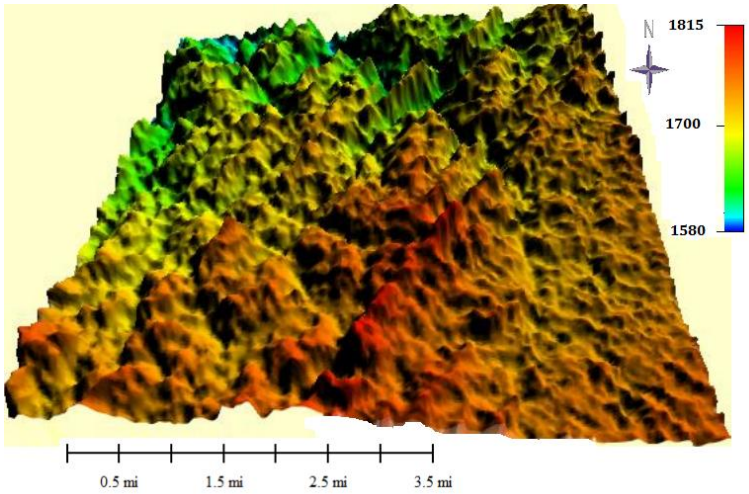

BY

MULUBRHAN GEBRESLASSIE

ADVISOR: Dr. MULUGETA ALENE

June, 2016

ADDIS ABABA UNIVERSITY

COLLEGE OF NATURAL SCIENCES

SCHOOL OF EARTH SCIENCES

DEFORMATION, METAMORPHISM AND CHEMICAL STRATIGRAPHY OF NEOPROTEROZOIC ROCKS IN KORARO-GELEBEDA AREA, NORTHERN ETHIOPIA

BY

MULUBRHAN GEBRESLASSIE

ADVISOR: Dr. MULUGETA ALENE

A Thesis Submitted to School of Graduate Studies of Addis Ababa University, in Partial Fulfillment of the Requirements for the Degree of Master of Earth Sciences

(Petrology)

June, 2016

ADDIS ABABA UNIVERSITY

COLLEGE OF NATURAL SCIENCES

SCHOOL OF EARTH SCIENCES

DEFORMATION, METAMORPHISM AND CHEMICAL STRATIGRAPHY OF NEOPROTEROZOIC ROCKS IN KORARO-GELEBEDA AREA, NORTHERN ETHIOPIA

BY

MULUBRHAN GEBRESLASSIE

APPROVED BY EXAMINING BOARD

	Signature
Dr. Balemwal Atnafu Department Chairman and Graduate committee	_____
Dr. Mulugeta Alene Advisor	_____
Prof. Dereje Ayalew Examiner	_____
Dr. Bekele Abebe Examiner	_____

June, 2016

ABSTRACT

An integrated study aiming at understanding metamorphism and deformation history, and chemostratigraphy of the basement rocks in Koraro-Gelebeda has been done. The exposed rocks represent Tambien Group exposures which are equivalents of Werii, Assem and Tsedia formations. Protolith mineral remnants and uncompleted reactions, primary bedding, fine grained textures and structures exhibited by the rocks such as pencil structure indicate a low to very low grades of metamorphism. The mineral assemblages are also typical of lower greenschist facies assemblage. Microstructures such as stylolites, fringe structures and indented grain contacts accompany the deformation at microscopic scale with the action of fluids. Mantled as well as fractured porphyroblasts and porphyroclasts resulting from non coaxial deformations show both dextral and sinistral sense. No deflection of foliation, random distribution of porphyroblasts but having strain shadow and fringe structure parallel to the foliations is interpreted to limit their development in the range of late- very late tectonic activity. Intertectonic ones without these microstructures are also common. Superimposed structures show foliation development due to first deformation phase; gently dipping folds, kink bands, crenulation cleavages and lineations due to second phase deformation; and joints and faults resulting from the third phase of deformation. The foliations generally trend NNE to SSW, and most of the lineation are gently plunging north. $\delta^{13}C$ values of the collected metalimestone samples fluctuate in the range of -7.6‰ -2.7‰. This fluctuation might be due to small level changes in the amount of primary organic carbon burial, interbedded siliciclastic materials associated with the influx of fresh water from continents during deposition or diagenetic effects. The metalimestones didn't show any glacial feature but all the $\delta^{13}C$ values are negative which is the same case elsewhere in the world as in Little Dal/Coates Lake Groups and Fifteen Mile Group (Canada), Bitter Springs Formation (Australia) and Hecla Hoek Group (Svalbard). These values are correlated to the Bitter Springs stage which is proposed to result from true polar wandering event.

Key Words: Metamorphism; Deformation; Porphyroblasts; Superimposition; Diffusive Mass Transfer; Chemostratigraphy; Bitter Springs Stage; True Polar Wander

ACKNOWLEDGMENT

First of all ‘thanks God’ for everything from the beginning of the work to the end. I would like to greatly acknowledge Addis Ababa University, German Academic Exchange Service (DAAD) and Princeton University for their logistical, financial and laboratory support.

My genuine and heartfelt gratitude belongs to my advisor Dr. Mulugeta Alene. His limitless support, valuable advices, comments and suggestions starting from the very beginning to the end were critical for the thesis and my future.

I would also like to express my sincere gratitude to Scott Angus MacLennan, Prof. Nicolas Swanson Hysell, Tadelle Tesema, Prof. Adam Maloof, Prof. Bereket Haileab, Yuem Park and Elliel Antila for their valuable suggestions and training during the reconnaissance survey. Besides, Scott runs the carbon isotope analysis and Tadelle help me in preparation of the carbonate chips.

My appreciation also goes to Ato Wendwossen Sisay for preparing the thin sections. The contribution from my family and friends is greatly acknowledged especially my brother Kahsay Gebreslassie who provides me some logistics during the field work.

Last but not least I thank inhabitants of Koraro town for their kind and memorable help during the field work.

Table of Contents

List of Figures

CHAPTER ONE

INTRODUCTION

1.1 Background

The basement rocks in Ethiopia which are exposed in southern, western and south western, northern and eastern part of the country are within southern part of ANS, a largely juvenile Neoproterozoic crust formed during Mozambique Ocean closure accompanying Pannotia/Greater Gondwana formation (Asrat et al., 2001; Stern, 1994, 2008; Fritz et al., 2013; Fig. 1.1 and 1.2).

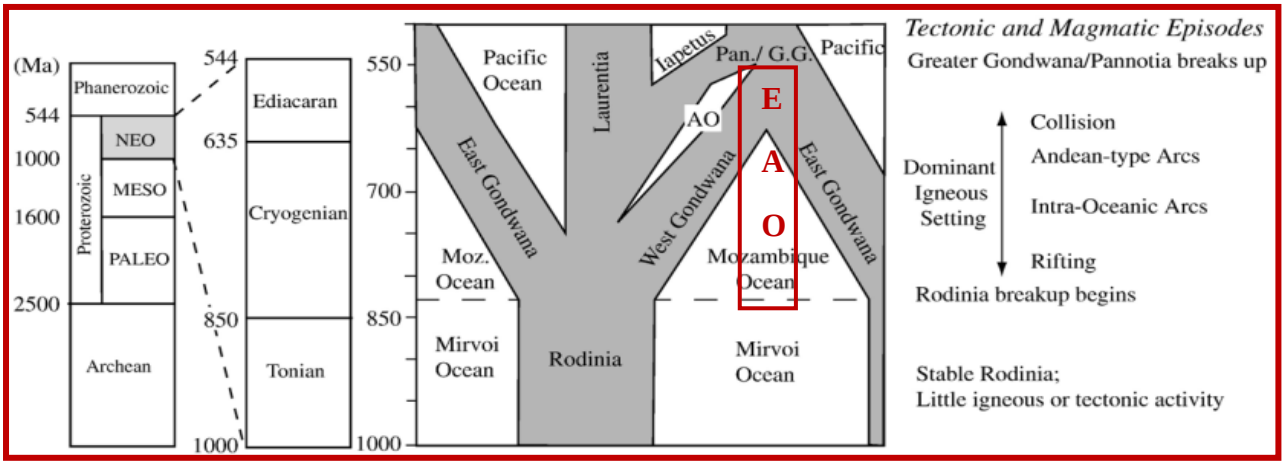

Fig. 1-1 Tree diagram representation of the Neoproterozoic transition from Rodinia to Gondwana and emergence of EAO (modified after Stern, 2008).

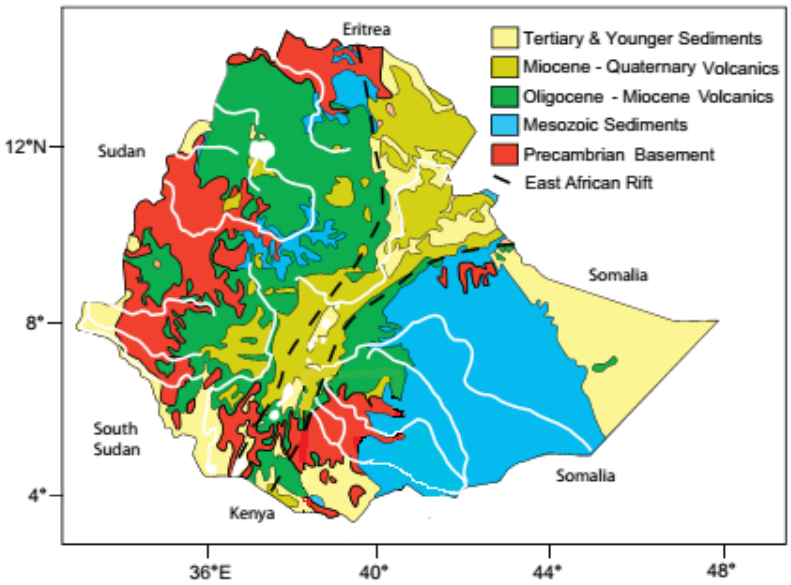

Fig. 1-2 Geological map of Ethiopia. White lines and white irregular shapes are rivers and lakes, respectively. Map modified from Tefera et al. (1996) cited in Stern et al. (2012).

The Precambrian geology of northern Ethiopia is grouped under two major sequences: Tsaliet and Tambien. The former represents the volcanic flows, agglomerates, tuffs, and volcanoclastic sedimentary rocks whereas the later constitutes interbedded clastic and carbonate sedimentary rocks. The Tsaliet Group which dominates most of the basement area outcrops in anticlinoria whereas Tambien Group does it in synclinoria. The Tambien Group is exposed in different parts of Tigrai including Mai Kenetal, Tsedia, Chehmit, Negash, Halagubi, Shiraro, East of Edaga Hamus and Samre areas (Beyth, 1972; Miller et al., 2009).

Two phases of deformation result in the development of various structures on these rocks. The D1 structures due to N- S compression are superimposed by the second phase of deformation which is due to E- W compression. Folded primary bedding, tight to isoclinal minor folds, elongation lineations and pervasive regional foliation are the products D1. D2 in turn results in large, upright, open folds with sub-horizontal axes without producing a pervasive cleavage. A low grade of regional metamorphism coeval with the first phase of deformation from pumpellyite-actinolite to lower greenschist facies is experienced by these rocks (Alene, 1998).

Chemical stratigraphy or chemostratigraphy uses chemical fingerprints stored in sediments and sedimentary rocks for stratigraphic correlation. Stratigraphic studies provided by isotopic chemostratigraphy are comparable to biostratigraphy in Phanerozoic formations. Its use in Neoproterozoic sequences will be pronounced where fossil record is low. Depositional C and Sr isotopic signatures varied markedly during this time providing a secular pattern of strong stratigraphic potential (Knoll and Walter, 1992).

In the last two decades more emphasis is given to the Tambien Group. This is because it contains a non glacial $\delta^{13}C$ negatively valued Assem limestone and glacial diamictite which are globally synchronous. Both are correlated to Bitter Springs Stage (BSS) and Sturtian glaciation respectively (Alene et al., 2006; Swanson-Hysell et al., 2015).

The present study area, Koraro-Gelebeda area, represents a least studied Neoproterozoic sequence containing several litho-units including siliciclastics, carbonates and volcaniclastics that are suitable for the study of chemo-stratigraphy as well as petrography. Structural analysis and microtectonics will provide evidence of deformation history experienced by the rocks.

1.2 Location

The study area is located between Koraro and Gelebeda towns of the Hauzien and Kola Tambien woredas respectively. Geographically it is bounded between the UTM coordinates 0520000-0526000E and 1528000-1534000N. It is at a distance of 48km south west of Freweyni town which in turn is 81km north of Mekelle (Fig.1.3).

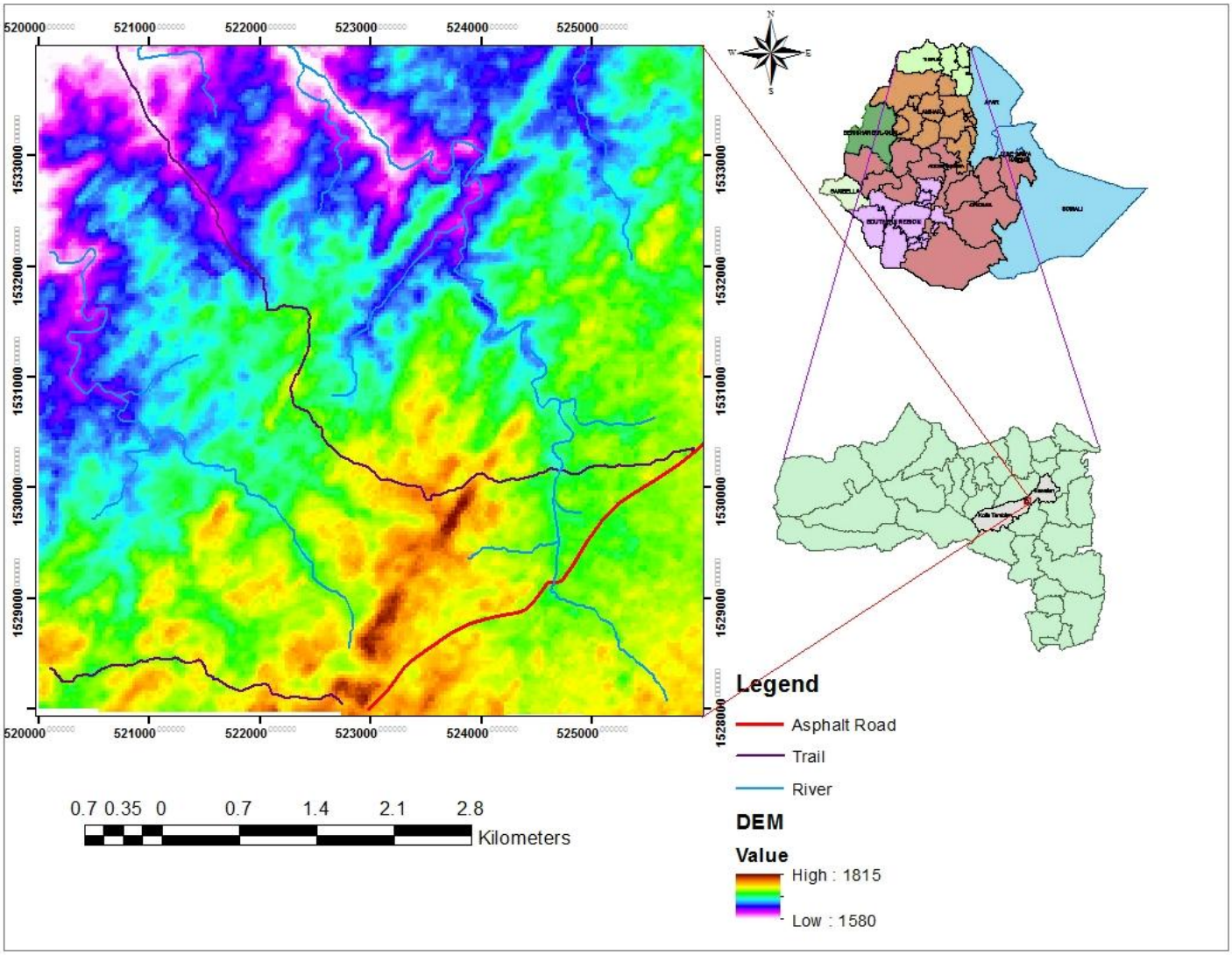

Fig. 1-3 Location map and digital elevation model (DEM) of the study area (Koraro- Gelebeda area)

1.3 Weather Conditions

According to Nedaw (2010) rainfall data of 1992- 2007 collected from Hauzien meteorological station shows that the rainy season is from June to September whereas dry seasons extend from September to June. The 2002-2007 temperature data displays a lowest

mean monthly temperature of 14.5 °C in January and the highest mean monthly temperature of 20.6 °C in May (Fig. 1.4).

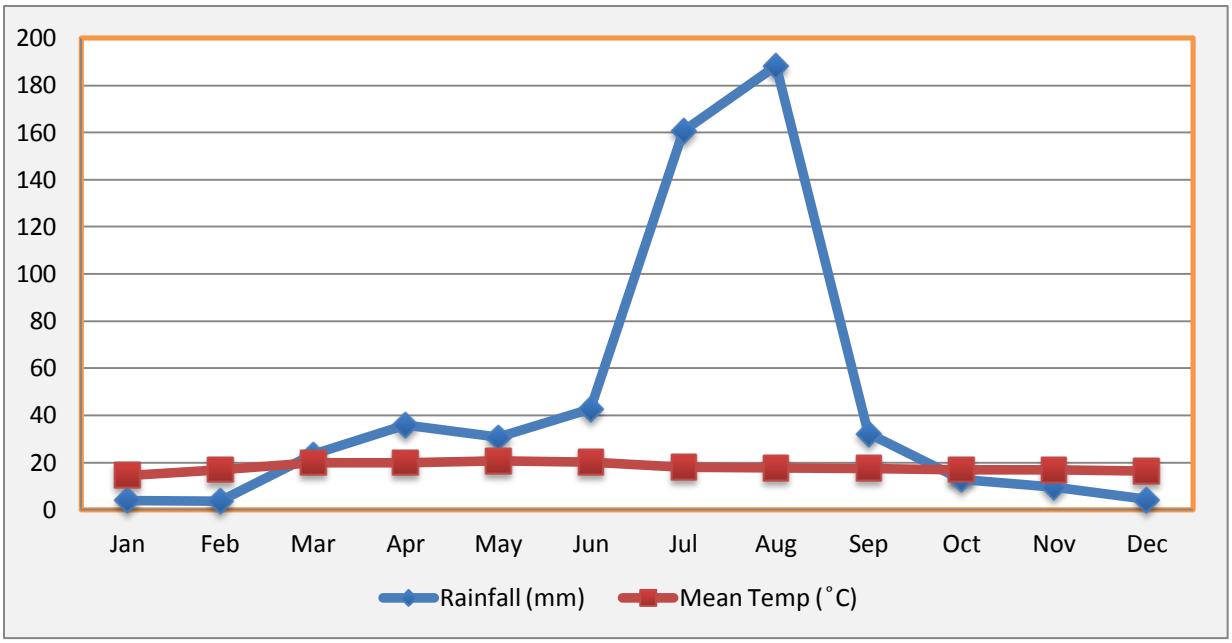

Fig. 1-4 Mean monthly rainfall and temperature plot of the Hauzien area

1.4 Accessibility and Physiography

The study area forms a relatively low land to the western side of a large hill of the Adigrat Sandstone. It is accessed by asphalt road running from Freweyni to Workamba town. Many trails commonly following the streams cross the study area. Newly founded small town of Koraro is densely populated where as the houses of village areas are sparsely distributed. Farming is the main way of life of the residents where honeybee production is also ordinary. The drainage is westwards and all the streams in the study area are intermittent. The stream forms deeper canyon on the metalimestone area but it is wider in the slates.

1.5 Objectives

1.5.1 General Objective

The study aims mainly at understanding of the metamorphism and deformation history of the rocks in Koraro-Gelebeda area. In addition, it is to carry out chemostratigraphic correlation of the metalimestones with other previously studied carbonates.

1.5.2 Specific Objectives

- Obtaining detailed description of the lithologies, including studying contact relationships of the various rock units.

- Identifying mineral assemblages and determine the metamorphic facies of the rocks
- Deciphering the phases of deformation in the area by examining macro and microstructures
- Correlation of the rocks in the area lithologically, texturally and stratigraphically to metamorphic rocks exposed on other areas
- Chemostratigraphic correlation of the carbonate rocks based on $\delta^{13}C$ values
- Producing a geologic map at a scale of 1:25,000

1.6 Problem of Statement

The abundant facies change within the siliciclastic, limestones and volcaniclastic units, and the presence of several small scale phases of folding makes the correlation of Tambien Group to regional geology difficult. In addition the identification of one formation from other is also equally challenging in the region. For example the same rock units north of the study area are mapped as Tambien Group by Arkin et al. (1971) and as Tsaliet Group by Garland (1972).

The carbonates found in the Tambien Group are used in global Neoproterozoic isotope signals i.e. paleoclimatic, paleogeographic interpretation and stratigraphic correlation with carbonates on different parts of the world (Alene et al., 2006, Miller et al., 2009). For example pronounced and globally correlative negative δ^{13}Ccarb anomalies apparently unrelated to glaciation occur at ca. 810 Ma (the "Bitter Springs" anomaly) and at the Precambrian–Cambrian boundary (Halverson et al., 2010). Tambien Group carbonates provide data which reveals the global synchronity of BSS (Swanson-Hysell et al., 2015).

The current study not only focuses on a new area where Tambien group rocks are exposed, but also provides data on lithological characteristic and similarity with other Tambien groups in Maikenetal, Tsedia, Chehmit, Negash and Samre areas in Tigrai. The δ^{13}Ccarb examination is of special interest in a sense it is vital for local as well as global chemostratigraphic correlations.

1.7 Methodology

The methods employed to achieve the objectives are classified generally into prefield work, during field work and post field work. Overall flow chart of the methodology is shown in Fig. 1.5.

1.7.1 Field Work

Before conducting the field works in the target area a regional survey and field work was done in Samre, Negash and Mai Kenetal areas from June 17 - July 18/2015. Review of published and unpublished papers related to the study has been done during and after this field work. Activities such as preparing maximized topo map, preparing Google Earth and satellite images and collecting all necessary materials for the work was also part of the preparation.

The field works on the study area, Oct 21-31/2015, started by doing regional mapping for two days to have general framework on the area. The intensive study in the delineated area was done by describing exposures of lithologies and contacts, Taking GPS reading and photographs during all activities and transferring the data to the topo map. Identifying of geological structures and relating them to the regional deformation history of the area were also carried out.

Sampling, labeling and sectioning were done for hand specimen description of the rock, petrographic investigation and C- isotope analysis. Section measurement was done to get the accurate depositional position of samples and true thickness of metalimestone unit. In doing so, sixty samples were collected for the $\delta^{13}C$ analysis. For the quality of the result samples free of quartz veins and unweathered part was slugged.

1.7.2 Petrographic Analysis

Twenty rock samples were chosen for petrographic studies. Rock samples were cut perpendicular to foliation and thin sections prepared at the School of Earth Science, Addis Ababa University. The petrographic analysis was done using a Leica microscope by capturing photographs from the ocular lens. Minerals assemblages and microstructural investigation of the thin sections has been done. All magnifications (4x, 10x and 40x) and bright illumination were used since there are fine grained samples.

1.7.3 Structural Data Analysis and Map Compilation

Orientation data of planes such as foliations and lineations such as fold axes, crenulation lineation and intersection lineations were collected for structural analysis using FieldMove ClinoPro mapping software and compass. These data are plotted on the stereonet to illustrate and evaluate mean orientations and relationships of the various structural components.

Openstereo version 0.1.2f and Stereonet_Windows version 9.5.3 are the free stereonet plot software used in the analysis. Schmidt net with representation in two and three dimensions displays the output of the orientation data. Erdas imagine 2014, Arc Gis 10.3, Global Mapper version 11 and stratigrapher software produced by GeoStru software are used in the analysis and presentation of the geological map and stratigraphic section.

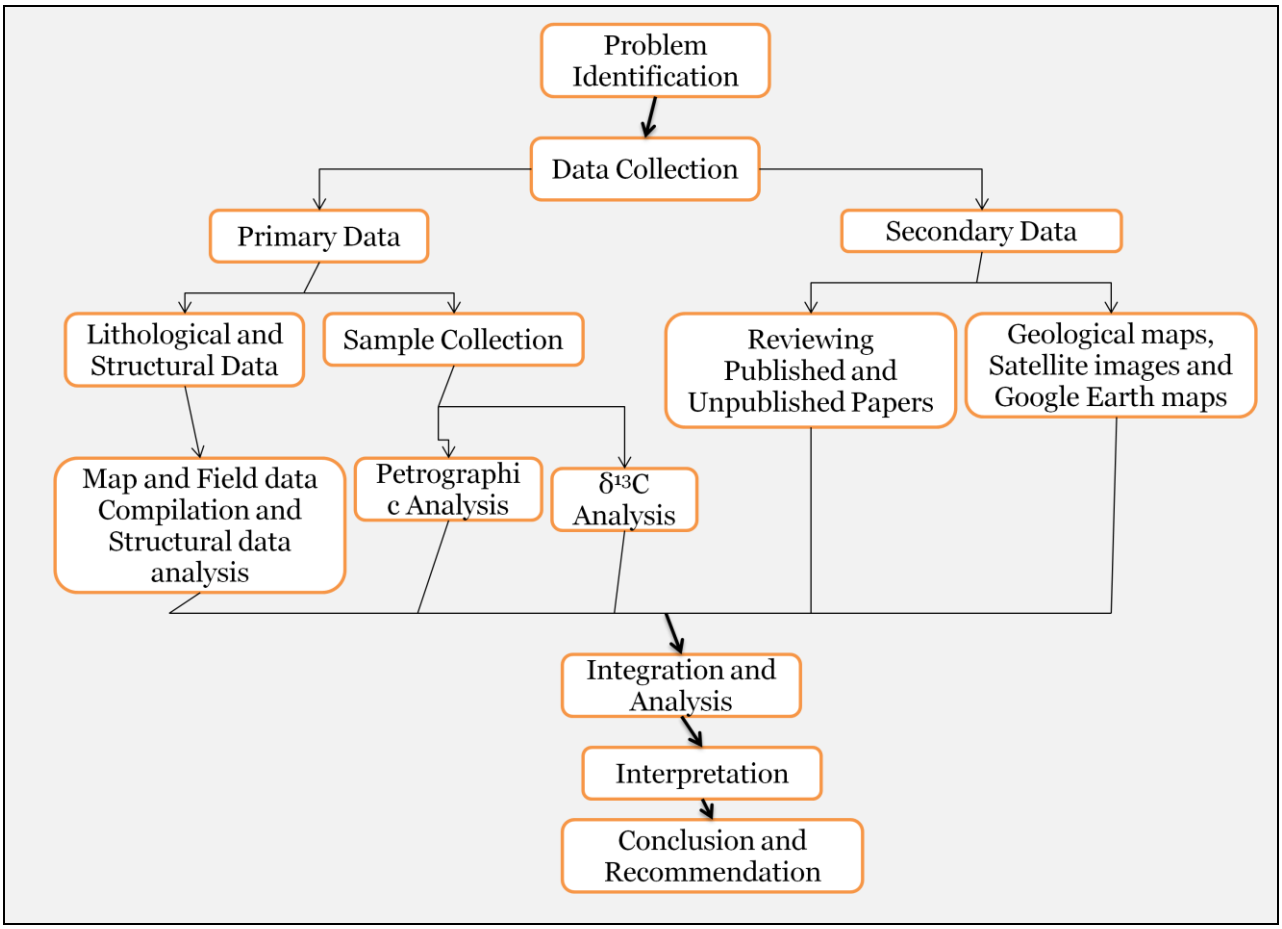

Fig. 1-5 Flow chart showing the order of activities

1.8 Significance of the Study

Regional geological mapping of the area has been done at a scale of 1:250,000 and 1:100,000 by Arkin et al. (1971) and Alene (1998) respectively. So far neither large scale geological map nor chemostratigraphic correlation has been done on this area. Detailed study and geological map (1:25,000) is believed to fill the existing gap regarding the area. The C-isotope analysis will also be new input of data and reference for other researchers working on the Tambien Group.

1.9 Previous Work

Since the 19th different professionals have been working on the basement rocks of northern Ethiopia (e.g. Blanford, (1870); Danielli, (1943) and Mohr, (1962) cited in Tarekegn, (1997)). The studies were more intensified in the early 70th when Levitte (1970); Kazmin (1971); Beyth (1971); Arkin (1971) and Garland (1972) started discovery on the basement rocks in Tigrai.

Levitte (1970) mapped the area around Mekelle. The Precambrian basement was divided into four main formations (Tsaliet metavolcanics, Werri slates, Assem limestone and Tsedia slate) and the overlying Mesozoic sedimentary rocks were divided as Adigrat sandstone and the Antalo limestone Group which was subdivided into five formations. According to Kazmin (1971) the basement rocks of Tigrai are part of the younger complex of the Precambrian of Ethiopia which represents a folded geosynclinal belt in the Mozambique Belt.

Beyth (1971) classified these complexes of northern Ethiopia in to two main units: the lower Tsaliet metavolcanics and the upper Tambien Group. The Tsaliet metavolcanics are formed mainly of intermediate to acid tuffs, welded tuffs, lappili tuffs and agglomerates which are very well bedded and with limestone at their upper parts. In the metasediments two facies were recognized: Mai Kenetal facies and Negash facies. In the first facies; Werri Slate, Assem Limestone, Tsedia Slate and Mai Kenetal Limestone were identified. Whereas in the Negash Facies; Black pebbly slate, black limestone, white dolomite (partly marble) interbedded with black slate, black slate with minor dolomitic beds, black greywacke, conglomerate conglomeratic in places were documented. The Forstage Diorite and Mareb granite intrude all the above mentioned sequence. The metamorphic grade of this complex is low and except for local changes around granitic intrusions it will never rises above the green schist facies. In addition to this history of deposition of the Paleozoic – Mesozoic sediments and the Tertiary Trap volcanics were discussed.

Garland (1980) during mapping the geology of Adigrat area, identified two complexes: the lower and upper complex. The lower complex has limited development and undifferentiated rocks. Thick and inhomogeneous unit of volcanic rocks and graywackes deposited in a geosynclinal basin overlain by sedimentary slates, limestones and sandy graywackes represent the Upper Complex. The rock units in the Upper Complex were classified in to: The Tsaliet Group, the Tambien Group, the Didikama Formation and the Matheos Formation. The Tsaliet group is represented by metavolcanics and the Tambien Group found was the three

lower members first recognized by Beyth (1971). These three members (Werri Slate, Assem Limestone and Tsedia Slate) were later named to Arequa Formation. The Didikama Formation where it gets its name after it outcrops at Didikama in Shiraro area was originally thought an equivalent formation to the metasediments of the Mai Kenetal section. Similar dolomite seen in Adi Arkay was named Amota Formation. Further work proved unconformity, where it rests in places on metavolcanics and others on the Arequa Formation thus appears to be a new unit above the Tambien Group. The Matheos Formation known only in Negash syncline is thought to be the youngest Precambrian formation in Ethiopia, composed of gray to black, well laminated and undisturbed limestone, partly detrital and veined with calcite.

The study of Tadesse (1997) aimed at producing 1:250,000 scale geological map of Axum sheet, covers large area from Shiraro to the west to Mai Kenetal in the East. Rocks exposed in these areas are contained in six tectonostratigaraphic blocks: Shiraro, Adi Hageray, Adi Nebrid, Chila, Adwa and Mai Kenetal blocks. He described each blocks in terms of stratigraphic, structural and metamorphic details, with the identification of five deformation phases regionally. The stratigraphy of the Mai Kenetal block from top to bottom is: Tselim Imni Limestone, Bliato Limestone and Slate, Logmitti Slate, Filafil Limestone and Segali Slate.

Alene (1998) and Alene et al. (2000) analyzed the geochemistry of metavolcanic and plutonic rocks from Mai Kenetal – Negash area in light of identifying magma type and original tectonic environment. The result suggests that majority of the metavolcanic and all the plutonic rocks are of the calc alkaline suite developed in a volcanic arc setting. In addition to this the lithological and stratigraphic description of the units in Mai Kenetal-Negash area (metavolcanic/ metavolcanoclastic unit, phyllite unit, slate and carbonate unit and plutonic unit) has been done.

A comprehensive review on the basement rocks of Ethiopia was done by Asrat et al. (2001). The classification of basement rocks of Ethiopia stratigraphically into lower, middle and upper complex is not in agreement with exiting data. In addition to this it is the tectonic evolution and degree of later denudation that results in lithologic difference between the ANS and MB being concurrent events during the Pan African Orogeny. The study conducted on the late tectonic Negash pluton provides an emplacement age of 608 ±7 Ma (Asrat et al., 2004). This constrain the minimum age of deposition of Tambien Group.

Since 2000 much attention was on the Tambien Group due to their intimate connection with Snowball Earth and true polar wandering hypothesis. Beyth et al. (2003) and Miller et al. (2003) come up with an idea of Snowball Earth hypothesis for the rocks in north Ethiopia. Rapid exhumation could have also resulted from extensive erosion. According to Beyth et al. (2003) the glaciation and especially deglaciation processes may provide a mechanism for erosion, crustal thinning and then rapid exhumation. This rapid exhumation together with the preliminary light $\delta^{13}C$ isotopic ratios (characteristic for cap-carbonates associated with Snowball Earth) suggests that at least one Neoproterozoic glacial event is documented in Ethiopia and Eritrea. Miller et al. (2003), by constraining the age of Tambien Group from granite intrusions post-dating early deformation and syn-tectonic granites elsewhere in ANS, concludes the Negash diamictite to be product of Sturtian glaciation.

Alene et al. (2006) provides a thorough work on four Tambien Group inliers: Mai Kenetal, Tsedia, Chehmit and Negash synclines. Detailed lithological description, structural and deformational history and stratigraphic correlation were part of the study. Chronostratigraphic age, $\delta^{13}C$ of carbonate and organic matter and $^{87}Sr/^{86}Sr$ value lead to correlation of Tambien Group globally (Australia and Svalbard) and deposition in the range ca. 800–735 Ma. These data further indicate the correlation of lower negative $\delta^{13}C$ with the non-glaciogenic Bitter Springs Stage and Negash diamictite to Sturtian glaciation. Non-glaciogenic Bitter Springs Stage is proposed to be result of a pair of Inertial Interchange True Polar Wander events. On the other hand, according to Miller et al. (2009) the initial negative $\delta^{13}Ccarb$ interval of the Tambien Group corresponds to recovery from perhaps the ca. 755 Kaigas glacial interval making the Assem Limestone the first and oldest cap carbonate sequence in the Arabian–Nubian Shield.

Recently Swanson Hysell et al. (2015) supported by new geochronological data renovate local and global correlation of the Tambien group and global synchronity of the BSS. The 815.29 ± 0.32Ma from the Werii Formation, 788.72 ± 0.24Ma from the upper Tsedia Formation, 774.4 ± 4.8Ma date from the volcanic unit below the Didikama Formation at Negash (Avigad et al., 2007), combined with ages from the Fifteenmile Group pre-BSS (811.51 ± 0.25Ma), constrains the maximum duration of the Bitter Springs Stage to be 22.8 ± 0.3Ma. It also leads to the conclusion that the Tambien Group deposition started ca. 820 Ma and continues up to Sturtian glaciation (ca. 717–662 Ma).

CHAPTER TWO

REGIONAL GEOLOGY

2.1 The Geologic and Tectonic Evolution

2.1.1 The Neoproterozoic Era

The Neoproterozoic era (1000-542Ma) is bracketed by the end of the Grenvillian orogeny (1000-900 Ma) and the Brasiliano-Pan-African system of orogenies (ca. 550-500 Ma). This implies a full supercontinent cycle happened during this era (Gaucher et al., 2009). It encompasses an eventful period in Earth history, comparable in length with the Phanerozoic Eon. Among the most notable events in the Neoproterozoic are the final amalgamation and demise of the oldest well documented supercontinent Rodinia, the fusion of its cratonic pieces into Gondwana through an immense network of orogenic events, the most severe glaciations in Earth history, large oscillations in the carbon and sulfur isotope composition of seawater in earth history, the advent of animals, the first skeletonized organisms, the oldest evidence of predation and the colonization of the infaunal niche. Thus the Neoproterozoic spans a time that is of particular interest across multiple disciplines (McMenamin and McMenamin, 1990; Hoffman et al., 1998; Seilacher, 1999; Rino et al., 2008; in Gaucher et al., 2009).

2.1.2 Assembly of Gondwana

The fragmentation of Rodinia results in the distribution of continental masses and opening of oceans which through time starts to assemble and form a composite megacontinent called Gondwana. Brasiliano/Pan-African orogenic belts welded together Amazonia, West Africa, Congo, Kalahari, Greater India and Australia-Antarctica cratons forming Gondwana (Fig. 2.1; Hoffman, 1999). Contemporaneous events include the closure of Adamastor (aka Brasilide) ocean which separates West Gondwana from the African cratons and Mozambique ocean which formed between East Gondwana and African cratons (Dalziel, 1992). The Congo and Kalahari Cratons were already joined at the Zambezi Belt, which closed at 850-800 Ma (Hanson et al., 1993, 1994; Mariga et al., 1998; Hargrove et al., 1998), although the western and central portions of the join reopened shortly thereafter and did not finally close, forming the Damaran and Katangan Belts, respectively, until 600-550 Ma (Stanistreet et al., 1991; Wilson et al., 1997).

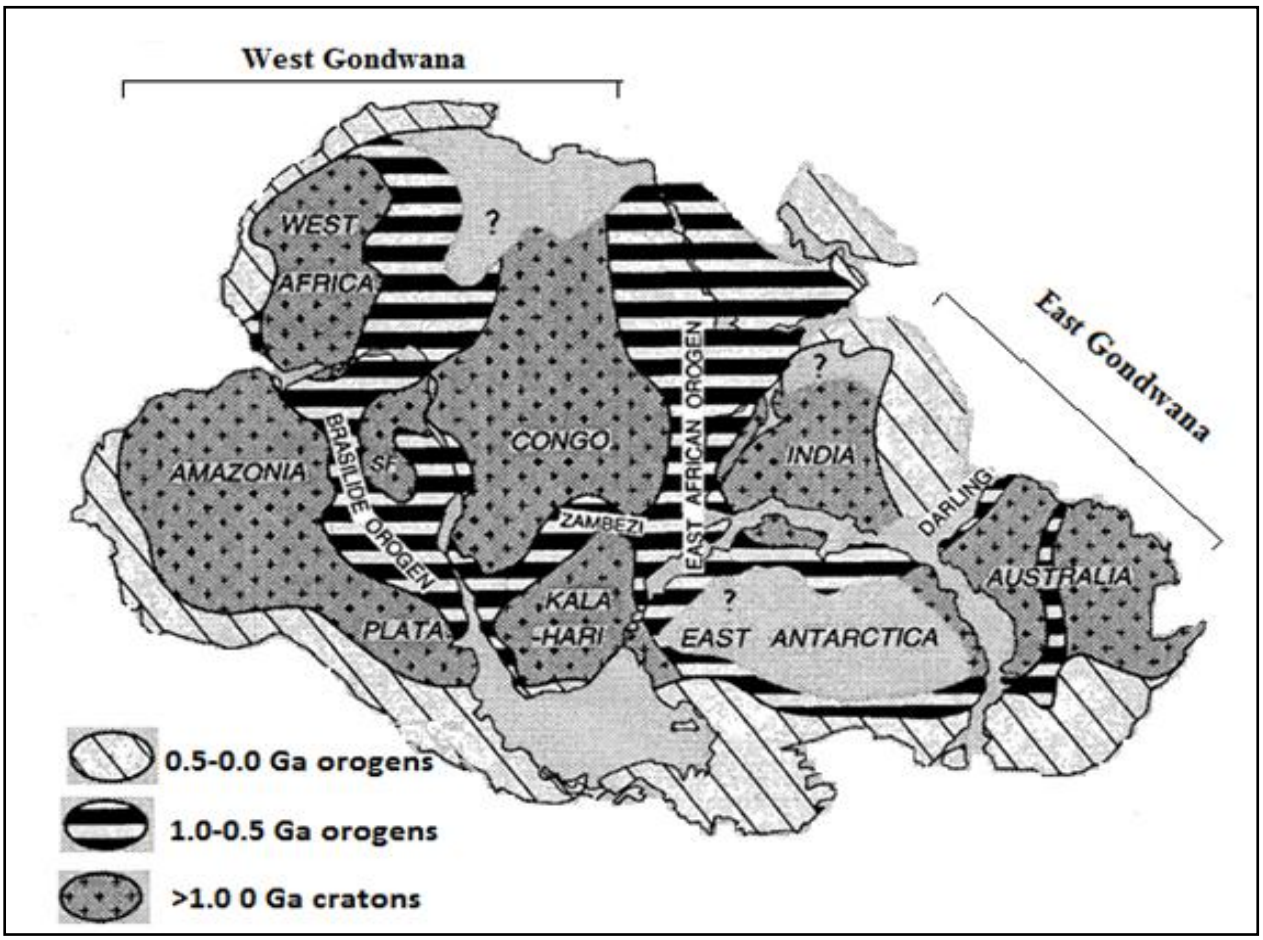

Fig. 2-1 Assembly of Gondwana, which is composite megacontinent comprised of six or more pre- 1.0 Ga cratons welded by Pan-African/Brasiliano orogenic belts (Hoffman, 1999).

2.1.3 East African Orogen

The East African Orogen formed as a result of consumption of Mozambique Ocean is a Neoproterozoic–early Cambrian mobile belt that today extends ~6000km from southern Israel, Sinai and Jordan in the north to Mozambique and Madagascar in the south (Stern, 1994; Fritz et al., 2013). According to Hoffman (1999), a widely accepted two stage model has been developed on the subject of Mozambique Ocean consumption. It combines the revised geochronological picture for East Gondwana with new paleomagnetic constraints (Meert et al., 1995; Meert and van der Voo, 1996, 1997).

According to their model, the older 'East African' Orogeny (~680 Ma) resulted from the collision of Greater India (i.e. India-Tibet-Seychelles-Madagascar-Enderby Land) with the conjoined Congo and Kalahari Cratons. The younger 'Kuunga' Orogeny (-550 Ma) represents the collision of Australia-East Antarctica with proto-Gondwana, accompanied by intraplate reactivation of the East African Orogen. The model accounts for the extensive Kuungan Orogeny (580-520 Ma) in East Antarctica and the polyphase nature of the East African

Orogen, with the older (~680 Ma) collision dominant from Tanzania northward and the younger (~550 Ma) one dominant from Mozambique southward.

Traditionally, the EAO is subdivided into the Arabian–Nubian Shield (ANS) in the north, composed largely of juvenile Neoproterozoic crust (e.g. Stern, 1994, 2002; Johnson and Woldehaimanot, 2003; Johnson et al., 2011), and the Mozambique Belt (MB) in the south comprising mostly pre-Neoproterozoic crust with a Neoproterozoic–early Cambrian tectonothermal overprint (Fig. 2.2A) (e.g., Fritz et al., 2005; Collins, 2006; De Waele et al., 2006; Viola et al., 2008; Bingen et al., 2009). It is unlikely that the EAO has similar tectonic styles along its entire length. Even a cursory inspection suggests that different processes were active in the ANS in the north and the MB in the south. Additional differences in temporal and geometric relations are seen in Tanzania and Mozambique where the E–W trending Damara–Zambesi–Irumide Belt intersects the N–S trending MB. Thus it is appropriate to define different orogenic styles, aiming to highlight major characteristics of the EAO segments (Fritz et al., 2013).

Fritz et al. (2013) discussed about the non extensive nature of pre-Neoproterozoic crust outcropping in the ANS. The ANS is southward narrowing belt internally structured by individual terranes, which covers Saudi Arabia, Egypt and Sudan in its northern part and Eritrea, Ethiopia and Kenya in its southern part. Assemblages with high-grade Neoproterozoic metamorphism and intense deformation constitute the southward continuation of the ANS from Kenya through Tanzania to Mozambique. These units have been classified as part of the MB (Holmes, 1951) but contain a collage of different crustal fragments. A key tectonic position is occupied by the Eastern Granulites in Tanzania (Hepworth, 1972) and the Cabo Delgado Nappe Complex in Mozambique (Viola et al., 2008) that are regarded as a coherent entity (Eastern Granulite–Cabo Delgado Nappe Complex: EGCD). Based on the formation ages of different groups, Maboko and Nakamura (2002) inferred that the Eastern Granulites of northern Tanzania represent Neoproterozoic juvenile crust coeval with the ANS.

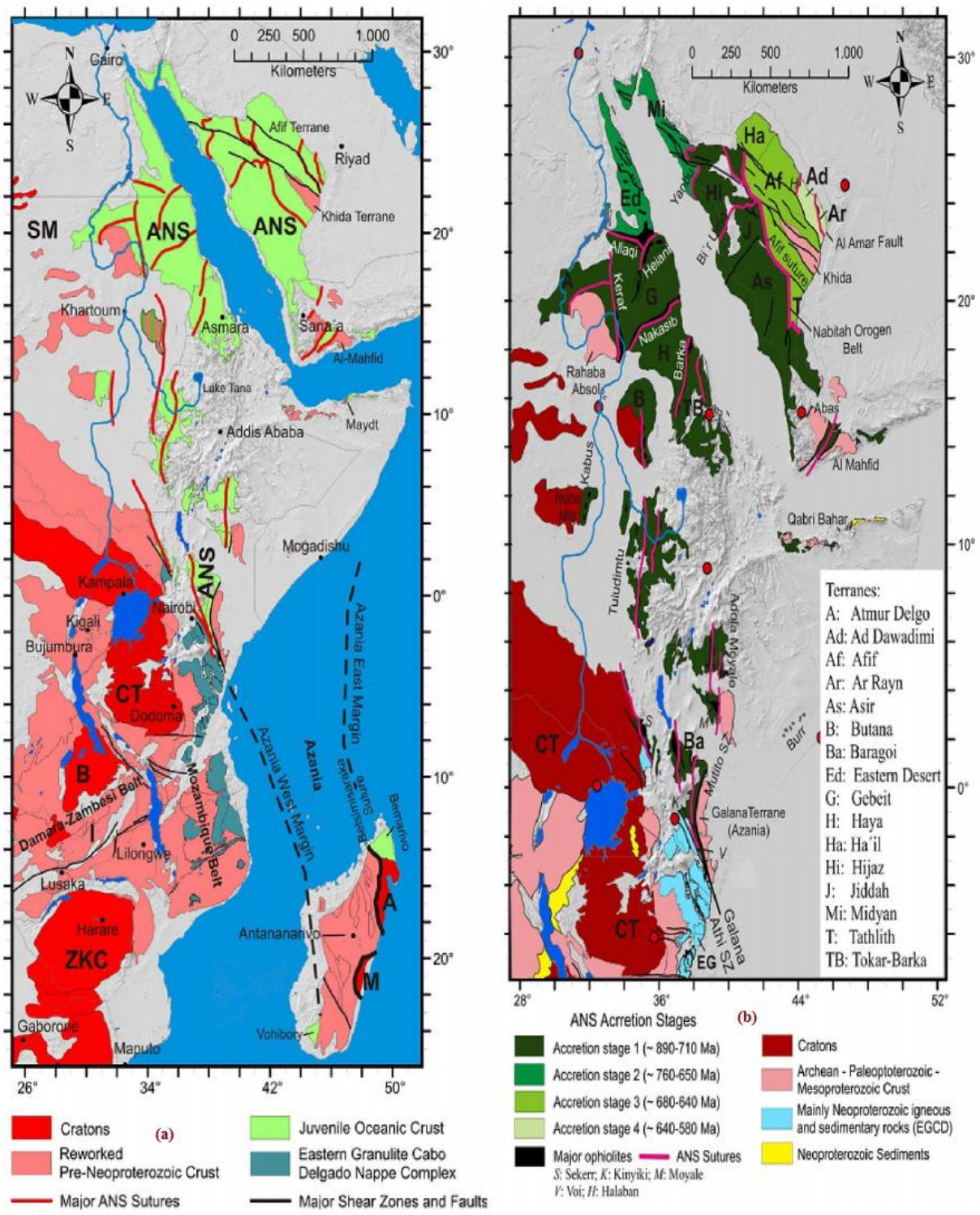

Fig. 2-2 (a) Distribution of crustal domains in the East African Orogen. (b) Crustal age domains in the northern East African Orogen and crustal growth phases in the Arabian–Nubian Shield. SM, Sahara Metacraton; CT, Congo–Tanzania cratons B-Bangweulu Craton; ZKC, Zimbabwe–Kalahari Cratons; I, Irumide Belt; A, Antogil Craton; M, Masora Craton; ANS, Arabian Nubian Shield; EG, Eastern Granulites (Fritz et al., 2013).

2.1.4 Evolution of Ethiopian Basement Terrane

The Ethiopian Basement is exposed in the Northern, West and South western, Southern and Eastern part of the country (Asrat et al., 2001). It is widely accepted that the Ethiopian Basement is constituted of two major structural units: ANS and MB, but it is less clear in defining the transition from one to the other (e.g., Asrat et al., 2001; Stern et al., 2012; Fritz et al., 2013).

According to Fritz et al. (2013) the evolution of the ANS is accomplished by four phases of crustal accretion: southern, northern, western arc and eastern part of ANS (Fig. 2.2b). The southern ANS, extending from southern Kenya through Ethiopia, Sudan and Eritrea to Yemen and Saudi Arabia, formed first (Johnson et al., 2003). This part of the ANS constitutes terranes that are internally partitioned by arc–arc sutures (Kröner et al., 1991; Abdelsalam and Stern, 1996; Stern et al., 2012; Johnson et al., 2011). The terranes are known as Tokar–Barka, Butana, Haya terranes in Eritrea, Ethiopia, and Sudan and Abbas, Asir, Jiddah, and Hijaz terranes in Yemen and Saudi Arabia. Protolith ages from these terranes extend back to 900–830 Ma.

The tectonic evolution of the southern ANS through a Wilson Cycle is well illustrated in the Tuludimtu belt of central Ethiopia (Woldemichael et al., 2010). Here, early rifting was initiated between 900 and 860 Ma; the transition from rifting to ocean floor spreading occurred between 860 and 830 Ma; subduction and formation of arc- and back-arc basins occurred between 830 and 750 Ma; and basin closure by accretion of island arcs commenced between 750 and 650 Ma. To the north, amalgamation of arc systems by closure of internal arc–arc sutures (e.g., Barka and Bir' Umq-Nakasib sutures) occurred between 800 and 700 Ma (Abdelsalam and Stern, 1996; Yibas et al., 2002; Woldemichael et al., 2010).

Unlike the northern, NE-trending Nakasib-Bi´r Umq suture, the ANS arc–arc sutures to the south (Barsaloi–Tuludimtu–Baraka sutures and Galana–Adola–Moyale–Ghedem-Araq sutures) trend N–S. They consist of meta-volcanosedimentary rocks such as garnet–staurolite and amphibole schists, metamorphosed up to amphibolite facies (Ghebreab, 1996, 1999; Yihunie and Hailu, 2007). Most are decorated by linear belts of mafic and ultramafic rocks with ophiolitic affinity. The sutures are flanked by partly migmatitic gneiss terranes (given different names in different places) where rocks show higher grades of metamorphism (Tsige and Abdelsalam, 2005; Yihunie et al., 2006; Yihunie and Hailu, 2007; Stern et al., 2012;

Woldemichael et al., 2010). The nature of these orthogneiss terranes is debated. They might represent either pre-Neoproterozoic crust or roots of Neoproterozoic arcs.

Asrat et al. (2001), supported with geochronological data from granitoids and others showed that basement rocks exposed in different parts of Ethiopia are comparable in age with differences in tectonic evolution and degree of later denudation. In line to this, recent zircon geochronology in southern Ethiopia (Stern et al., 2012) establishes that the bulk of these gneisses are Neoproterozoic. However, one sample from undeformed granite intruding a migmatitic gneiss has abundant ~2500 Ma old zircons. Stern et al. (2012) took this as argument that Archean crust exists locally at depth in southern Ethiopia.

The western Barka sinistral shear zone is probably a northward continuation of the Tuludimtu Belt in Ethiopia, and the eastern Ghedem–Araq shear belt (Asmara–Nakfa Shear Belt) a continuation of the Adola–Moyale Belt. Two pulses of magmatism (at 860–850 and 795–785 Ma) are discerned in the Tuludimtu region (Woldemichael et al., 2010), and four magmatic episodes (890–840, 790–700, ~660 and 630–500 Ma) in the Adola Moyale Belt (Stern et al., 2012).

In Kenya and Ethiopia, W- and E-directed thrusting of individual units above the high-grade gneissic terranes are interpreted as an early phase of deformation between 800 and 650 Ma (Yibas et al., 2002; Yihunie and Tesfaye, 2002; Allen and Tadesse, 2003; Yihunie and Hailu, 2007). This event was related to collision of individual terranes after consumption an ocean along a possibly E-dipping subduction zone (Bulbul and northern Moyale belts: Tsige and Abdelsalam, 2005). N-trending strike-slip shearing was initiated soon after or contemporaneous with thrusting. The Adola Moyale belt has been described as a positive flower structure (Tolessa et al., 1991; Ghebreab, 1992) and all subsequent authors typify the southern ANS belts as a transcurrent orogen with an oblique NW–SE to NE–SW shortening component. Regional E–W shortening resulted in both lateral and pronounced vertical flow of rocks as suggested by the involvement of metamorphic terranes exhumed from 25 to 35 km (Johnson et al., 2004; Tsige, 2006) or even 45 km depth (Ghebreab et al., 2005). The superposition of strike-slip shearing with thrust-related fabrics produced the complex fold interference pattern typical for these belts (Bogliotti, 1989; Bonavia and Chorowicz, 1993).

2.1.5 Geology of Northern Ethiopia

Three main rock complexes make up the geology of the northern Ethiopia; the Precambrian basement complex and its intrusives, Paleozoic-Mesozoic sediments and Tertiary trap

volcanics and the young sediments and volcanics of the Danakil depression. The first is a geosynclinal succession of low grade metavolcanics and metasediments forming large submerdional anticlinoria and synclinoria. The Paleozoic-Mesozoic sediments unconformably overlying Precambrian basement are composed mainly of horizontal glacial rocks of Paleozoic age, overlain by Jurassic to Lower Cretaceous sandstone and limestone. Paleozoic glacial rocks in northern Ethiopia are described as Edaga Arbi glacial deposits and Enticho Sandstone. The tillite facies informally named Edaga Arbi glacials, grades northward, eastward, and westward, into the sandstone conglomeratic facies, called the Enticho Sandstone. The Enticho sandstone is deposited after unconformity where the Neoproterozoic orogens are eroded across North Africa and Arabia, producing Afro-Arabian peneplain (Avigad et al., 2003). Paleozoic – Mesozoic sediments are controlled by E-W and NW-SE set of normal faults along which the Mekelle dolerites were emplaced. These structures are cut by the rift valley faults to the east. Flood basalts of Tertiary age unconformably overlie the sedimentary rocks (Dow et al., 1971; Beyth, 1972).

Metamorphic rocks exposed in Tigrai are the southward extension of the Bizen domain of Nakfa terrane of Eritrea (Fig. 2.3) (Beyth et al., 2003; Alene et al., 2006; Miller et al., 2009, 2011). They are broadly divided into the Tsaliet and Tambien Groups (Beyth, 1971, 1972).

According to Garland (1980) the Tsaliet Group which covers the greater part of the basement is formed by heterogeneous series of rocks with obvious volcanic association. They are breccias, agglomerates, bedded tuffs and lavas all interbedded with marine clastics, rare limestones, tuffaceous slates, redeposited ash and greywacke composed partly of volcanic fragments.

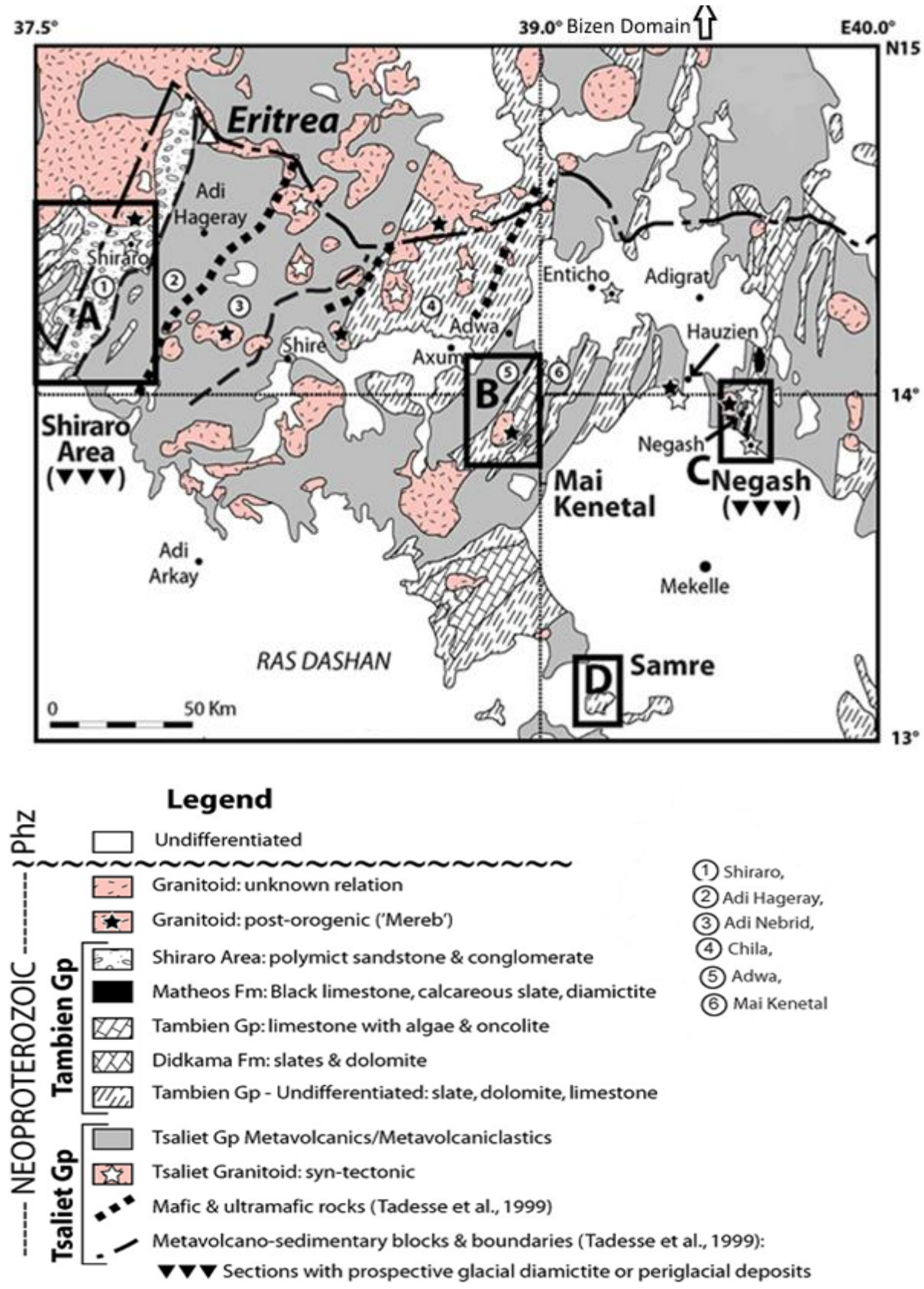

Fig. 2-3 General geological map of Tigrai region. White and black stars respectively show locations of dated arc-related (syn-tectonic) and post-orogenic intrusives (Miller et al., 2009, 2011).

Cessation of Tsaliet arc volcanism was followed by deposition of Tambien Group, a mainly marine siliciclastic and carbonate sedimentation within the Mozambique Ocean. The Tambien Group exposed in different parts of Tigrai is preserved in NNE- trending upright/ overturned synclinorium formed by D_2 deformation (Sifeta et al., 2005; Alene et al., 2006; Miller et al., 2011). The Mai Kenetal, Tsedia, Chehmit and Negash synclines are more studied than other exposures (Fig. 2.4). From oldest to youngest: Lower Slate, Lower Limestone and Upper Slate are exposed in the first three synclines with an additional Upper Limestone lying on top of these in Mai Kenetal syncline (Alene et al., 2006). According to Swanson-Hysell et al. (2015) the complete stratigraphy of the Tambien Group is ~5km thick and contains nine formations (Fig. 2.5A).

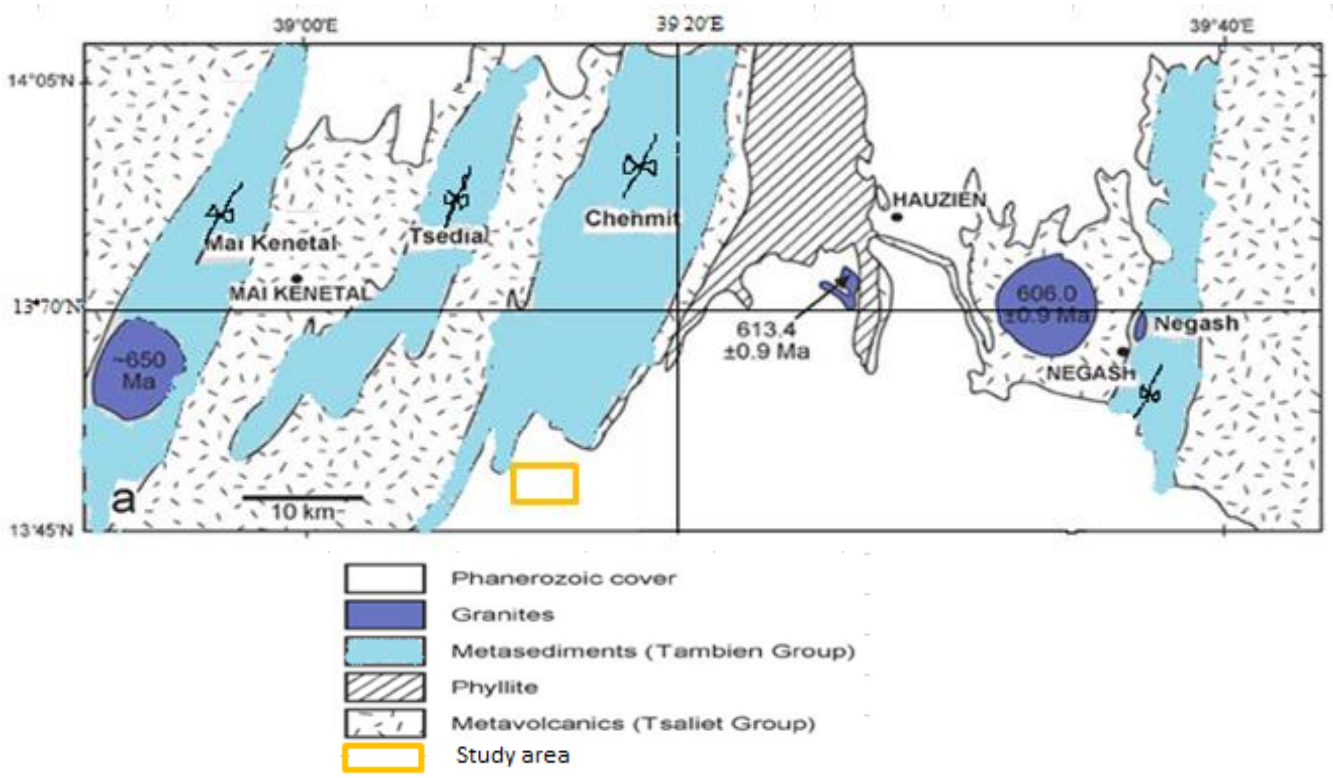

Fig. 2-4 Geological map of the Mai Kenetal – Negash area. The age of the pre D_2 intrusives are from Miller et al. (2003) for the Negash and Hauzien and Beyth (1972) for the Mai Kenetal granites (Alene et al., 2006).

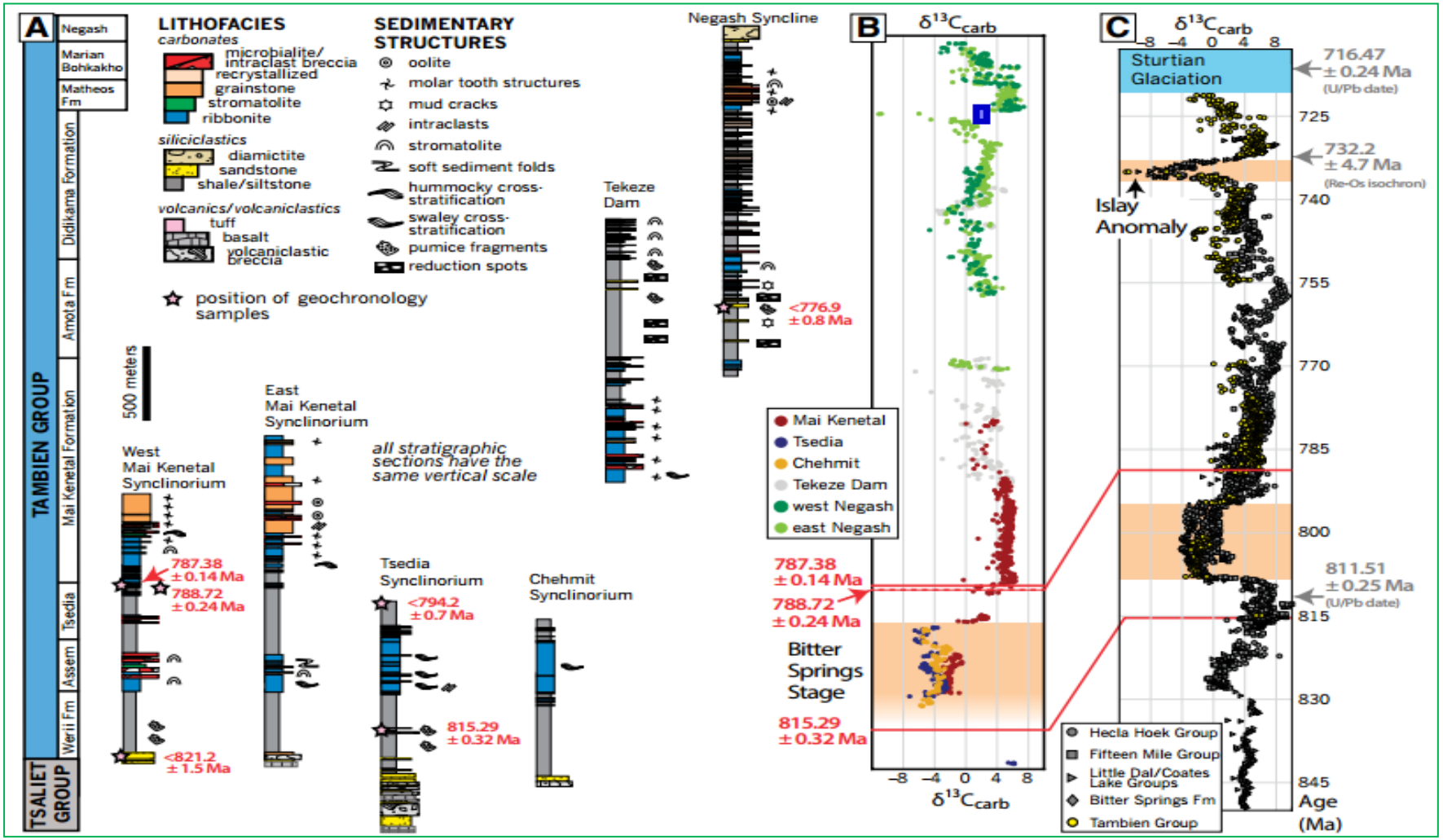

Fig. 2-5 Regional and global correlation of Tsaliet and Tambien Groups on the basis of: A: lithostratigraphical sections. B: New U-Pb geochronology and $\delta^{13}C$ chemostratigraphy. C: Composite of pre-Sturtian carbon isotope data that incorporates new U-Pb dates from the Tambien Group and dates from northwestern Canada (gray) (Swanson-Hysell et al., 2015).

Beyth (1972) described the contact relationships between the metavolcanic and metasedimentary successions as unconformable however; Alene et al. (2006) called it gradational. The contact is poorly understood varying from sharp contact formed by faults and lineaments to gradational contacts to blurred unconformable contacts (Sifeta et al., 2005). Dateable volcanic ashes were added to the successions of the metasediments and the contact is transitional (Swanson-Hysell et al., 2015). Tsaliet metavolcanics experienced a regional metamorphism from pumpellyite - actinolite to lower greenschist facies (~245–375^{0}C) where as <250^{0}C is attained by Tambien Group (Alene et al., 2006).

Intrusive rocks of different age i.e. syntectonic and post tectonic granites, granodiorites and diorites are found within the Precambrian basement. The syntectonic ones are weathered, medium grained epidotised with slight foliation and are elongated along the strike. On the other hand the post tectonic granites are coarse grained with mineral composition microcline perthite, zoned sodic plagioclase, biotite and hornblende with sphene and apatite as accessory minerals. The granite is cut by aplitic dykes. Intermediate rock types between granite and diorite were discovered in all the intrusions (Garland, 1980). Asrat et al. (2003) discussed the presence of regional structures in the Negash pluton which will make it to be late tectonic rather than post tectonic. According to Alene et al. (2006), it is intruded between D_1 and D_2 where D_1 is due to N-S compression and resulting in tight minor folds, elongation lineation and pervasive regional foliation and D_2 is due to E-W compression and resulting in long wavelength, upright folds without producing a significant cleavage.

2.2 Chemostratigraphy

2.2.1 Definition

Chemostratigraphy, or chemical stratigraphy, is the study of the chemical variations within sedimentary sequences to determine stratigraphic relationships. The field is relatively young, having only come into common usage in the early 1980s, but the basic idea of chemostratigraphy is nearly as old as stratigraphy itself: distinct chemical signatures can be as useful as distinct fossil assemblages or distinct lithostratigraphies in establishing stratigraphic relationships between different rock layers.

In geochemistry, paleoclimatology and paleoceanography δ^{13}C (pronounced "delta thirteen c") is an isotopic signature, a measure of the ratio of stable isotopes ^{13}C: ^{12}C, reported in parts per thousand (per mil, ‰).

The definition is, in per mil:

$$\delta^{13}C = \left(\frac{\left(\frac{^{13}C}{^{12}C}\right)_{sample}}{\left(\frac{^{13}C}{^{12}C}\right)_{standard}} - 1 \right) * 1000\ ‰$$

Where the established standard reference material was the Pee Dee Belemnite (PDB) and which is based on a Cretaceous marine fossil, *Belemnitella americana*, which was from the Pee Dee Formation in South Carolina. Other standards calibrated to the same ratio, including one known as VPDB (for "Vienna PDB"), have replaced the original (Rey and Galeotti, 2008; Libes, 2011; Miller and Wheeler, 2012).

2.2.2 Carbon Isotope Excursions

Isotopes have the potential to improve the relatively coarse stratigraphic resolution provided by Neoproterozoic fossils. Isotopic shifts in the global ocean atmosphere system are superimposed on regional and local variability, so that carbon isotope profiles from widely separated localities are often strikingly similar despite differences in the absolute value of $\delta^{13}C_{carb}$. Large oscillations in the isotopic records show that the Neoproterozoic Era was characterize by noticeable tectonic and biogeochemical change (Ripperdan, 1994; Kaufman, 1995).

Variations in the isotopic composition of carbon ($\delta^{l3}C$) in the marine environment are a function of: the fraction of available CO_2 undergoing photosynthesis reduction or synthesis to organic carbon, the amount of fixed organic carbon buried in sediments, and the fractionation between the inorganic and organic carbon reservoirs, which is ultimately regulated by pCO_2 and temperature. The $\delta^{13}C$ value of marine bicarbonate ion, $HC0_3^-$, is sampled by $CaCO_3$ deposition of marine limestones and carbonaceous skeletons with a minor fractionation of 1-2‰ that is only slightly dependent on temperature (Anderson and Arthur, 1983). Since the burial flux of organic compounds with low $\delta^{13}C$ values ($\delta^{13}C$ org ~ -25‰) ultimately controls the isotopic composition of HCO_3^-, the $\delta^{l3}C$ of shallow-water marine carbonates ($\delta^{13}C_{carb}$) serves as a measure of net worldwide carbon deposition during long-term steady-state conditions (Ripperdan, 1994).

The efficient burial of organic matter in ocean basins, perhaps as a consequence of high erosion rates related to widespread orogenesis and abundant nutrient availability causally related to an increase in the oxygen content of the atmosphere result in the ^{13}C-enriched intervals of Neoproterozoic successions. On the other hand negative excursions seen in the C-isotopic record can be contributions from weathering and erosion of organic-rich rocks or the

vigorous ventilation of the deep sea following an interval of ocean stratification (Kaufman, 1995; Calver et al., 1996). More emphasis is given to the negative excursions as it suggests decline in biological productivity in the ocean surface for millions of years (Hoffman et al., 1998).

During snowball Earth, ice cover would block out sunlight ensuing in severe declining of oceanic photosynthesis for millions of years. On its rapid termination the atmospheric carbon dioxide raised due to subaerial volcanic outgassing resulted in extreme greenhouse conditions. Carbonate rocks with negative carbon isotope anomalies are formed from the transfer of atmospheric carbon dioxide to the ocean (Hoffman et al., 1998). Although this being the case, there are cases in which negative carbon isotopes are measured in non glaciogenic rocks (Fig. 2.6) (e.g. Alene et al., 2006; Hoffman et al., 1998; Swanson-Hysell et al., 2015).

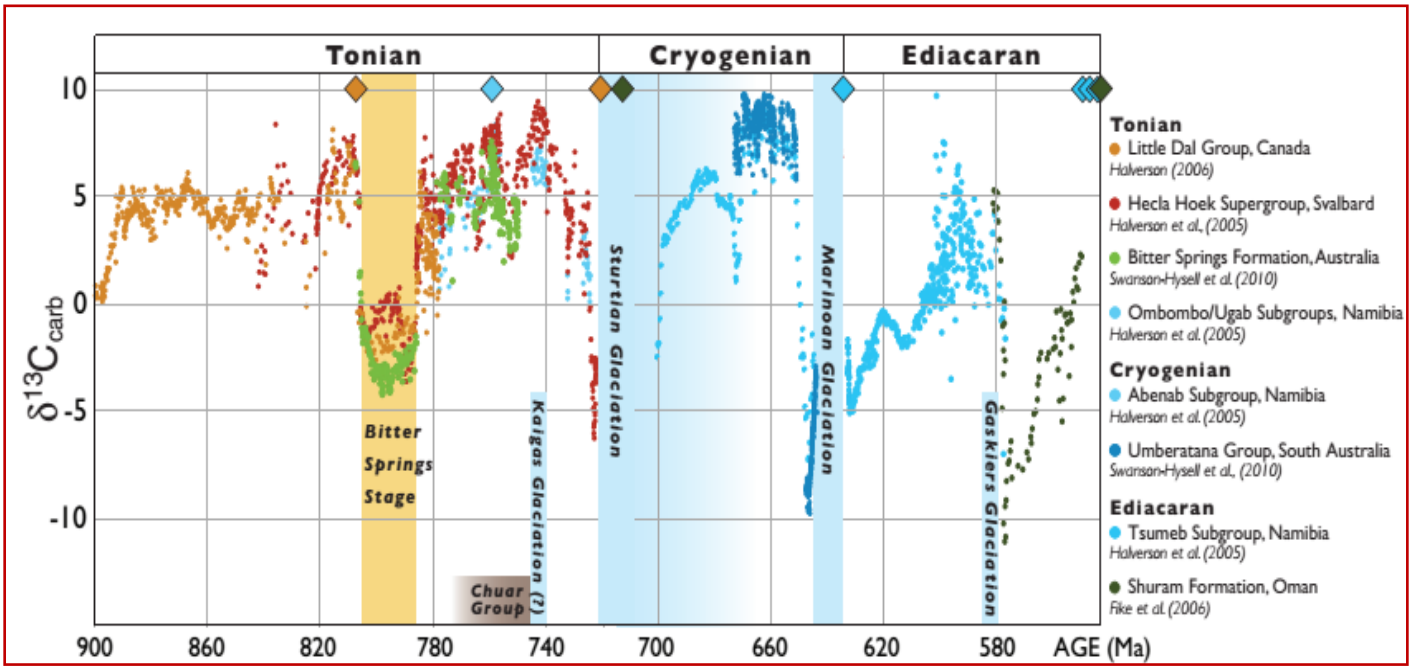

Fig. 2-6 Secular variations of composite carbonate carbon isotope values during Neoproterozoic era, from Swanson-Hysell et al. (2012).

According to Alene et al. (2006) the Negash diamictite and lower negative C-isotope anomalies are correlated to Sturtian glaciation and Bitter Springs Stage respectively. Swanson-Hysell et al. (2015) supported with geochronolical data discussed the global synchronity of Bitter Springs Stage using Assem Formation as evidence (Fig. 2.5B, C). True polar wander hypothesis, any rotation of the entire silicate shell of the Earth, down to the core-mantle boundary, relative to the diurnal spin axis, for the Bitter Springs Stage is proposed (Alene et al., 2006; Maloof et al., 2006; Swanson-Hysell et al., 2015).

CHAPTER THREE

GEOLOGY AND PETROGRAPHY OF THE STUDY AREA

3.1 Introduction

A panoramic view on the study area shows continuous ridges and lithologically distinctive units trending NE-SW. Following the approaches mentioned in the methodology part data are analyzed and compiled to depict the geology and deformation history of the area. Primary name of lithological units were given during the field work based on textural and mineralogical compositions, latter confirmed through petrographic analysis. Thin sections from representative rock samples have been prepared and examined for modal compositions, alterations, texture and microtectonics.

Broadly categorizing, the lithological units exposed are para and ortho metamorphic rocks unconformably overlain by sedimentary rocks. Figure 3.1 shows seven lithological units representing the geology of the study area at a scale of 1:25,000. These lithological units listed from bottom to top are: variegated slate, metavolcanic, spotty phyllite, metalimestone, slate, slate and phyllite unit and pebbly sandstone (Fig. 3.2). Unmappable units include metagraywacke, graphite slate, metasubvolcanics and psammites. Almost all the units are intruded by syn-late tectonic aplite dikes. The detail field and petrographic description of the lithological units is given as follows:

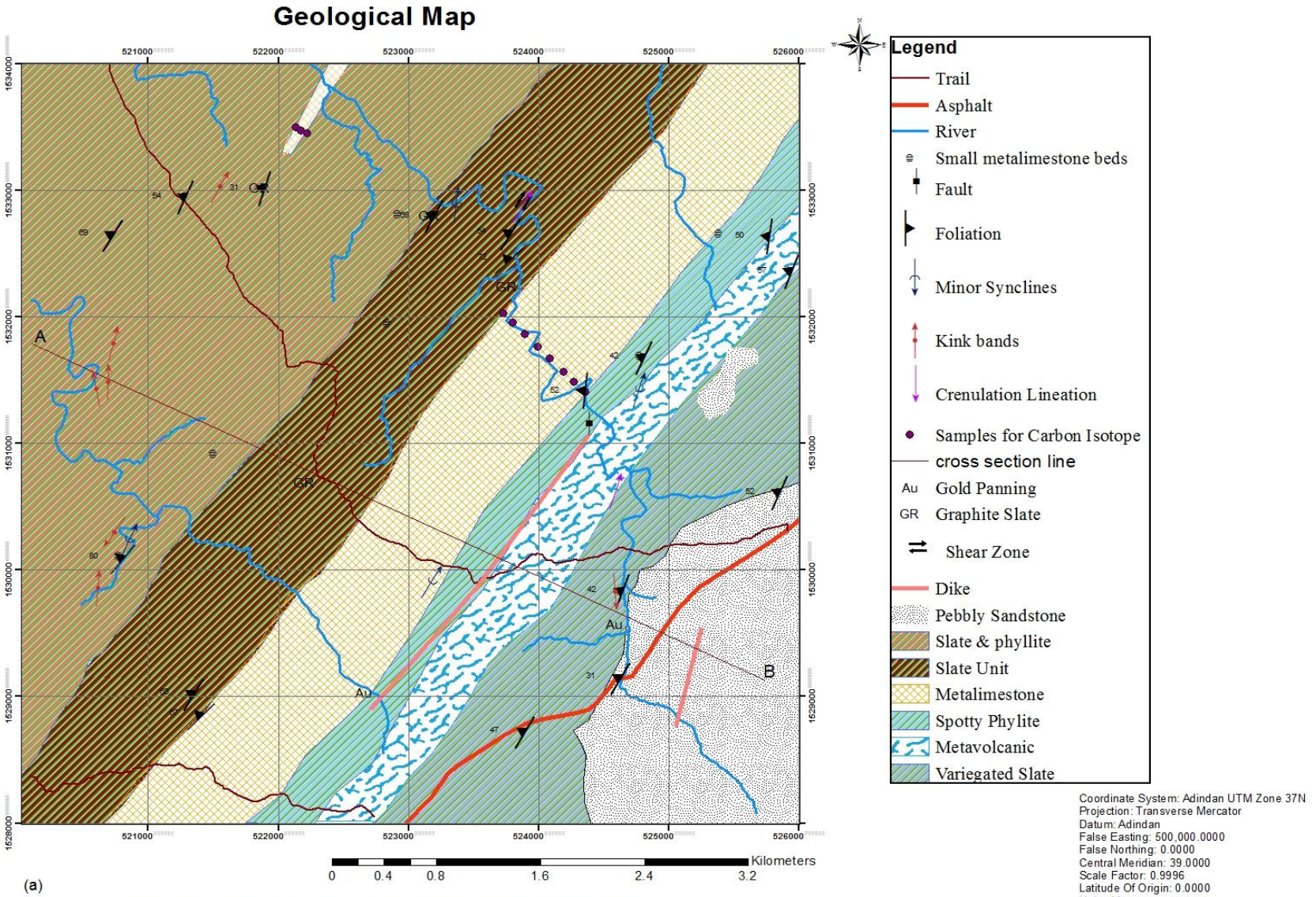

(a)

Fig. 3.1 (a) Geological map of Koraro- Gelebeda area and (b) Cross section along the line A-B

Cross section

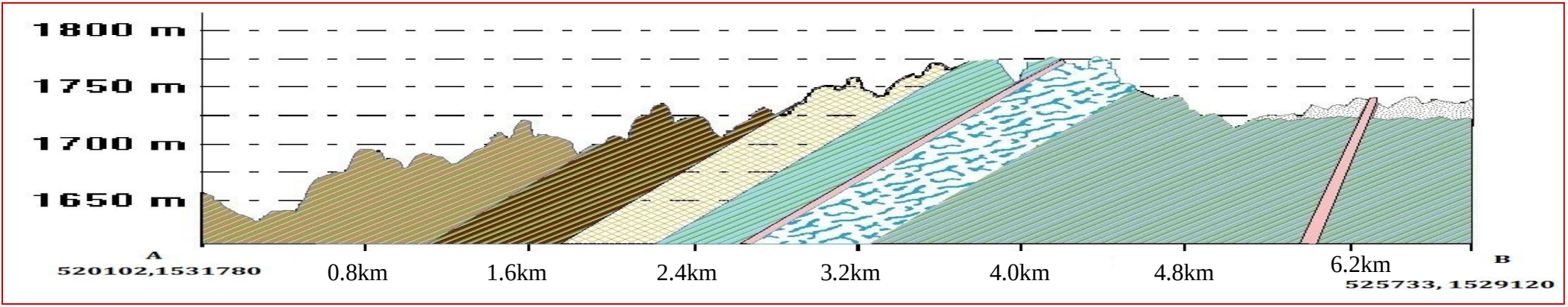

(b)

Vertical scale = 1:5000

Horizontal scale = 1:27500

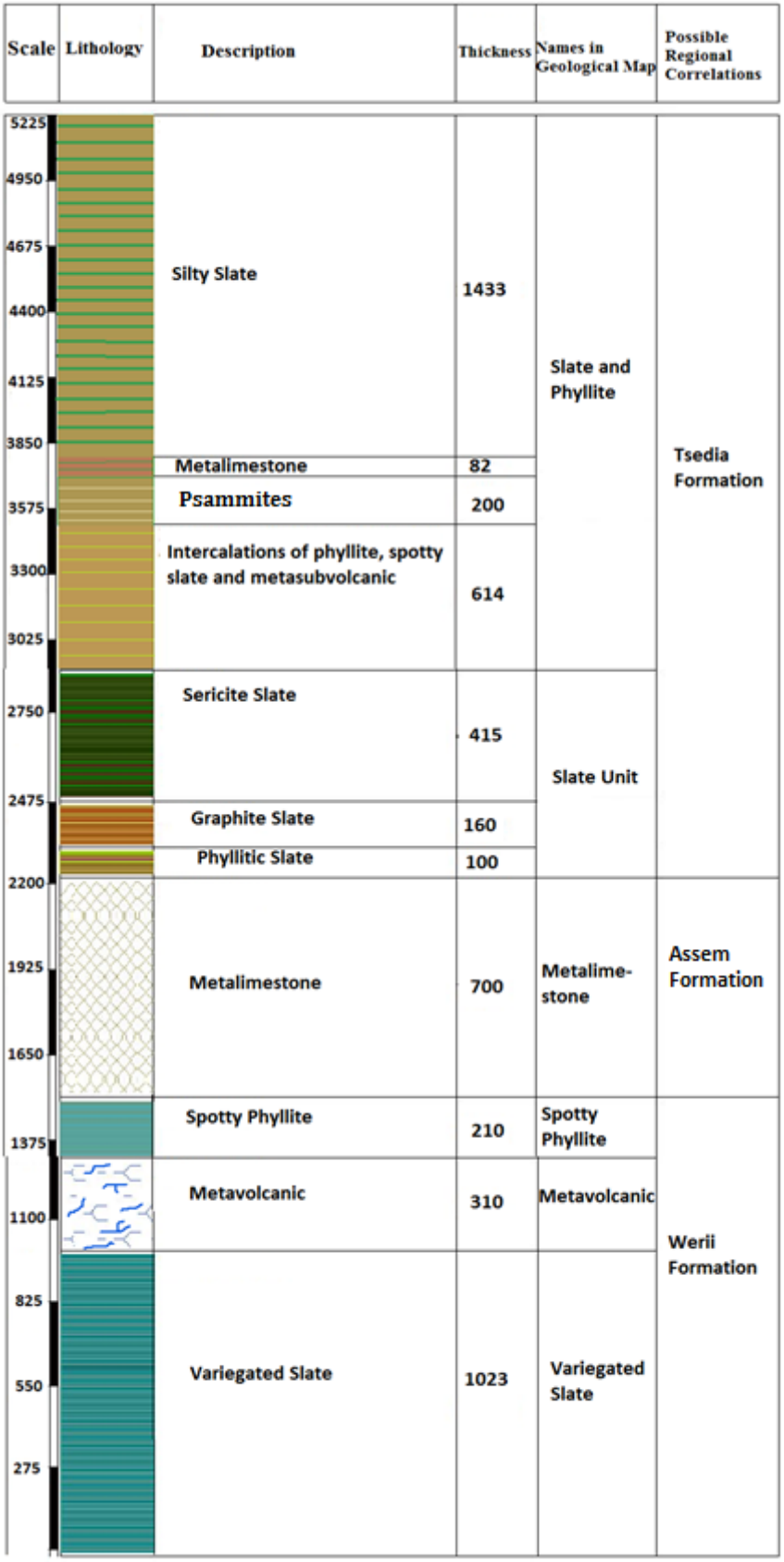

Fig. 3-2 Stratigraphy of the study area

3.2 Variegated Slate Unit

This is the oldest unit in the study area, its lower boundary is not observed but it is overlain by a metavolcanic unit. It is also unconformably overlain by pebbly sandstone rock on the eastern part of the study area. The estimated thickness of this unit is ~1023 m. It is largely composed of gray, greenish gray, purple and pink slates layers (Fig. 3.3A). Spotty slates with secondary brown minerals in it are also recognized. Quartz veins trending parallel to strike of the beds are common in the unit. High variation in dip of the beds from 31^0-82^0 is documented which is due to folds. There are several gently plunging upright and recumbent folds on the slate rocks and the quartz veins (Fig. 3.3C, E).

Up stratigraphy it grades to phyllite with shiny surfaces and crenulation lineations (Fig. 3.3C). Conformably overlaying the phyllite rock is a thick metavolcanic unit without slate interbeds. Relatively this slate unit forms lowland and is used for farming but interbedded metavolcanics and metagraywackes form ridges. On weathered surface of the metagraywacke rocks are sub-rounded quartz crystals which might be due to short distance transportation. Limestone beds ranging in thickness from 5-10cm with black and pinkish color are found.

The petrographic analysis of greenish gray slate shows that it is composed of 55% sericite, 40% quartz/k-feldspar and 5% opaque minerals. Alignment of micas and stretching of quartz grains define slaty cleavage. Quartz grains show altered boundaries. Subparallel relationship of bedding to foliation is clear. It has many shear sense indicators and sigmoidal microveins. Foliation are crenulated where it is mica enriched (Fig.3.3B).

The phyllite unit is composed of 50% sericite, 30% muscovite, 25% quartz, 3% k-feldspar and minor opaque minerals. Micas grow parallel to cleavage and microlithon domains. Asymmetric folds with different wavelength on both domains and only in the cleavage domain are prevalent. Folded quartz veins with coarser and brighter grains than grains in microlithon domains cut the bedding. Fold axes of these veins are parallel to fold axes of the crenulation which may be due to same deformation phase (Fig.3.3D).

Spotty slate is composed of 60% muscovite/sericite, 15% quartz/k-feldspar and 25% brown secondary minerals. Most of the brown porphyroblasts overprint the slaty cleavage. Foliation is crenulated with the bending frequently occurring on the margins of the porphyroblasts. This provides evidence for their genesis stage (Fig. 3.3E). Quartz minerals of up to 0.2mm large and the brown minerals ranging from 0.6-2mm are common.


A
23 Oct 2015

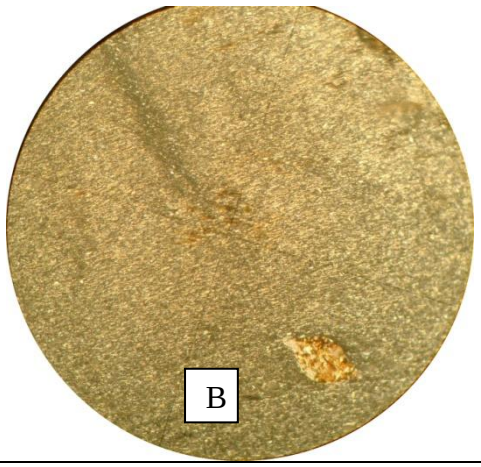
B


C

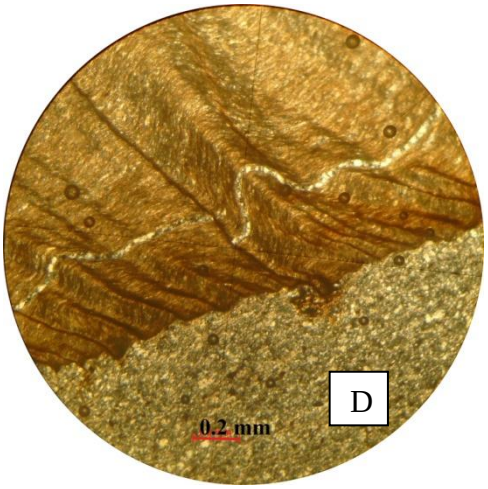
D
0.2 mm

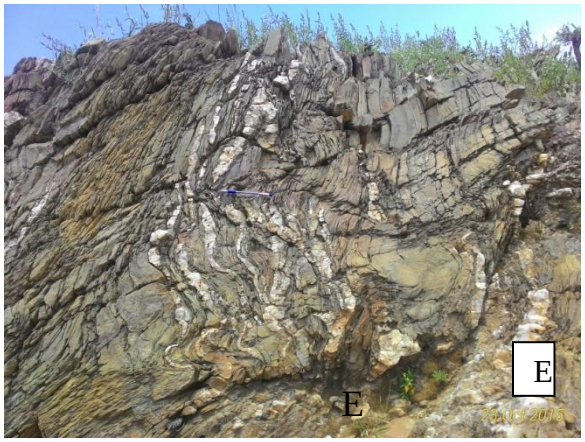
E
E

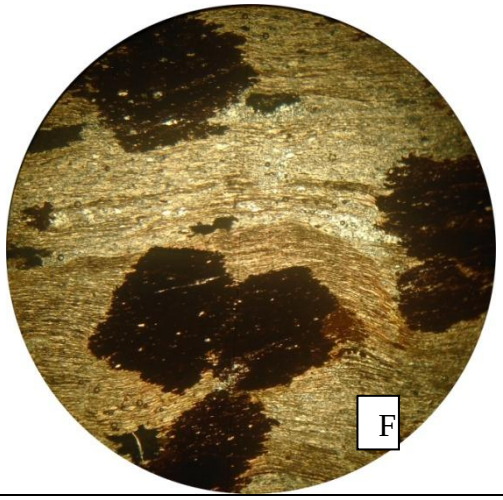
F

Fig. 3-3 Field photographs and photomicrograph of rocks in variegated slate unit.

(A) Variegated slate showing alternating purple and greenish gray colors which typifies bedding. Foliation and bedding are parallel and dip 42/290. E- 0524598, N-1529845,

(B) Slaty cleavage defined by sericite minerals and elongated quartz-feldspars. Mica enriched zones show secondary deformation, crenulation of the main foliation. Mantled porphyroblast looks a pseudomorph after brown minerals since residue of brown material is noticeable with the mica. It is porphyroblast because it grows over the foliation without any deflection or pressure shadow. Tails of the blast are parallel to foliation. Sinistral sense of shear. 10x, Xpl. E-0524591, N-1529794,

(C) Phyllite unit in the variegated slate. The reddish line bound a small bed, and is parallel to foliation. It is shown that these beds are folded by gently plunging upright folds. Viewed from top are clusters of lines which are parallel to axes of these folds. These define crenulation lineation which is common in phyllites. Top left (opposite side of the river) is ridge of metavolcanic. Attitude of lineations 15/013, E- 0524603 N- 1530657,

(D) It is a thin section (xpl view) of sample grabbed from C showing primary bedding. Crenulation cleavage is seen in the mica rich zone trending top left to lower right. Where it is well developed sericites are recrystallized offsetting quartz vein (center). Xpl. E-0524603, N-153065,

(E) Highy deformed zone of greenish gray slate in the variegated slate. The host rock and quartz veins show recumbent type fold. Most of the hinge zones of the slate are affected by approximately east- west joints. E-0524732, N-1530734.

(F) In this specimen abundant brown minerals (25%) are subidiomorphic. The foliation on the matrix is continuous through these minerals with out deflection or rotation. Most of the crenulations with the fold axis perpendicular to the main foliation are seen on the margins of the brown minerals which act as starin barrier. Sericites are almost grown to muscovites with various colors (blue, yellowish and purple) on diverse position of the thin section. 4x, Xpl. E-0524773, N-15316693.

3.3 Metavolcanic Unit

It is dark greenish and distinctive from others by forming hills. Going along strike of the metavolcanic bed it changes from weakly to less foliated but generally it is weakly foliated unit (Fig. 3.4A). It has an approximate thickness of ~310 m. Bedding defined by compositional variation is visible (Fig. 3.4B).

Modal composition of this rock shows 40% plagioclase, 30% chlorite, 10% k-feldspar, 10% brown alteration (mafic remains?), 5% quartz, with calcite veins and opaques. Another thin section shows less altered calcite minerals as larger grains (after plagioclase?) in the matrix of fine grained authigenic minerals. It is composed of 30% chlorite, 25% opaque, 23% muscovite/sericites, 10% quartz, 10% calcite with remnant feldspars and mafics (Fig. 3.4C).

Texturally, weak foliation is defined by elongation of calcite and opaque minerals (Fig. 3.4D). Muscovite minerals are only noticeable at 40x magnification. High concentration of these muscovite flakes forming some shapes is implication of pseudomorph after feldspars. High amount of chlorite and xenoblastic opaque minerals also suggests high abundance of mafic minerals in the protolith. Random distribution of opaque minerals through the whole thin section indicates results of chemical reaction of primary minerals instead of association with veining.

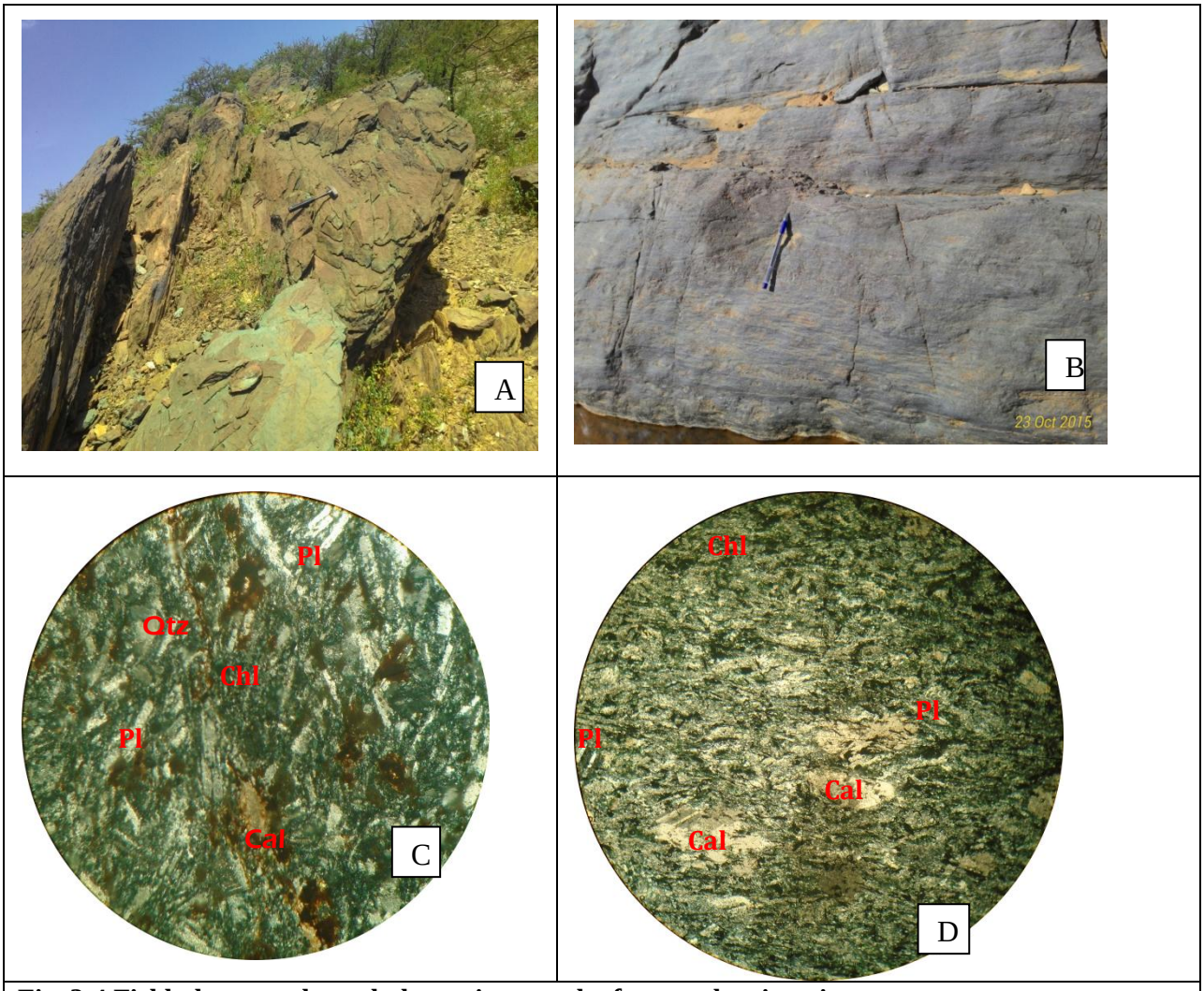

Fig. 3-4 Field photographs and photomicrograph of metavolcanic unit.

(A) Metavolcanic exposed in variegated slate interbedded with slates. On the bottom right a foliated part of the massive block is seen along same strike. E- 0524864, N-1530560,

(B) Bedding in metavolcanic defined by alternating colors of compositional difference. E-0524396, N-1530713,

(C) Abundant elongated minerals with first order gray are the plagioclases. A closer looking at these minerals show alteration to micas. Unlike felsic minerals the mafic minerals are completely altered to chlorite as shown by blue black color of the groundmass. Calcite at the center is vein filling associated with quartz grains showing deformation. Xpl, 10x. E-0524294, N-1530107,

(D) The porphyroclasts are stretched defining a foliation. Protolith plagioclase's polysynthetic twinning showing high order birefringence might be due to alteration to calcite. The plagioclases are more altered than in plate C. Xpl, 10x. E-0524385, N-1530797.

3.4 Spotty Phyllite Unit

This unit is different from phyllitic rocks exposed in other areas due to its lack of crenulation lineation and the abundance of subidioblastic to xenoblastic brown minerals. It exhibits a gray shiny surface and has an estimated thickness of ~210 m. The brown minerals are weathered and holes preserving their shape are abundant on surface of the rock. Size of these minerals varies from microscopic up to 3cm. Their orientation is random on the rock and didn't show any relation with foliation (Fig. 3.5A).

It is composed of 70% muscovite/sericite, 20% quartz/k-feldspar and 10% pyrite mineral. Most of the quartz rich domains are not continuous as the muscovite domains. The main foliation is overgrown by pyrite minerals indicating that it grew relatively late with respect to foliation formation. Nevertheless some of those pyrites which grow on the quartz rich domain show a fibrous fringe structure parallel to main foliation (Fig. 3.5B). This can be explained as last part of the deformation which creates the main foliation postdates pyrite growth; the random orientation of these porphyroblasts might be due to very late growth. Slight bending of foliation near pyrites may be due to the deformation responsible for crenulation.

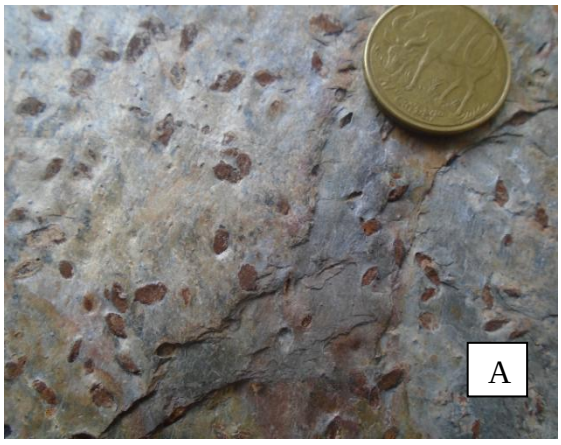

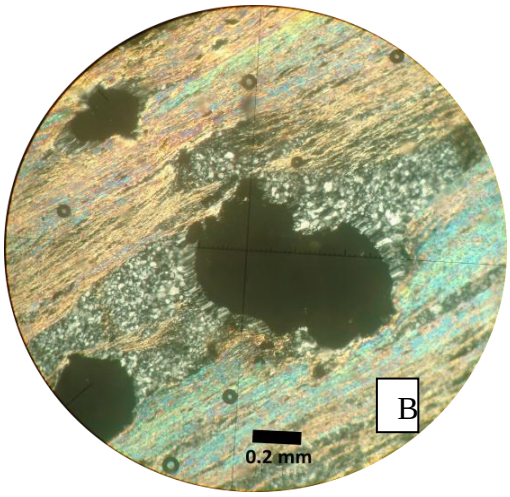

Fig. 3-5 Field photographs and photomicrograph of spotty phyllite unit.

(A) Abundant elliptical pyrites giving it spotty appearance. These minerals are randomly oriented and weathered. Seen also are holes near the coin and filled by secondary materials on the central left. E- 0524699, N-1531490.

(B) Muscovites with varying interference colors define the phyllitic cleavage. Xenoblastic pyrite growing in quartz rich domain exhibits fibrous quartz fringes on both sides parallel to the foliation.

There is no deflection of foliation around the pyrite rather is pushed by the fibrous quartz. From the same location as outcrop photo, xpl.

3.5 Metalimestone Unit

This unit lies conformably over spotty phyllite. Both ribbonite and grainstone limestone with black color is found. On the lower part it starts with distinct beds of limestone, less than 0.5m, interbedded with slates. Upper half of this metalimestone unit has calcareous metavolcanic beds and is intermingled with highly calcareous slates which react readily with HCl. These slates become dominant and phyllitic towards the upper part of the unit. It has a thickness of about ~700 m. Few fully recrystallized beds are seen during section measurement and sampling for the carbon isotope analysis. Smaller folds of different wavelength on quartz veins filling metalimestones and metalimestone beds itself decorate the lithology (Fig. 3.6A).

Most of the grains from lower limestone are less than 0.05mm with some sparse grains 0.1mm long. It shows a foliation by elongation of calcite minerals. Syntaxial veins cutting the foliation at about 45^0 are observed (Fig. 3.6B, Section 4.2.2E). On average it consists of 95% calcite and 4% quartz and minor fine opaque minerals.

The completely recrystallized sample consists of numerous coarse calcite minerals of 5mm long. Microstylolites are common with remnants of quartz, micas and small dark minerals (Section 4.2.2B).

On the northwestern part of the study area there is an eighty two meter thick black metalimestone grainstone and ribbonite just above the psammites unit. Averagely 2m thick pure metalimestone is interbedded continuously with thin beds of slate (Fig. 3.6C). Unlike the lower metalimestone where there are abundant slate rocks enclosed in a metalimestone rock i.e. intermingled, the upper one has distinct beds of metalimestone alternating with beds of slate. This metalimestone exposure is not continuous throughout the study area but continuous outside the study area (see the geological map). The thickness decreases to the direction where it ends. Fresh cubic to rectangular shaped brown minerals (pyrites?) are abundant which are unusual in the lower metalimestone.

Under the microscope it shows more pronounced foliation compared with the lower metalimestone. It consists of 98% calcite with trace amounts of black impurities, quartz and brown minerals. The brown minerals post date the main foliation (Fig. 3.6D).

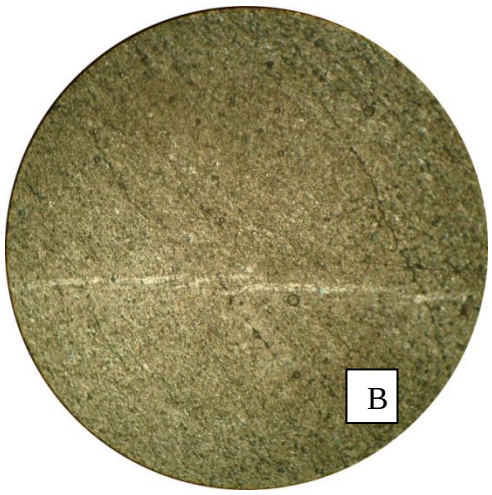

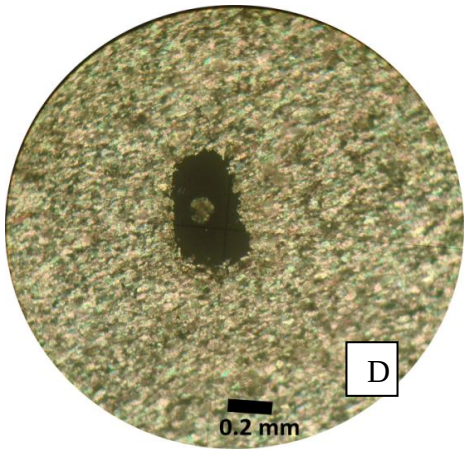

Fig. 3-6 Field photographs and photomicrograph of metalimestone unit

(A) Metalimestone unit with a sub horizontal plunging fold of metagraywacke passing through the center. Black fresh surface is seen on the lower part of the photo. The Overlapped photo shows this fresher surface due to abrasion from the stream. E-0524187, N-1531389,

(B) Fine grained texture of metalimestone, defining a foliation running from top left to bottom right. Gray brighter minerals scatterd through out are quartz. Brighter enchelon looking vein with coarser calcite grains than the matrix (syntaxial veins) cuts the foliation at about 45^0. Black lines parallel to the foliation are due to dissolution effect, stylolites. 4x, xpl. E-0523202, N- 1529931,

(C) Exposure of two meter thick limestone unit. It is limestone ribbonite with white calcite veins. Gray colors to the right (base of the limestone bed) are interbedding of slate where trees grow. E-0521965, N-1533250,

(D) Foliation is prominent than lower limestone. Calcites also show higher birefringence. The brown subidiomorphic mineral postdates foliation. Xpl. E-0521965, N- 1533241.

3.6 Slate Unit

Two compositionally different units are described under the slate unit.

3.6.1 Graphite Slate

Graphite slate has a fresh black color and a whitish weathered surface due to oxidation of carbon (Fig. 3.7A). This suggests a source of organic rich sedimentary rock such as shale. Tiny shiny minerals are seen in the black background. It is underlain by a phyllite unit at the top of metalimestone and overlain by the ridge of sericite slate unit. It is about 160m thick.

This unit is composed of 40% graphite, 40% sericites and 20% quartz/k-feldspar ground mass. Maximum dimension of quartz minerals is 0.1mm. Graphites do not have a particular shape, it flows parallel to the foliation. Fringe structures of 0.1mm long show bends on both sides of a host mineral which is half smaller in size (Fig. 3.7B). The bends are interpreted to result from changes in orientation of instantaneous stretching axes (ISA) with respect to fabric in the wall rock (Passchier and Trouw, 2005).

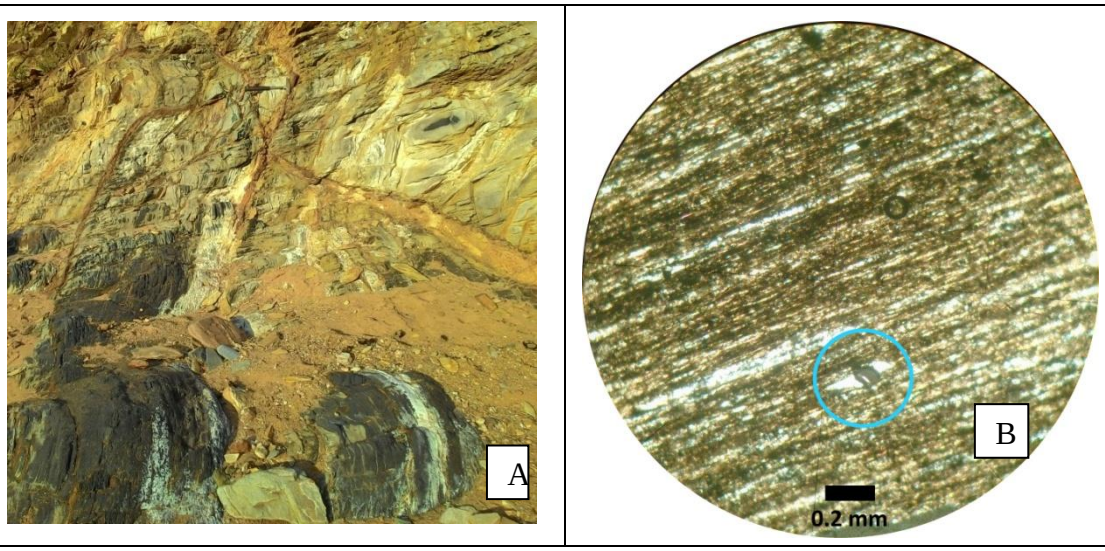

Fig. 3-7 Field photographs and photomicrograph of graphite slate unit

(A) Graphite slate showing a weathered gray surface and fresh dark in the vicinity of the flowing river,

(B) Bedding parallel foliation is defined by sericites, graphite and elongated quartzes. In the circle is fringe structure developed on two sides of central mineral and show S- shaped spiral (dextral shear sense). Xpl. E- 0523741, N- 1532472.

3.6.2 Sericite slate

At its base it forms a large ridge with brown weathered surface (Fig. 3.8C). Its fresh surface is blackish gray to greenish gray (Fig. 3.8A). Small idiomorphic crystals of pyrite are widespread. This large ridge is foliated but not as variegated slate. This unit is remarkably

covered by *'kitkta'* shrubs in all traverses. The area between ridge of the slate and metalimestone below, which is about 260m thick, is covered by graphite slate and phyllite. Up stratigraphy small 3cm thick folded limestone beds are interbedded with spotty slates and phyllites. These and other units far to west, mapped as slate and phyllite unit, make a relatively flat topography compared to the ridge below it. It has an estimated thickness of ~415 m.

In thin-section the slate is composed 65% sericite and 35% quartz/k-feldspar ground mass and porphyroclasts. Sparsely distributed are mantled and fractured porphyroclasts of quartz and feldspar of up to 0.6 mm developed in to sigma type shear sense indicator (Fig.3.8B). Feldspars are identified because of alteration by the micas. All these clasts show a sinistral shear sense (Fig.3.8B). Orientation of the fracture and overall shape of the mantled aggregate shows opposite shear sense. However the fragment geometry not only depends on bulk shear sense but also on initial orientation of microfaults in grains, which may be partly controlled by crystallographic directions in the porphyroclasts, flow type and original grain shape. As a result their use as shear sense markers is relatively unreliable (Passchier and Trouw, 2005).

The other thin section consists of 50% sericite, 25% graphite, 10% pyrite and 15% quartz/ k-feldspar groundmass. Foliation which predates the idiomorphic pyrite minerals makes 5^0 angles with bedding (Fig. 3.8D).

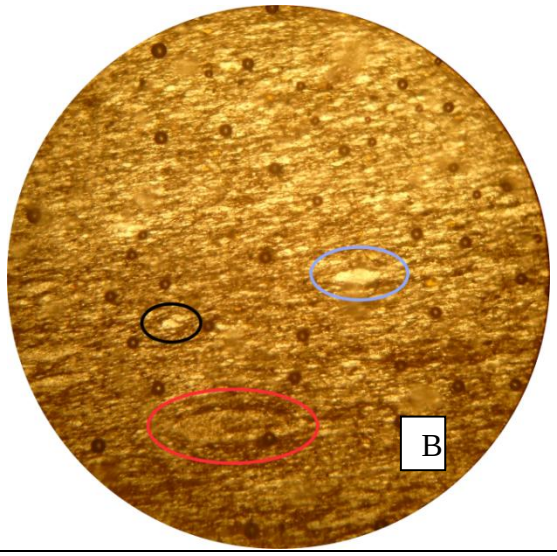

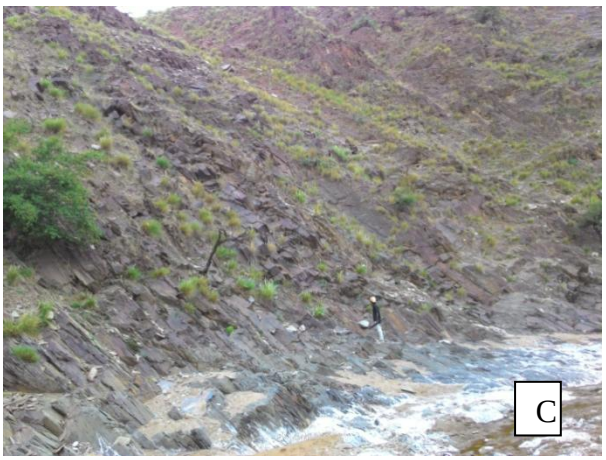

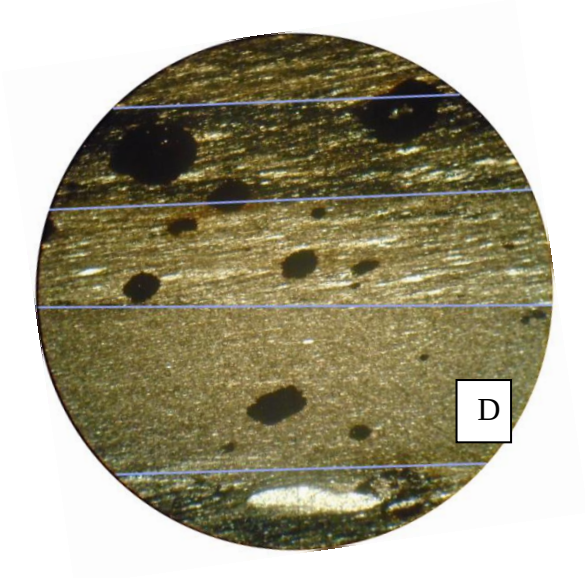

Fig. 3-8 Field photographs and photomicrograph of sericite slate unit.

(A) Less foliated, steeply dipping slate unit. E-0521313, N-1529036,

(B) Fine grained sericite and stretched quartz/feldspar grains define slaty cleavage. Surrounded by the top two ellipses are mantled porphyroclasts which are less altered, might be quartz. Clast in the dark ellipse is fragmented. Lower larger porphyroclast is altered to sericite but preserve a specific shape, pseudomorph after feldspar. 10x, Xpl. E-0521313, N-1529036,

(C) Partial view of the ridge. Brown weathered surface on top is seen changing to the fresh gray color on the river bed. White covers on the river are powders from limestone unit. Photograph taken facing south. E- 0523746, N-1532678.

(D) Primary bedding outlined by the sky blue lines makes a 5^0 angle to foliation as clearly seen on the central lamella by elongated quartz minerals. Idiomorphic pyrites simply rests on the foliation but the longest dimension of most of the black grains seems to have been aligned parallel to the foliation, which is due to late growth stage of the pyrites relative to the foliation. Elongated mantled porphyroclast on the bottom end shows a sinistral shear sense. Xpl, 4x. E-0523746, N-1532678.

3.7 Slate and Phyllite Unit

Slate unit lithologic characteristics changes when intercalation of different rock unit starts to appear above it. These lithologies are spotty slate, phyllite, metasubintrusive, psammites, metalimestone and silty slate as described below:

3.7.1 Spotty Slate and Phyllite

These units are well exposed on south western side of the study area next to ridge of upper slate. It is about ~600m thick. Spotty slate has abundant weathered brown minerals on its surface giving it mottled appearance (Fig.3.9A). Phyllite on the other hand owns shiny

surface and cleaves readily along the phyllitic cleavage. Structures such as kink bands and different types of folds are seen on this rock unit (Fig. 3.9C).

Under the microscope the spotty slate has porphyroclasts as well as porphyroblasts. Sericites curl around porphyroclasts in an anastomosing manner. Porphyroclasts are overgrown by small quartz and sericite minerals showing beard structure (Fig. 3.9B, see also section 4.2.2D). The porphyroblasts are xenoblastic in shape and postdate the main foliation.

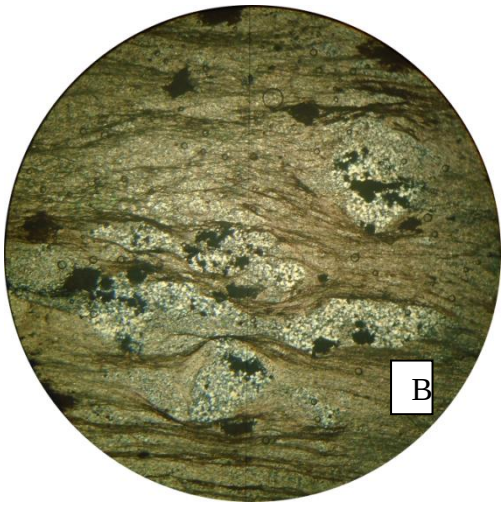

Fig. 3-9 Field photographs and photomicrograph of spotty slate and phyllite unit

(A) Spotty slate on which weathered brown minerals gives it mottled appearance. E- 0521543, N- 1530126.

(B) Sericites become coarser and colored (muscovites). The rock is grading to phyllite. Anastomosing of micas is seen around quartz rich patches. 4x, Xpl. E-0520669, N- 1529927.

(C) Phyllite unit with asymmetric kink bands on its shiny surface. Kink bands are curved. E-0520710, N- 1530271.

3.7.2 Metasubvolcanic unit

Intercalated with the slates and phyllite is metasubvolcanic unit. It occurs as ridges parallel to the regional strike, perhaps sills. The ridges have thickness varying from 1m to 5m (Fig. 3.10A). Perfectly cube shaped pyrite minerals of up to 0.04cm^2, which can be picked by hand are scattered on this rock. High density in some part of the rock is due to veinlets.

Petrographic studies show that it is composed of 45% chlorites, 35% calcite, 10% iron patches, 3% k-feldspar, 3% quartz, 3% amphibole/pyroxene and trace amount of opaque. As

in the metavolcanic rocks chlorite minerals are products of alteration of the mafic minerals (Fig. 3.10B). Interesting ferruginous residual septa which are cleavages of amphiboles and pyroxenes are seen in some incomplete reactions where chlorites are available (Fig. 3.10C). Brown aggregates of these residual materials are primary iron of detrital minerals. In addition to the larger grains of shaped calcite, xenoblastic altered calcites with inclusions are abundant. Approximately perpendicular and oblique relationship of these septa matches with cleavage directions of pyroxenes and amphiboles respectively. Except the brownish patches/aggregates all minerals have a size of greater than 0.5mm, and some elongated feldspars reaching up to 3mm.

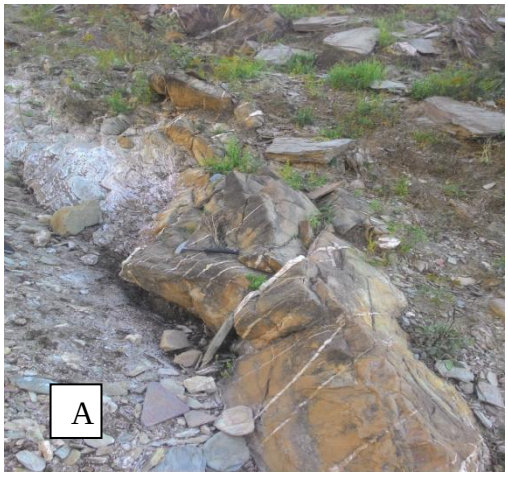

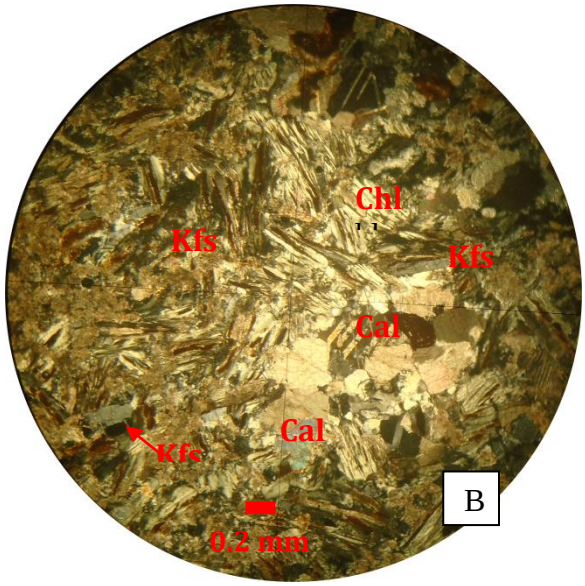

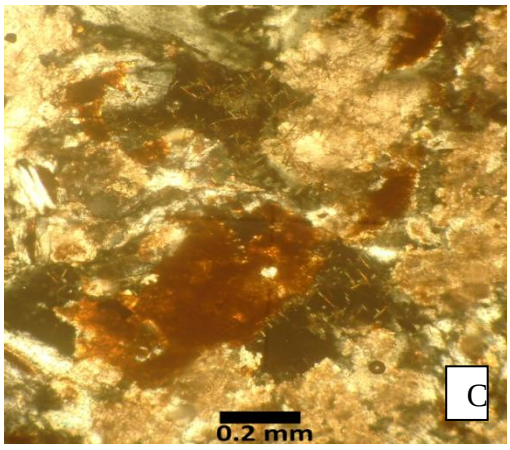

Fig. 3-10 Field photographs and photomicrograph of metasubvolcanic unit

(A) Metasubvolcanic layer which is parallel to main foliation. It is affected by quartz veins with average trend perpendicular to the main foliation. Cubic pyrite minerals are found in it. E-0520855, N-1530465.

(B) Abundant chlorites are after ferromagnesian minerals. Brown patches surrounding the chlorites are iron residuals from the reaction. Elongated feldspars are seen cutting the chlorites. Xpl. E-0522678, N-1532093.

(C) Ferriginous septa and brown patches are iron left from parent mineral. In this case the septa are perpendicular implying pyroxene parent minerals. chlorites are formed on the top center. The sugary (gray brown) material is altered calcite which covers the whole thin section in fine grained cloud as the brown residual. Xpl. E-0522678, N-1532093.

3.7.3 Psammites

This unit is differentiated from the pelites because it shows weak foliation and fine sand size texture. It has greenish gray color and is affected by abundant non systematic joints (Fig. 3.11A). It is about 200m thick. Conformably laying above the psammite unit are two lithological units, the eighty two meter metalimestone and graphite slate. This is possible because the metalimestone is not continuous throughout. But the graphite slate continues above the metalimestone.

It comprises 50% quartz, 30% k-feldspars, 15% sericites growing to muscovite, 3% plagioclase and 2% opaque. Although there are finer-grained, most of the quartz and feldspar minerals grain size is in between 0.1 to 0.2mm. This is in the range of fine to very fine sand. Weak foliation is defined typically by the elongated quartz and feldspars and the general trend of sericites. Sericites follow contacts between quartz i.e. didn't get space to become parallel and define the foliation on their own. There are also some muscovites partly replacing larger k-feldspar grains (Fig. 3.11B).

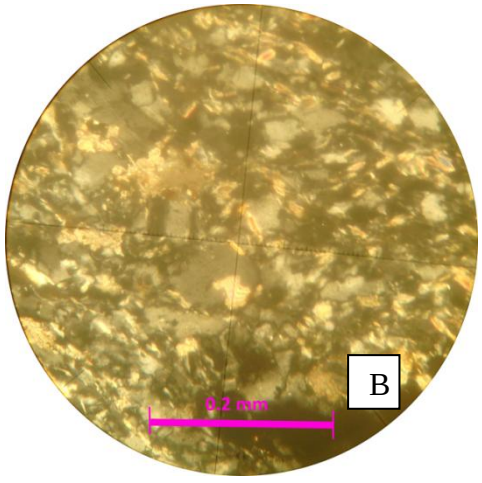

Fig. 3-11 Field photographs and photomicrograph of psammite

(A) Exposure of psammites taken facing east. It shows weak foliation which cannot be readily seen but breaks along foliation. Numerous non systematic joints are seen on the surface. E- 0522138, N- 1532748.

(B) A k-feldspar grain is partially replaced by muscovite (center). Micas together with the stretched sands define weak foliation.

3.7.4 Silty Slate Unit

This unit covers extensive area to the west of the study area. It shows greenish gray color as the psammites but no grains are seen using naked eye. Sporadically kink bands are encountered although not extensive as in the phyllites (Fig. 3.12A). It has an estimated thickness of ~1433 m.

It has same mineralogical composition as the sericite slate unit. Fine grained sericite minerals and elongated quartz/feldspars define slaty cleavage. Grain size of the granular quartz mineral in one sample is greater than or equal to 0.05mm which categorizes it in the coarse silt to very fine sand class. Foliation makes 2^0 angles with bedding (Fig. 3.12B). During rotating the stage a specific shape becomes dark but is completely overgrown by sericites which might be protolith feldspar grain. Curved kink bands are also visible in the thin-section (Fig. 3.12C).

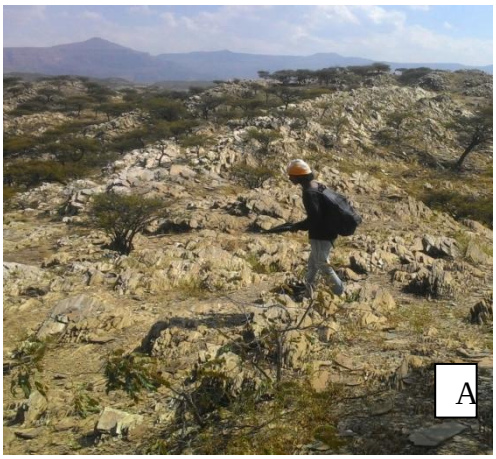

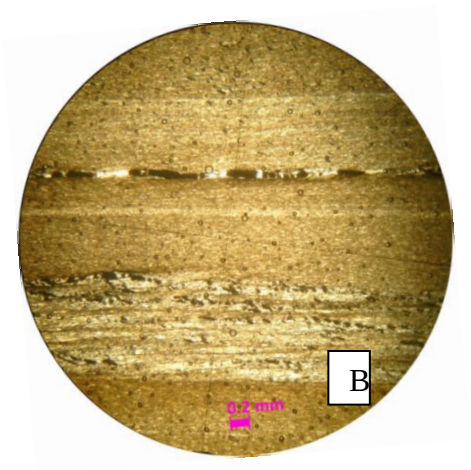

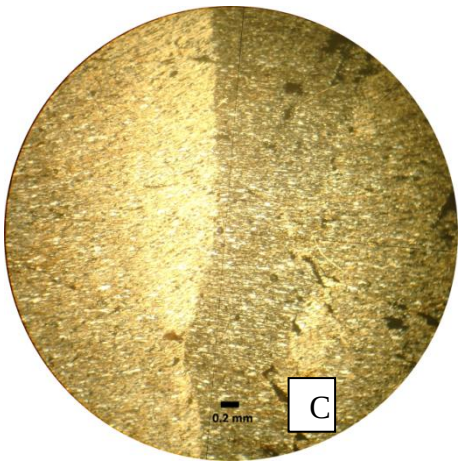

Fig. 3-12 Field photographs and photomicrograph of silty slate unit

(A) An open view of silty slate unit taken facing east. E-1520690, N- 1532665,

(B) Distinct bedding by alternating mica rich and poor zones at an angle to foliation. Laminae are almost equally thick (1.5mm). Xpl. E-1520690, N-1532665,

(C) Most of the quartz minerals are elongated. Granular quartzes are greater than or equal to 0.05mm in size, elongated ones are longer. This classifies them to be at least coarse silt. Curved kink band is perpendicular to foliation. Xpl. E-0521557, N-1533058.

3.8 Aplitic Dyke

It has sharp contact with the country rocks and occurs towards the top part of the variegated slate and within the pebbly sandstone unit. Each is 2m thick with massive structure. At outcrop level foliation of the country rock is deflected against the dike (Fig. 3.13A). This leads to the verdict that it could be syntectonic- intertectonic instead of pretectonic. It lacks foliation but the rather weathered nature and alterations seen in the thin section are not characteristics of post tectonic granites around the study area (e.g. Asrat et al., 2004). In both cases there is no distinct contact metamorphism on the host rocks.

Under the microscope, half and half is composed of coarse matrix and finer grained groundmass. Coarse grains are quartz and plagioclase with a size of up to 4mm long. Indenting grain contact of these coarse grains is abundant due to diffusion mass transfer via solution (see also section 4.2.2C). This indentation contact gives plagioclase minerals a microcline appearance. Both coarse and relatively finer grains of plagioclase show sieve texture due to sericitization which grow to muscovite for the most part (Fig. 3.13B). The modal composition of these intrusive rocks is 25% plagioclase, 20% quartz, 10% sericite/muscovite and 45% ground mass of quartz and feldspar. It doesn't show foliation. Deformed quartz grains with undulose extinction and mica minerals development testify that it is not post tectonic. It is anticipated that sulphide and quartz vein mineralization have occurred in association with these dikes since these minerals are late tectonic in age.

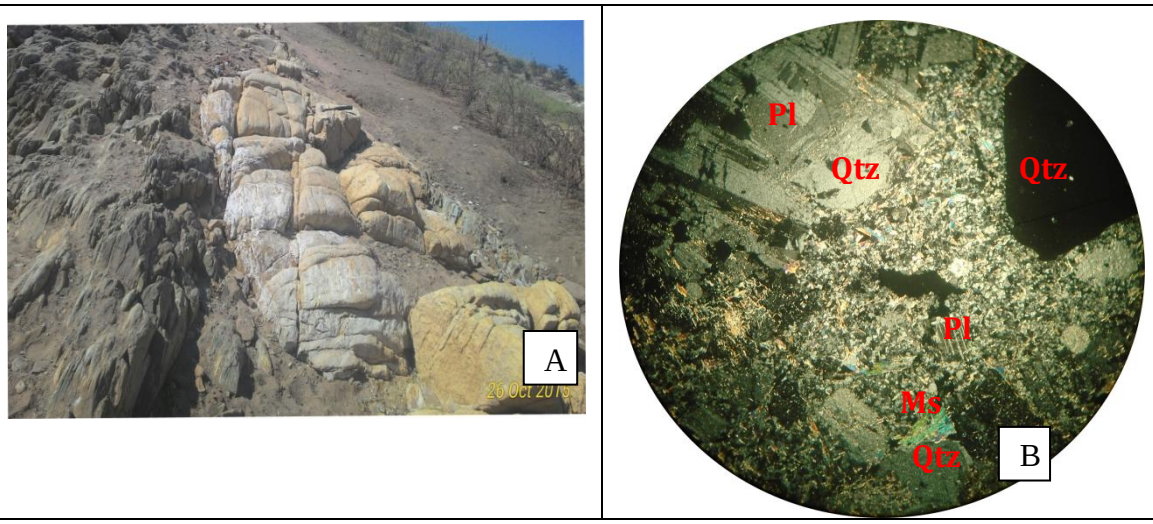

Fig. 3-13 Field photographs and photomicrograph of aplitic dikes

(A) Aplitic dike truncating NNE-SSW running foliation. On the right side of the intrusion is a small outcrop of country rock with a deflected foliation which indicates syn-intertectonic character of the dike. E- 0522590, N-1528995.

(B) Larger grains of plagioclase and quartz are seen on a relatively finer grained matrix of quartz and feldspar. It is shown that sericite minerals are overgrowing coarser and finer grained feldspars. 4x, Xpl. E-0522592, N-1528997.

3.9 Pebbly Sandstone

Angular unconformity is visible on its contact with the metamorphic rocks (Fig.3.14A). It is poorly sorted which has large pebbles up to 50cm. The pebbles are sub rounded and includes granite and metavolcanics (Fig. 3.13B). The lithological characteristics correlate it regionally to the glacial part of Ordovician Enticho sandstone which is deposited after Afro-Arabian peneplain (Avigad et al., 2007).

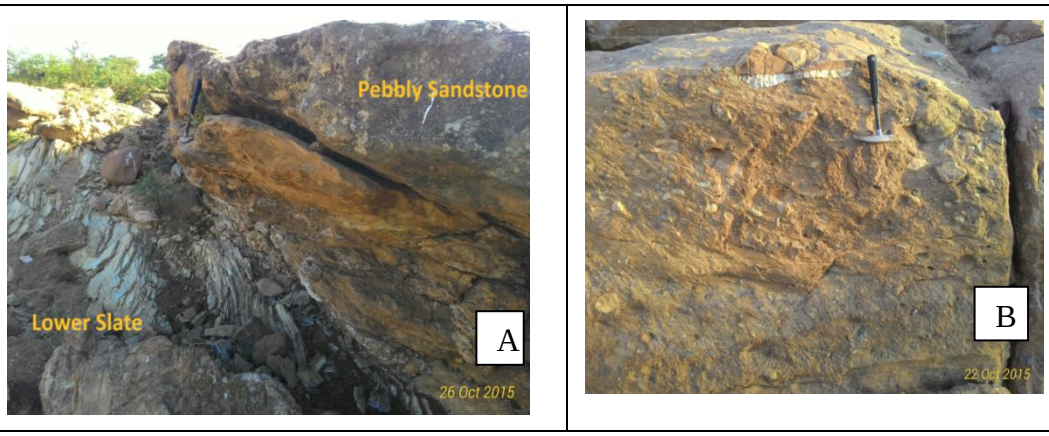

Fig. 3-14 Field photographs and photomicrograph of pebbly sadstone unit

(A) Angular unconformity between lower slate which is the underlying foliated gray unit and pebbly sandstone, the massive jointed upper unit. E- 0524588, N-1529159.

(B) Poorly sorted, compositionally different grain sizes of sub rounded pebbles on the base of the sandstone. Sand supported is deposited above this mud supported debris. E-0524650, N- 1529870

3.10 Quartz vein

It is found cutting all the Precambrian metamorphic rocks. It ranges in thickness from microscopic to as large as 1.5m. Gently plunging in the slate units and steeply plunging in the limestone units are mesoscopic scale asymmetric folds of the quartz veins. Both concordant and discordant types are seen with respect to the regional foliation (Figs 3.15A, B). The microscopic analysis shows that these quartz veins are of different generations from pre to post D2.

Fig. 3-15 Field photographs and photomicrograph of quatz veins.

(A) Concordant quartz vein on slate and phyllite unit. E- 0520819, N-1531746. Superimposed photograph shows a gently plunging folded quartz vein on the limestone unit,

(B) Discordant quartz vein cutting at an angle the spotty slate of variegated slate. E-0524461, N-1531592.

3.11 Gold Mineralization

The extensive quartz veins cutting the Precambrian rocks are known to be the hosts of gold mineralization in the area. This is evident from the mining activities, panning on river sediments by digging to 2m deep well, by the local people in search of placer gold (Fig. 3.16).

Fig. 3-16 Panning for gold in the greenish gray of variegated slate. E- 0524703 N- 1530601.

CHAPTER FOUR

DEFORMATION AND METAMORPHISM

4.1 Introduction

Geological structures at a scale of microscopic to megascopic are recognized on the basement rocks of Koraro-Gelebeda area. These metamorphic rocks have experienced different phases of deformation. Polyphase deformations are observed by superimposed structures one on another such as folded and kinked foliations and crenulation lineations. At least three phases of deformation have occurred which are recognized based on superimposition principle. Foliations produced during the first phase of deformation are folded, kinked and crenulated during another phase of deformation. The youngest structures which are formed due to brittle deformation mechanisms include faults and different types of joints.

Primary structures such as bedding and lamination (Figs. 3.3D, 3.8D, 3.12B) are distinguished by compositional and color variation in the rocks. The deformational structures are classified into ductile, brittle and structures associated with diffusion mass transfer. Here the various deformational structures are described and analyzed as follows.

4.2 Deformational Structures

4.2.1 Ductile Structures

4.2.1.1 Fold

Folding is the most common structure seen on metamorphic rocks of the study area. These folds are of different types including recumbent, upright synclines and anticlines. Majority of the folds have amplitude and wavelength less than a meter. The stereographic plot shows that most of the folds are plunging gently toward NNE (e.g. Fig. 4.1B, C) but few moderately plunging are also found as in Fig. 4.1A.

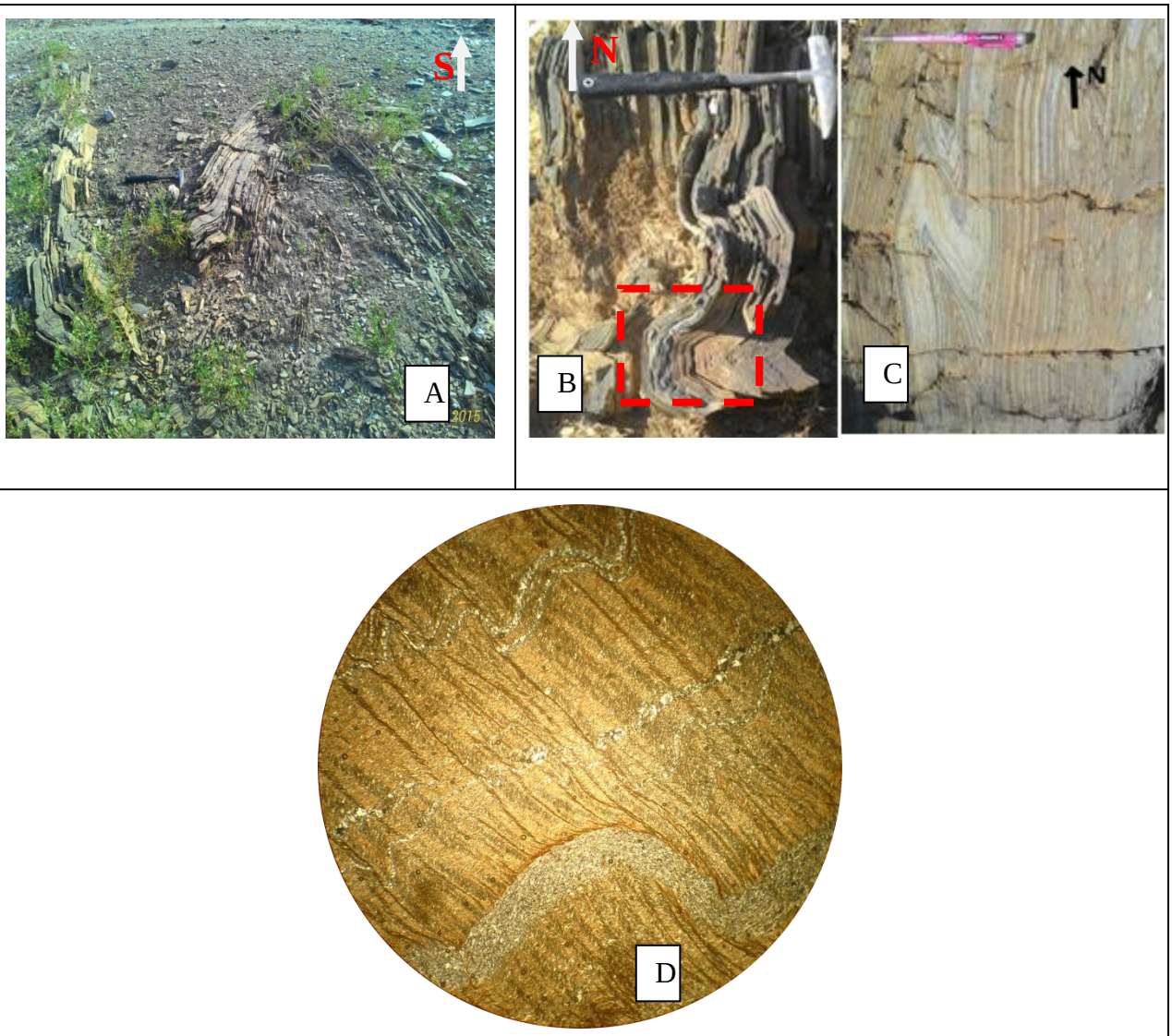

Fig. 4-1 Field photographs and photomicrograph of different folds.

(A) Steeply dipping fold on the limestone unit. Exposed on flat topography (photo taken from almost top view). Fold axis 49/191 at E-0523202, N-1529931,

(B) Box and (C) upright folds in the phyllite rock of phyllite and slate unit. Both have gently plunging axes. E-0520860, N-1530266 (photo taken from side view, facing north)

(D) The bottom half shows folded primary bedding. At least two generations of quartz veins are seen: one folded and the other not so. These quartz veins may be formed by pressure solution which involves dissolution and precipitation of quartz during the development of phyllitic cleavage. This provides evidence for the existence of a metamorphic fluid at these grades. Difference in wavelengths of quartz vein folds from micaceous and quartz rich domains show the dependence of folding on contrast in viscosity and thickness of the layers. Xpl, 4x. E- 0524603, N- 1530657.

4.2.1.2 Foliations and Shear Sense Indicators

All metamorphic rocks in the study area exhibit foliation though the intensity varies. High cleavage of phyllites and slates is largely from alignment of micas although stretched felsic minerals also contribute to the foliation development. In most cases when micas are concentrated the foliation is crenulated. Mean direction of the measured foliations trend 028.6^0. Mantled porphyroclasts and sigma type indicators in the foliation show sinistral sense of deformation (Fig. 4.2).

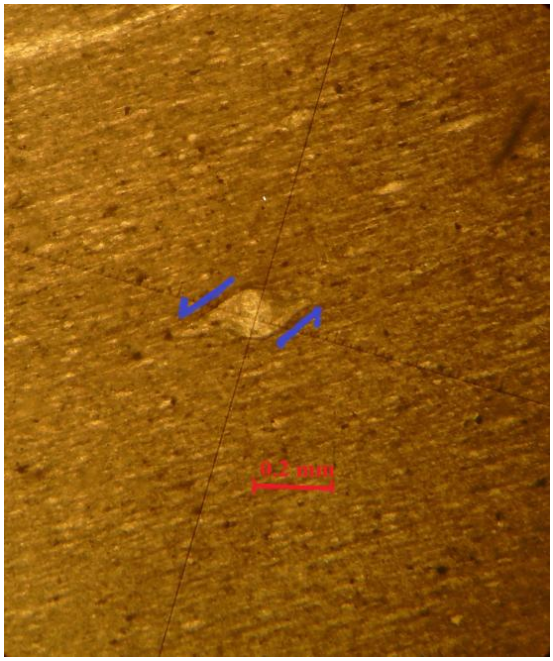

Fig. 4-2 Sigma type shear sense indicator: tails are parallel to foliation and show sinistral sense of deformation during main foliation development. Xpl. E-0524591, N-1529794.

4.2.1.3 Crenulation Cleavage and Lineations

Crenulation lineations are parallel to fold axes of parasitic fold in the sub horizontal folds (D2) (Fig. 4.3A). Fig. 4.3B is a sericitic phyllite showing S_0, S_1 and S_2 on the microscale. The bedding plane (S_0) is defined by the contact between quartz-rich and quartz-poor layers. The phyllitic cleavage (S_1) is sub-parallel to S_0 and is marked by sericite and muscovite. The crenulation cleavage (S_2) defined by sericites is a discrete cleavage which is only seen in the mica rich layers. Since S_2 is formed by layer parallel shortening, it is developed at high angles to S_0 and S_1.

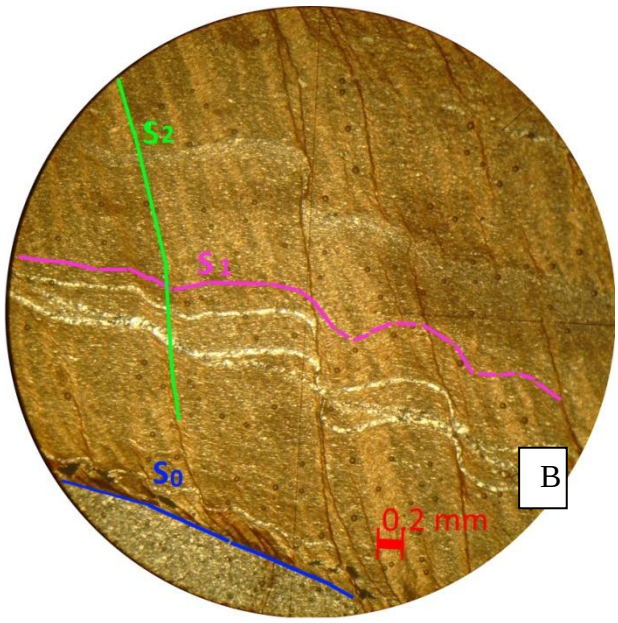

Fig. 4-3 Field photograph and photomicrograph of crenulation lineations and cleavages.

(A) Crenulation lineation parallel to fold axis of small folds (both ends of the scale) with orientation of 32/188 at E- 0523881 N- 1532915,

(B) Bedding denoted as S_0 is shown as compositional variation from mica rich to Qtz/fels rich domain. This is affected by pervasive foliation (S_1). Then later deformation results in folding of the lamella including quartz veins. In addition to folding, crenulation cleavage is formed where the sericites are recrystallized and define S_2 cleavage. Xpl. E-0524603, N-1530657.

4.2.1.4 Kink bands

Kink bands are frequently seen on the phyllitic units. Generally trends parallel to strike of the foliation on which it rests. The kink bands have variable width and are not straight. Two kink bands joining to form one are also seen (Fig. 4.4A). Kink bands are identified in both field and thin section as alternating shiny and dull colors, due to their orientation differences (Fig. 4.4B). Phyllites on the north western part of the study area have to some extent steeper angle.

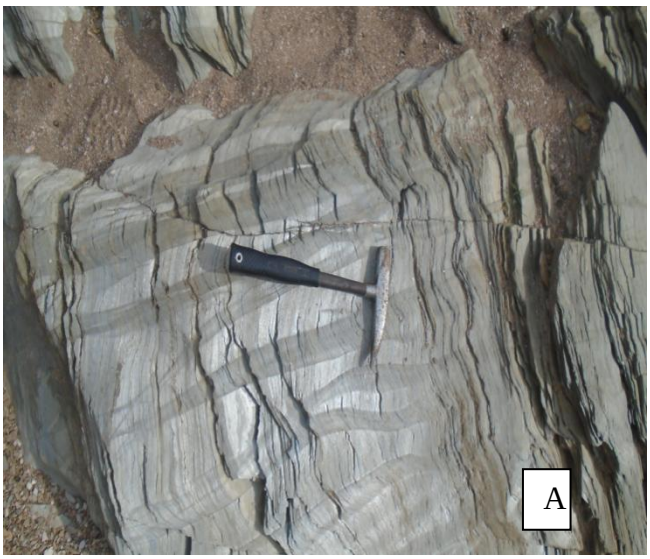

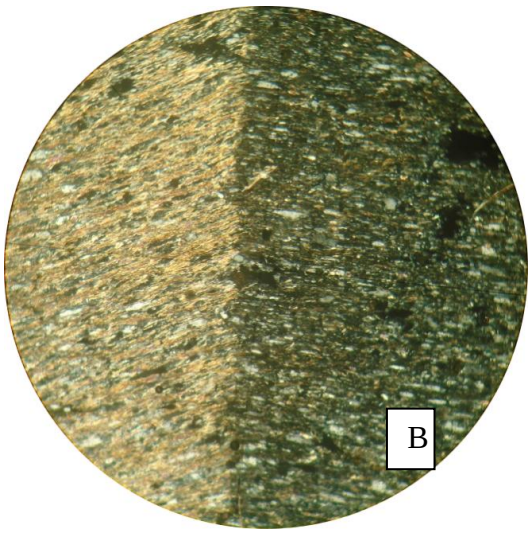

Fig. 4-4 Field photographs and photomicrograph of kink bands.

(A) Kink bands of different width on the phyllite rock. E- 0520710 N-1530271,

(B) Right side at extinction position due to kinking and different orientation from the left side. Xpl, 10x. E-0521557, N-1533058.

4.2.1.5 Shear zones

Outcrop as well as microscopic scale shear zones are seen. On the upper slate is 2.40m thick highly deformed zone rich in quartz veins. Near the contact of the shear zone with the country rock are small folds with crenulation lineation parallel to the fold axis. The remaining large part of the zone looks brecciated since lacks foliation (Fig. 4.5). Collectively they are evidence of deformation by both brittle and ductile mechanisms. The systematic joints in the wall rock are absent in the shear zone since the sheared zone is not stiff enough to show fracturing. Micro shear zone is described in section 4.2.2E. Shear sense indicators on the foliation and shear zones are abundant. These indicators include mantled porphyroclasts including sigma type and sigmoidal veins. Both dextral and sinistral senses are identified from these indicators.

Fig. 4-5 Shear zone on the ridge of slate unit. Systematic joints on the bottom left of the country rock are not observed in the shear zone. E-0523881 N- 1532915.

4.2.1.6 Pencil Structure

According to Davis and Reynolds (1996) pencil structure is a linear structure associated with folded and cleaved mudstones and siltstones. Fossen (2010) rather uses the term pencil cleavage for rocks fracturing in to pencil shaped fragments. Regardless of calling it linear structure for the pencil shaped fragments or exhibiting pencil cleavage for the rock unit, it is a structure formed when a rock unit fractures equally along S_0 and S_1 (Fig. 4.6). This structure is seen on the highly folded zone of slate rock where axial plane cleavage intersects bedding fissility. Small folds shown on the figure are within the core part (no dip) of larger fold.

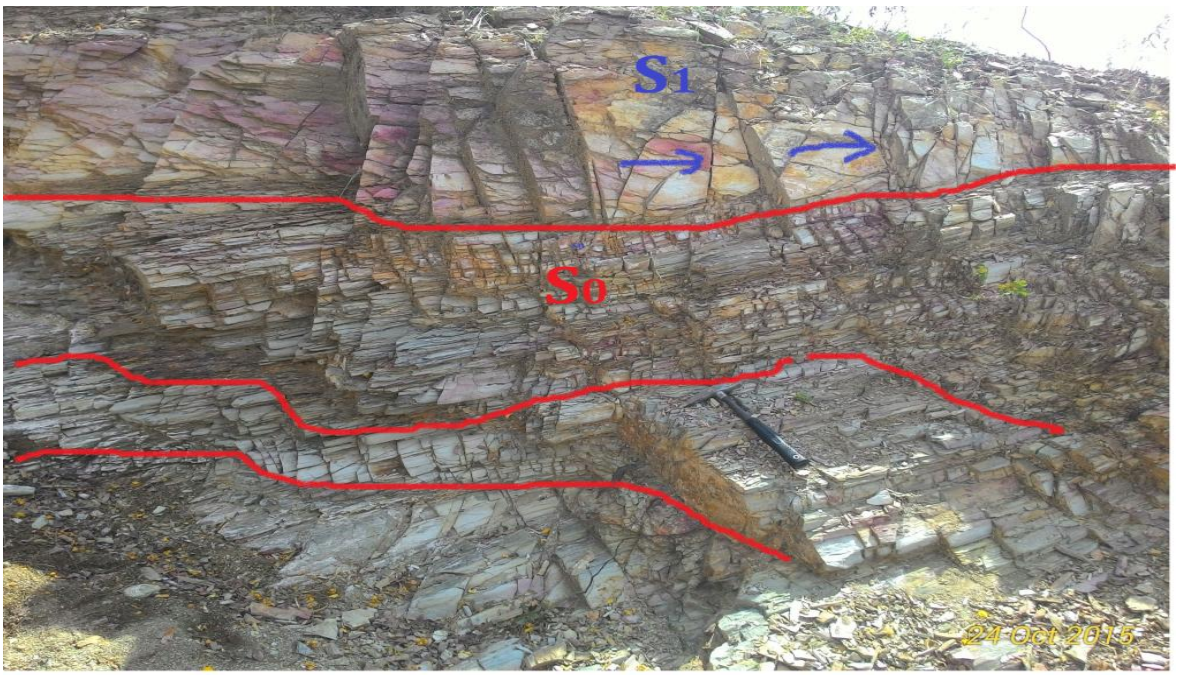

Fig. 4-6 Pencil Structure: pencil like shards, especially on the center of the photo, result from intersection of the two foliations. S_0 represents original fissile bedding with compositional variation shown. S_1 is axial plane cleavage of a larger scale fold and small folds clear on the lower gray bed bounded by red lines. The larger fold is out of sight, core part is only seen. E-0521837 N- 1529871.

4.2.1.7 Boudinage

As shown in the figures below boudinaged limestone and quartz veins are common.

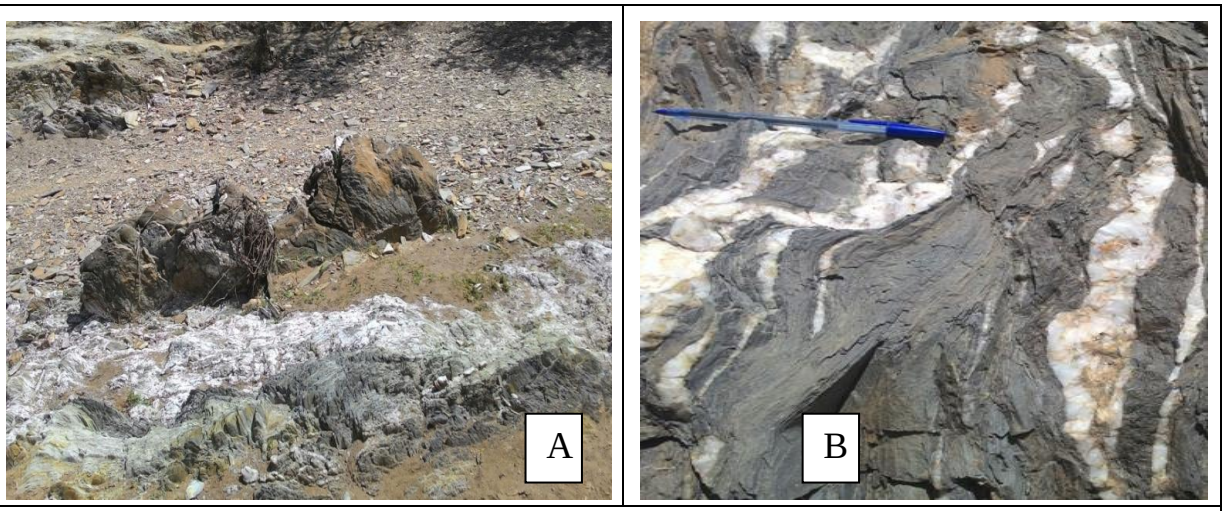

Fig. 4-7 Field photographs of boudins. (A) Limestone boudin (center) in a slate rock exposed in river bed. E-0523359, N-1532044, (B) Quartz vein to the right side shows boudin structure in the limestone host rock. E-0524780, N-1531451.

4.2.2 Diffusion Mass Transfer by Solution

A) Microstylolites

These stress induced solution surfaces are frequent in the metalimestone rock samples. It is distinguished as thin dark lines on the fine grained metalimestone and thicker with coarse residuals on recrystallized samples. Both are Undulating (sinusoidal) surfaces which run almost parallel to foliation. According to Barker (1998) it generally develops perpendicular to principal compressive stress. Boundaries of the large calcite grains are prone to dissolution (Figs. 4.8A, B). The remaining material after dissolution is quartz and dark insoluble residuals.

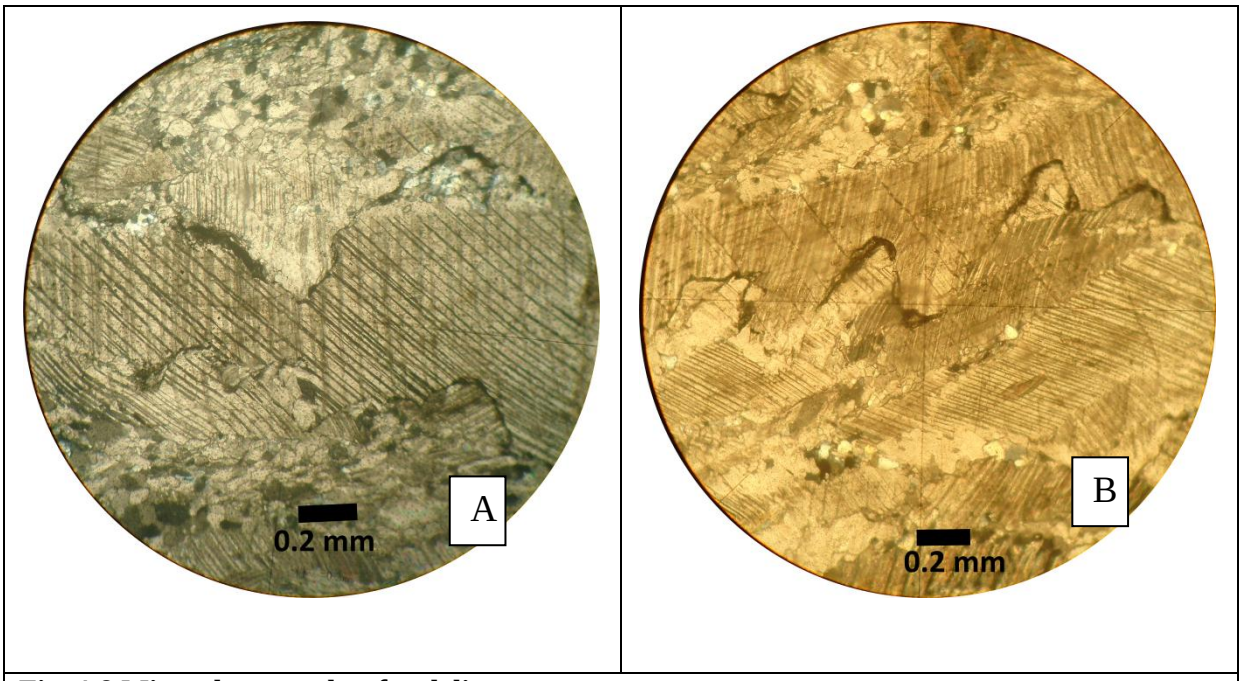

Fig. 4-8 Microphotographs of stylolites.

(A) Microstylolites surrounding calcite minerals. One passing through the center has accumulated quartz grains (central right and left) as residual material. To the bottom is another pressure solution consuming calcite mineral. Xpl,

(B) Sinusoidal microstylolite with fine grained dark residues. A and B from the same sample, E-0523913, N- 1531762. Xpl.

B) Fringe Structure

This structure is formed when increased pressure solution occurs adjacent to a rigid object on the side of shortening instantaneous stretching axes (ISA) and new elongate crystalline material grows on the extensional gashes opened on contact of the object and matrix on the side of extensional instantaneous stretching axes (ISA) (Passchier and Trouw, 2005).

Under the microscope this structure is shown growing adjacent to pyrite minerals. It grows only on two sides of pyrite crystals. The fringes have lengths varying from 50µm-100µm. It grows normal to the faces of the host and parallel to the main foliation (Fig. 4.9). Pyrite minerals growing on the mica rich domain didn't show fringe structure.

Interpretation of the fringe structure

Pyrite minerals post date the first deformation event which results in the formation of regional formation. This is because there is no curling of the foliation around these minerals. Development of the fringe structures on the side of pyrite minerals reveals these minerals have been affected by a deformation phase, since these structures are formed by ductile deformation around rigid objects causing local perturbation of stress and flow pattern. This puts growth stage of the pyrite minerals to be late tectonic during development of the main foliation.

Number of faces on which the fringes grow depends on shape, stress field and fluid pressure (Bons et al., 2012). Undulose extinction exhibited by the fringes might be associated with the deformation resulting in crenulation though not significant in this specimen. Simple fringe geometry i.e. absence of complex shaped fringes suggest coaxial deformation. Pyrites resting in the quartz rich domain are the only showing fringe structure which could be associated with availability of quartz and nucleation site?.

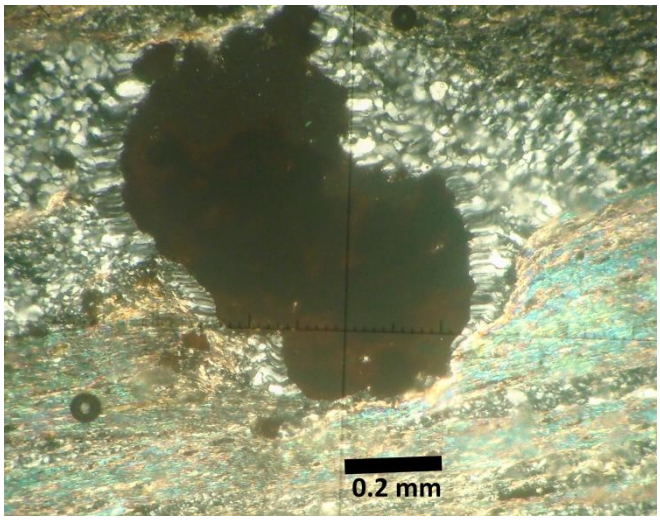

Fig. 4-9 Microphotographs of fringe structures. Fringes grew on both sides of the host mineral parallel to main foliation. It lies on quartz rich domain and the growing fringes tend to push micas. Xpl, E- 0524699, N-1531490.

C) Indenting Grain Contact

According to Blenkinsop (2002), it is generalized that up to amphibolite facies, majority of DMT occurs via solution because solid-state diffusion occurs very slowly at these temperatures. Corroded appearance on the contact of the grains is grain surface textures created by solution (Fig. 4.10). Of the two quartz grains, the grain with smaller radius of curvature typically penetrates into the grain with larger radius of curvature. This creates an indenting grain contact.

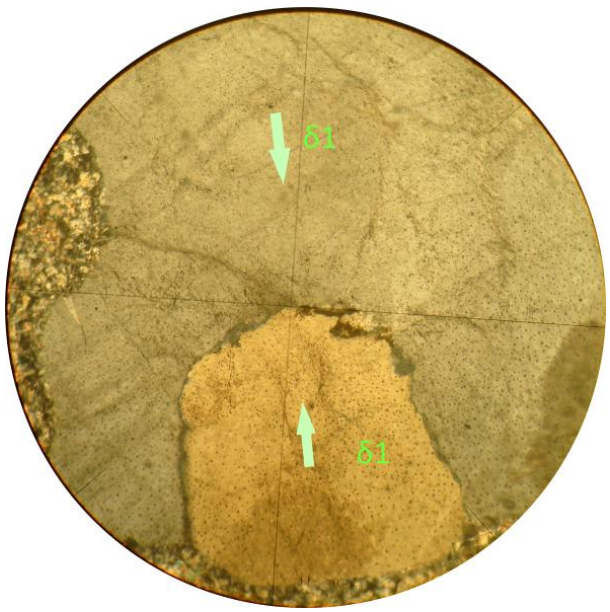

Fig. 4-10 Indenting grain contact: smaller grain of quartz to the bottom indents larger grain of similar composition (quartz).

D) Beard Structure

Beards are roughly triangular intergrowths of mica, chlorite and quartz or feldspar on detrital grains in weakly metamorphosed sedimentary rocks (Pluijm, 1984). A slate sample from slate and phyllite unit shows a cleavage defined by well aligned sericite minerals anastomosing around porphyroclasts producing an augen looking texture as shown in the Fig. 4.11. The porphyroclasts show a shape as if it was a single mineral and rotated to different positions during formation of the main foliation. But now it is overgrown by small granular as well as aligned quartz and sericite minerals. Beard structure is shown by the intergrowth of sericites and quartz on both sides of the clast parallel to the main foliation. There are also alignments at an angle ranging from almost perpendicular to oblique to the foliation.

Fig. 4-11 Microphotograph of beard structure. Aligned sericites anastomosing around the clasts defining slatey cleavage. Shown also is triangular aligned intergrowths of sericite and quartz (beard structure) adjacent to a porphyroclast. 4x, Xpl. E-0520669, N- 1529927

E) Micro vein

A syntaxial and antitaxial type are seen where the calcite mineral fills a vein in metalimestone and brown mineral (sulphide?) on slate unit respectively (Fig. 4.12). In the former case vein filling minerals are not fibrous rather granular. Since growth starts from wall rock it shows optical continuity with wall rock minerals (Fig. 4.12A). The later shows an en echelon tension gashes forming a feather veins. Feather veins are probably formed when a continuous vein grows over a chain of en echelon tension gashes (Passchier and Trouw, 2005). These en echelon tension gashes are generally formed in brittle- ductile shear zones during simple shear. The veins are rotated as deformation progresses and develop sigmoidal shape. 'Z' – shapes twisted tell us dextral shear sense (Fig. 4.12B). The shear zone defined by these veins is at about 30^0 to the main foliation. Instantaneous stretching axes directions are shown in the figure.

The sigma type shear sense indicator (sinistral sense, Fig. 4.2) is also from the same thin section with this one. It can be discussed that during formation of the main foliation sinistral shear sense was prominent. Moreover the en echelon veins reveal later shearing after formation of the main foliation with dextral sense.

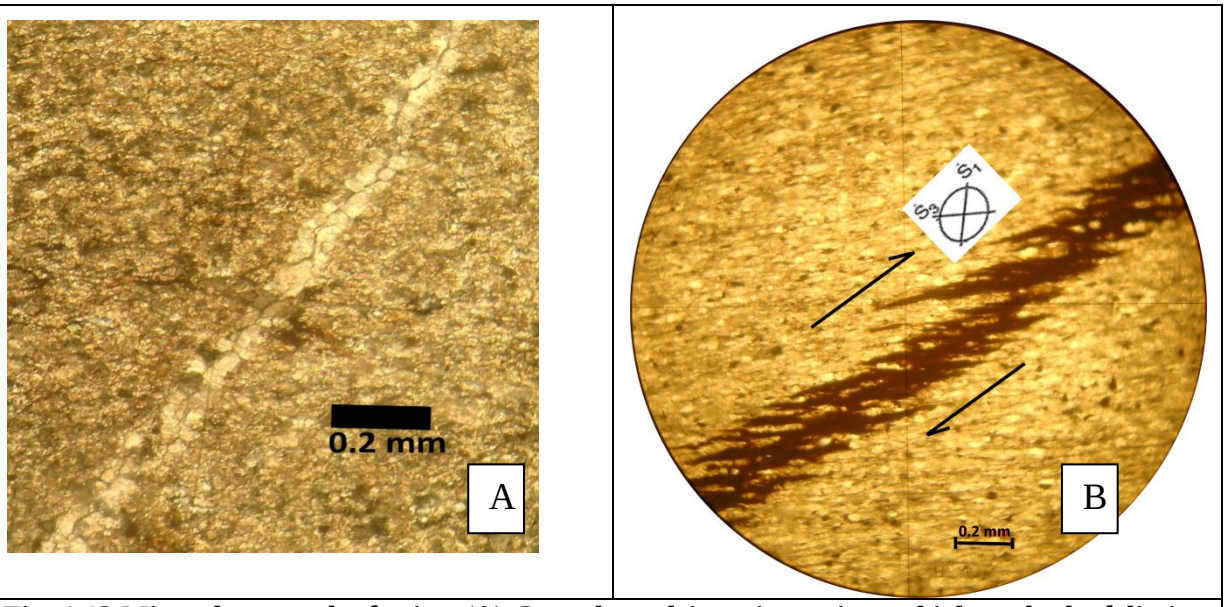

Fig. 4-12 Microphotograph of veins. (A) Granular calcite vein cutting at high angle the foliation defined by the matrix. Grain at the center is at extinct position at the same time with the host rock mineral. Xpl, E- 0523202, N- 1529931. (B) Brittle- ductile shear zones defined by the single set of en echelon- feather veins. Xpl. E-0524591, N-1529794.

4.2.3 Brittle Structures

4.2.3.1 Faults

ENE-WNW trending fault occurs on phyllite unit recognized by the offset in a metagraywacke bed. It is offseted dextrally with a net slip of 1.5m (Fig.4.13).

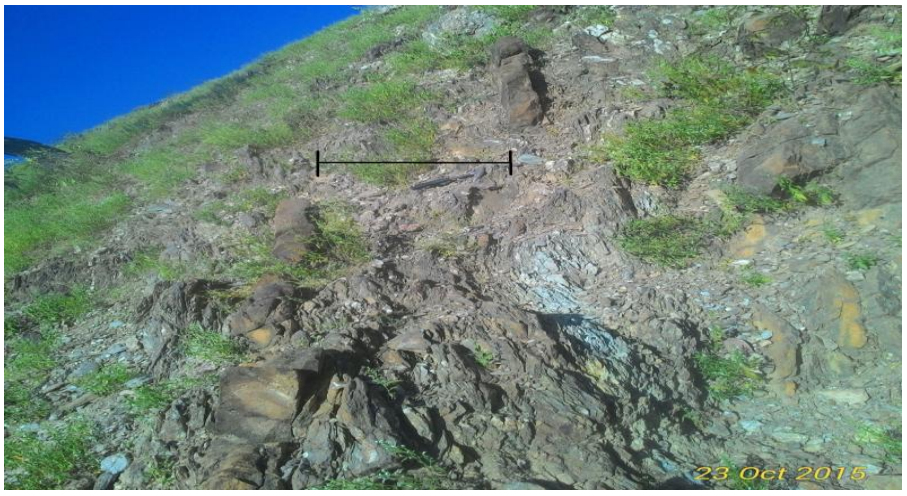

Fig. 4-13 Dextral fault in the spotty phyllite unit. E- 0524392, N- 1531117.

4.2.3.2 Joints

Both systematic and non systematic sets of joints are common in the study area. The non systematic joints are found in all rocks and show different orientations. In most cases are curved which might be due compositional variation. Y and T intersections are common in

these types of joints (Fig. 4.14A). The systematic joints on the other hand are common in the slate rocks and rarely in the metavolcanic. Two sets of perpendicular joints with an average joint spacing of 0.5m are shown in Fig. 4.14B.

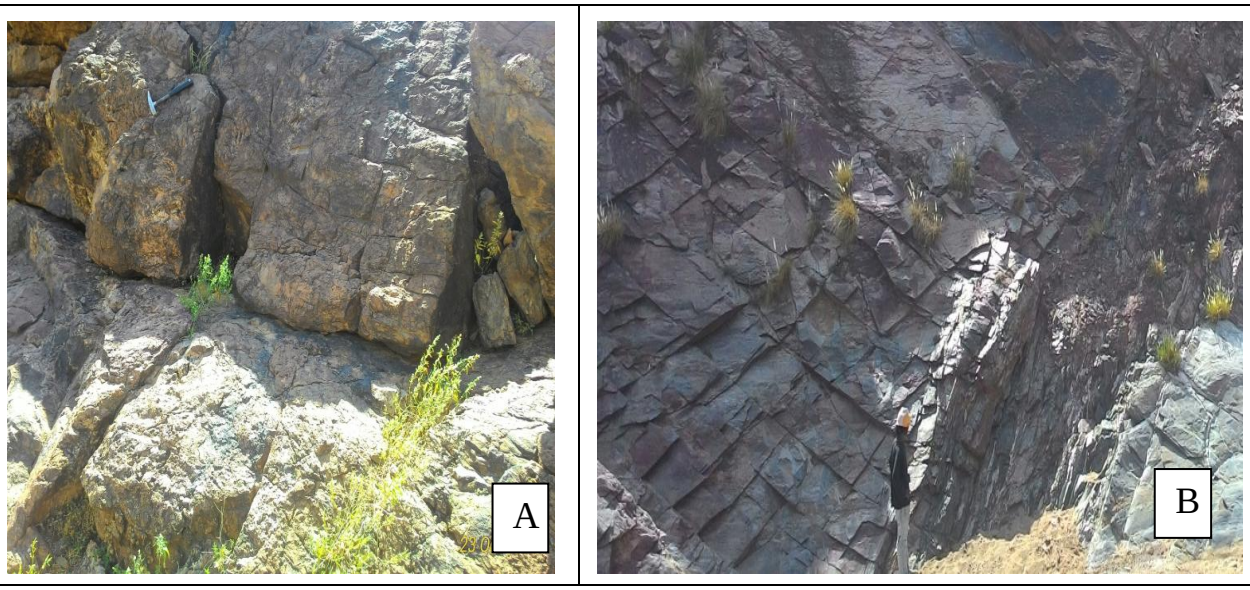

Fig. 4-14 Field photographs of joints. (A) Non systematic joints with irregular joint surface on the metavolcanic, E- 0524513, N-1530650 (B) Perpendicular systematic joints in the slate unit, E- 0523881 N- 1532915.

4.3 Metamorphism

The mineral assemblages and textures i.e. relict minerals, primary bedding, fine grained textures and structures exhibited by the rocks indicate a low to very low grade metamorphism. For instance the pencil structure seen is a fabric developed by superimposition of a tectonic preferred orientation on a bedding parallel fissility at very low grades of metamorphism. The assemblage chlorite-muscovite-quartz of the pelitic rocks is also a typical green schist facies assemblage and defines the chlorite zone. The absence of biotite mineral further classifies it to the lower green schist facies. Although the degree of metamorphism varies, all rocks in the study area are metamorphosed except the sandstone unit. Most of the metamorphic minerals are coeval with D_1 with some simultaneous with D_2 and porphyroblasts which are late-intertectonic between the two deformation phases. The remaining minerals in the assemblage are the relict minerals from the protolith. The mineral assemblages of the lithological units are (critical minerals are in bold):

1. **Variegated slate:**

Sericite + quartz + k-feldspar + **muscovite** ± opaque ± brown secondary mineral (pyrite?)

2. **Metavolcanic:**

Plagioclase + **chlorite** + k-feldspar + mafic residue + quartz ± **muscovite/sericite**

3. Limestone:

Calcite + quartz + opaque ± brown mineral

The petrographic examinations of the limestone units indicate that in contrast to the detrital sedimentary texture of the limestone there are also completely recrystallized samples.

4. Slate Unit:

Sericite + quartz + k-feldspar + pyrite ± opaque

5. Metasubvolcanic

Chlorite + calcite + remnant iron + k-feldspar + quartz ± amphibole /pyroxene

In these rocks the incomplete reactions of the pyroxenes and amphiboles to chlorites is seen.

6. Psammites:

Quartz + k-feldspar + **sericite** + plagioclase + opaque

Muscovite minerals less abundantly seen on the quartz feldspar sink.

7. Silty Slate:

The mineral assemblage of this unit is similar to the slate unit.

8. Aplitic intrusion:

Plagioclase + quartz + k-feldspar + **sericite** + **muscovite**

4.4 Timing of Deformation and Metamorphism

The main foliation (S1) is defined by the orientation of mica minerals and stretching of the other minerals. Micas grow perpendicular to the general strike of the foliations. The extensive metamorphism of the area is during development of the foliation. Then mineralization of some of sulphides and quartz veins happens as revealed from the thin sections. The pyrites overgrow the primary foliation but strain shadows and fringes parallel to the foliation put them to be late tectonic. Some of the brown minerals without the strain shadows and fringes are post the foliation but act as strain barriers during the deformation that result in crenulation of the foliation i.e. intertectonic.

In the rocks of the study area D2 is responsible for the formation of outcrop scale folds with the parasitic folds in it and crenulation cleavage. During this phase of deformation metamorphism is not obvious but few recrystallized sericites define crenulation cleavage (Fig. 4.3B). Crenulation lineations (L2) trend almost parallel to strike of the foliation (S1) as it is shortened in a direction at low angle to the micas.

4.5 Stereographic Projection

In structural analysis it is important to use stereographic projection i.e. plotting attitude measurement on the stereonet independent of their location. This is because bulk measurements are displayed easily and can be placed in a small plot. Fig. 4.15A, below shows stereographic projection of foliations as poles. Poles are preferred to great circles because great circles hold more space and crowd making it difficult to interpret.

In addition to poles, rose diagrams and contours are plotted for further interpretation. In all cases lower hemisphere equal area projection stereonets are used. The two dimensional data represented by rose diagrams of all foliations and lineations measured during the study are generated by azimuth frequency and interpreted.

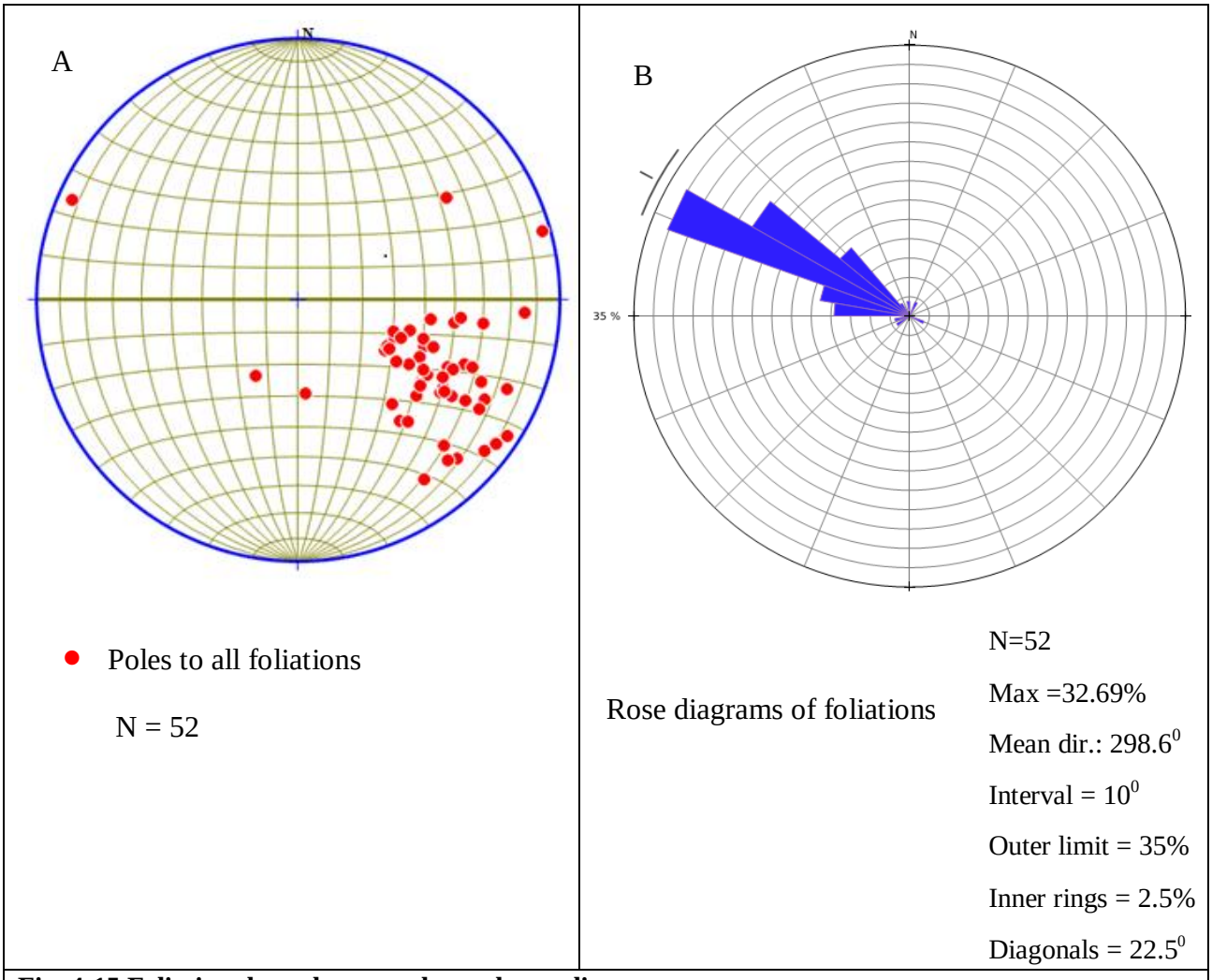

Fig. 4-15 Foliation data plots as poles and rose diagrams

Poles of these foliations which are almost parallel to bedding are clustered on the SE quadrant of the stereonet indicating NW dip. The longest wedge of the rose diagram holds 32.69% of the data. This wedge shows the value between N60^0 - 70^{0}W to be the orientation

with maximum value as shown in Fig. 4.15B. These orientations of highest value go with the regional trend in the area. The other intervals with low values are due to the folds.

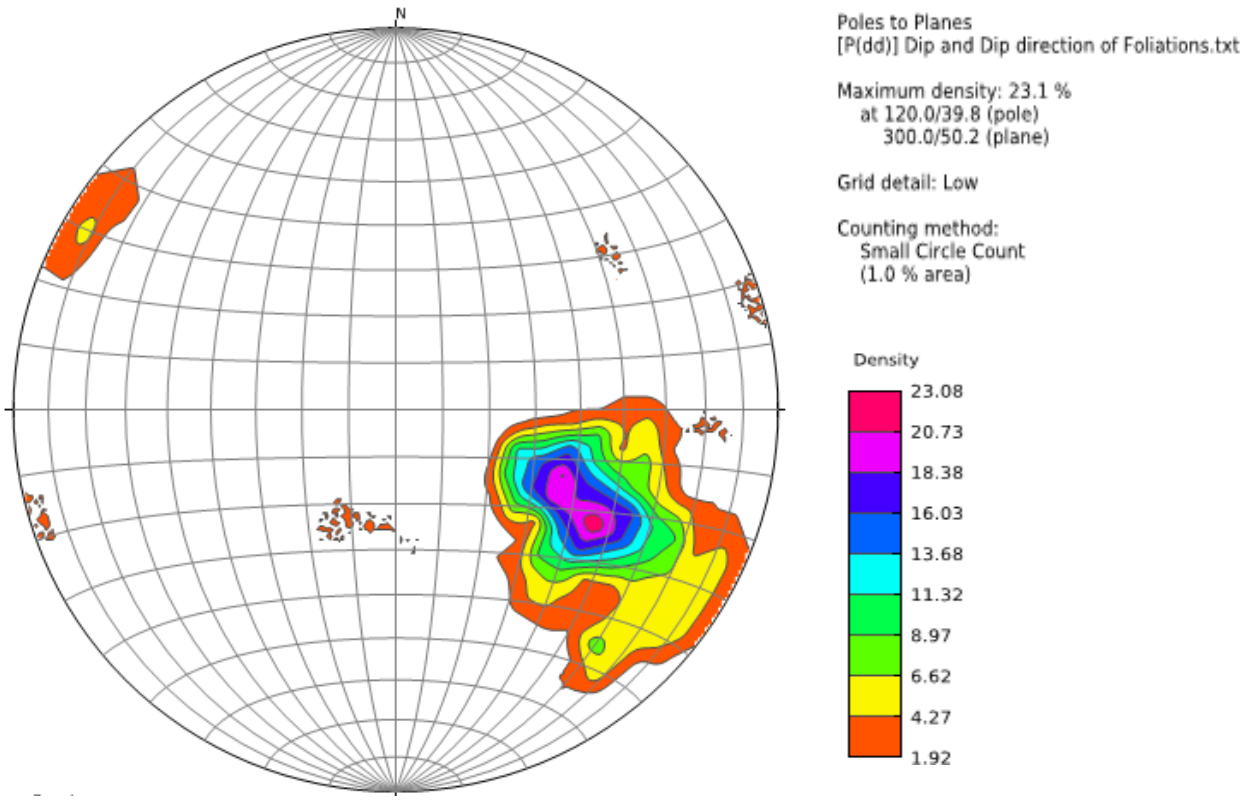

Fig. 4-16 Contour diagram of the poles to foliations (Open Stereo, v- 0.1.2f)

The contour plots represent both an azimuth and an inclination of the measured foliations (Fig. 4.16). It shows the density distribution of these data by the various colors. It is plotted by small circle counting of 1% area and the contour interval is 2.35%. Area represented by the red color (densest part) embodies greater than 20% of the data. The plot shows the maximum density which is 23.1% is at 300/50.2 foliation.

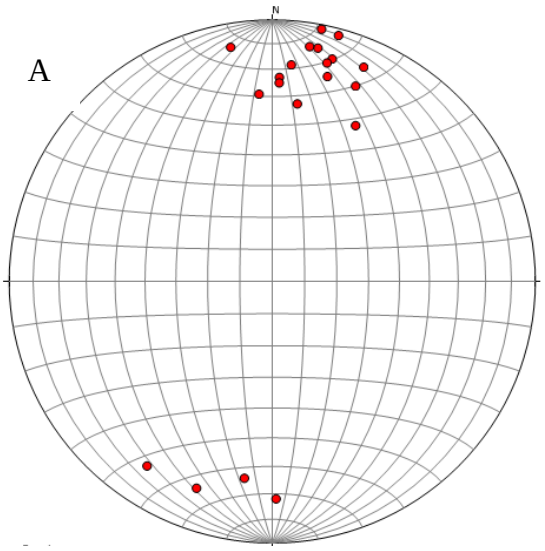

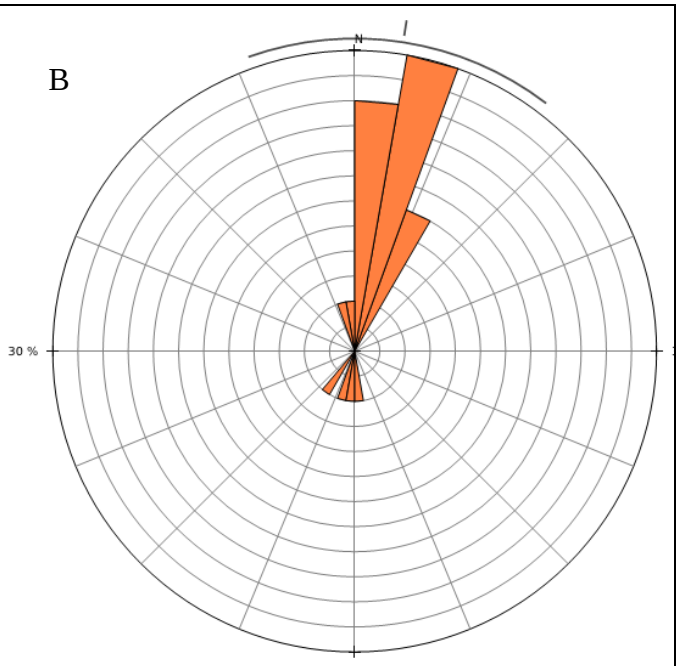

Rose diagrams of lineations

N=20
Max =30.00%
Mean dir.: 8.9^0
Interval = 10^0
Outer limit = 30%
Inner rings = 2.5%
Diagonals = 22.5^0

Fig. 4-17 Lineation data projections and rose diagrams

Fig. 4.17A shows the plots of the linear features: fold axes of the metamorphic rocks and quartz veins, crenulation lineations and kink bands. The pattern formed shows most of the lineations are gently plunging towards north with some to south. From the Rose diagrams it is seen that 30% of the data have a preferred orientation between $N10^0 – 20^0E$ (Fig. 4.17B).

Generally the plots of the linear features (gently plunging fold axes of the metamorphic rocks and quartz veins, crenulation lineations and kink bands) lie on a particular area making it to be formed at similar deformation phases (D2). Even in the out crop level it is perceptible the crenulation lineations are parallel to the fold axes of the minor folds.

CHAPTER FIVE

CHEMICAL STRATIGRAPHY AND CORRELATION

5.1 Introduction

The need to understand global changes brings with it the need to understand geologic history of oceans. In the past twenty years the applications of temporal changes in the isotopic compositions of marine carbonates and organic matter for regional and global correlation is well developed. Carbon isotope plays an important role in studies of biogeochemical change. This is because carbon isotope compositions of unaltered carbonates (δ^{13}Ccarb) precipitated in equilibrium with seawater closely approximate the composition of the dissolved inorganic carbon pool of that seawater. The longer term C-isotope trend for carbonates has been punctuated by sudden shifts over short time intervals named "carbon isotope events". Ages of some Neoproterozoic metasedimentary carbonate sequences can be inferred on the basis of their carbon isotope fluctuations versus the δ^{13}C (Vienna Pee Dee Belemnite, V-PDB) chemostratigraphic curve for Neoproterozoic marine carbonates (Kaufman and Knoll, 1995; Sial et al., 2000; Misi et al., 2006; Halverson et al., 2006; Hoefs, 2009).

Neoproterozoic stratigraphic successions usually include carbonates deposited in a range of sedimentary environments. If isotopic composition correlates strongly with facies rather than time, isotopic chemostratigraphy cannot work in these sections. In Neoproterozoic successions studied to date no longer or systematic variation among facies has been found within a single succession (Kaufman and Knoll, 1995).

In the Koraro area metalimestone samples were collected for chemostratigraphy purpose. The chemostratigraphy of these carbonates have not been studied by previous researchers. Results and interpretations of the δ^{13}C analysis will be discussed in the following sections.

5.2 Sampling Procedure

A meter stick set with the dip amount of the metalimestone unit is used to measure the stratigraphic section. This is to get the true thickness of the unit during deposition. Limestone samples were collected from one formation in the study area (Fig. 3.1). The section measurement is done perpendicular to the strike of the bedding. A total of sixty carbonate rock samples, ten from the upper eighty two meter thick bed, were collected. Samples which are fresh, free of veins and minimum siliciclastic constituent were selected. It is done at a

meter scale where good beds are exposed. Labeling of the samples is based on the stratigraphic level where it is located starting from zero at the base of the section.

5.3 Analytical Procedure

The collected samples were cut perpendicular to the foliation using the cutter machine in Addis Ababa University. Limestone chips were sent to Princeton University for analysis. The cut surfaces were polished and 5mg powder were micro-drilled from the laminations. All powders were placed in individual borosilicate reaction vessels and heated to 110^0C to remove volatile contaminants and water. Samples were then reacted at 72^0C with 5 drops of H_3PO_4 in a GasBench II preparation device coupled directly to the inlet of a Thermo DeltaPlus continuous flow isotope ratio mass spectrometer. $\delta^{13}C$ data were acquired simultaneously, and precision and accuracy of data are monitored through analysis of 12 standards for every 10 measured unknowns. All values are presented as ‰ differences from the isotopic composition of the V-PDB (Vienna Pee Dee Belemnite) international standard. Measured precision is maintained at 0.1‰ (1σ). The carbon isotopic values are displayed using Microcal Origin 6.0 software. All $\delta^{13}C$ measurements are reported in appendix one.

5.4 Results

Results of the isotopic analysis are displayed in Fig. 5.1. The values range from -5.379 at 181m to -2.726 at 356m for the larger metalimestone and from -7.627 to -5.287 for the small metalimestone unit.

.

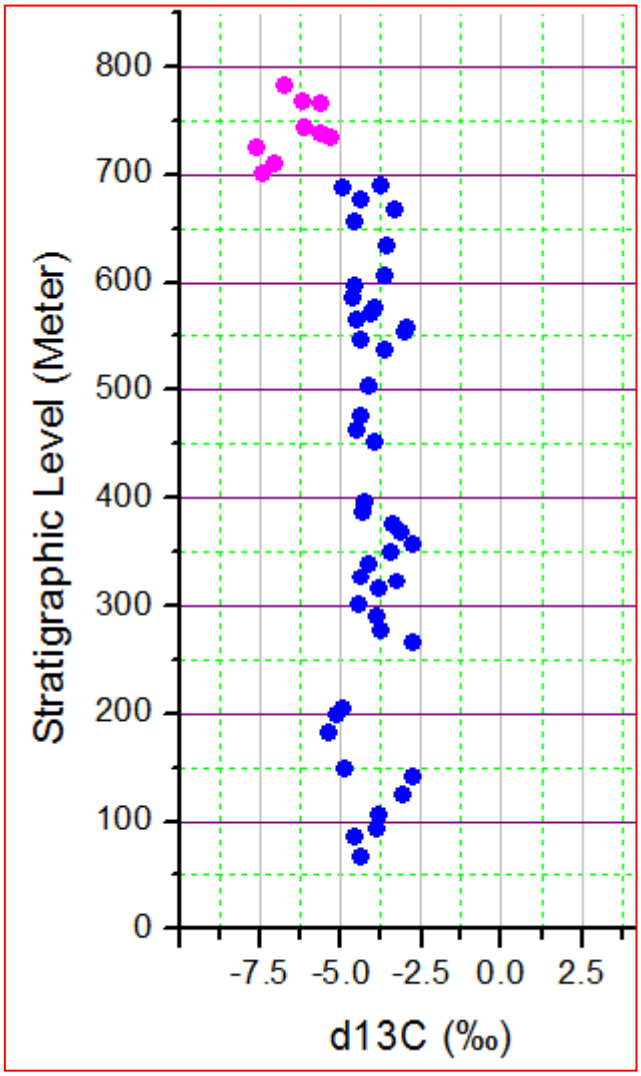

Fig. 5-1 $\delta^{13}C$ distribution data from the metalimestone units. Blue circles are from the large metalimestone unit and the purple/magenta circles are from the eighty two meter thick metalimestone in the slate and phyllite unit.

As it is seen from the graph, up to 600m the values show a repetitive increase and decrease patterns and above the 600 m thickness level the values decrease continuously from -3.70 to -7.5 ‰. The magenta colored circles are from the small metalimestone bed which is exposed in the slate and phyllite unit. It is plotted just above the larger metalimestone to reduce the space in between. Although these results don't show much variation from the lower metalimestone it occupies another column to the left of the blue ones. The consistency of all the data together with the higher stratigraphic position leads to the argument that the pattern is primary. This primary sea water signal might be due to large eustatic drops in sea level or low sedimentation rates (Halverson et al., 2005).

5.5 Carbon Isotope Fluctuations during Neoproterozoic Era

According to Kaufman and Knoll (1995) the fluctuation of the isotopic values in the Neoproterozoic successions is high compared to the Phanerozoic rocks. This suggests that the Neoproterozoic time was a time of tectonic and biogeochemical change. During Photosynthesis ^{12}C is taken preferentially over ^{13}C leaving the dissolved inorganic carbon (DIC) of the surface ocean relatively enriched in ^{13}C. Highly ^{13}C-enriched intervals typical of interglacial times are as a result of unusually efficient burial of organic matter in Neoproterozoic ocean basins, perhaps as a consequence of high erosion rates related to widespread orogenesis and abundant nutrient availability. Negative $\delta^{13}C$-shifts may indicate a decrease in the rate of carbon burial and/or enhanced oxidative weathering of once buried organic matter.

A snowball earth hypothesis characterized by negative carbon isotope anomalies as a result of declining biological productivity in the surface ocean for millions of years has been interpreted by Hoffmann et al. (1998). This ended abruptly when subaerial volcanic outgassing raised atmospheric carbon dioxide to about 350 times the modern level and transferring to the ocean would result in the rapid precipitation of calcium carbonate. Alternatively negative carbon isotopes have been recorded during Neoproterozoic not associated with glaciation (e.g. Halverson et al., 2005; Alene et al., 2006). This low δ13C interval referred to as the Bitter Springs Stage is reproduced precisely in different formation across the world. The perturbation to the carbon cycle is related to a global scale event that also drove large changes in sea level (Halverson et al., 2005; Maloof et al., 2006).

Due to the association between $\delta^{13}C$ anomalies and glaciation in the Neoproterozoic (Knoll et al., 1986, Kaufman et al., 1997, Hoffman et al., 1998), it is tempting to speculate that the Bitter Springs isotope stage is related to a glaciation. Indeed, this possibility cannot be ruled out, even though no sedimentological evidence for glaciation has been found. However, paleomagnetic data from Svalbard suggest instead that the Bitter Springs isotope stage and associated fluctuations in sea level may be related to a pair of large-scale true polar wander (TPW) events (Maloof et al., 2006 cited in Xiao and Kaufman, 2006).

5.6 Alteration of Carbon Isotopic Signal

Variations of $\delta^{13}C$ value can be due to primary or secondary effects. According to Knoll et al. (1986), primary effect reflects changes in the isotopic composition of carbonate in the water column beneath which the sediments initially accumulated. The secondary effects alter the

original seawater isotopic signatures. It includes bacterial reworking of organic material, precipitation and admixture of new carbonates, isotopic exchange with species in solution, diagenetic and metamorphic overprints. In decarbonation, carbonates and quartz or feldspar react to produce Ca- or Mg – silicates plus CO_2. The CO_2 is enriched in the ^{13}C, lowering the $\delta^{13}C$ value of remaining carbonates. These are always a concern in ancient carbonates, and it is safe to assume every carbonate sample we have analyzed has experienced some degree of chemical alteration during these processes (Kaufman and Knoll, 1995; Halverson et al., 2005).

5.7 Do the Collected Samples Represent Primary Isotopic Signal?

As discussed in sections 5.2 and 5.3, necessary precautions are made from sample collection to preparation to get the least altered product. Samples are micro-drilled to obtain the least altered material from each which can show chemical and isotopic evolution of sea water as discussed in Jacobsen and Kaufman (1999).

Carbon in sedimentary carbonate rocks is buffered against significant isotopic exchange during rock–fluid interactions. The ratio of the amount of carbon in the rocks to the amount of carbon dissolved in fluids is orders of magnitude higher and because the fractionation between calcium carbonate is relatively small at near surface temperatures (Sial et al., 2000; Jones et al., 2010). The idea that carbonates are generally impermeable to the influx of externally-derived fluid is evidenced by experimental study of Holness and Graham (1995). The result shows carbonate rocks will not have a stable interconnected fluid- filled network of pores at pressures up to 7 kbars. In harmony to this the units in the study area including the metalimestone has undergone only low grade of metamorphism (section 4.3).

Moreover, $\delta^{13}C$ signatures are resistant to overprinting and major trends are reproducible basin wide even below major exposure surfaces and in rocks in contact with paleoaquifers. Many previous studies have addressed the reliability of $\delta^{13}C$ signatures in Neoproterozoic carbonates and the typical conclusion is that even clearly diagenetically altered and dolomitized carbonates appear to preserve their original $\delta^{13}C$ composition (e.g., Kaufman et al., 1991; Derry et al., 1992; Kaufman and Knoll, 1995; Halverson et al., 2002, 2004 cited in Halverson et al., 2005).

As shown in Fig. 5.1 the results shift from left to right forming patterns but it doesn't show association with specific effects. For example samples collected near the slates at different

locations have different value. Samples which seem to show similar grain sizes have different value. Therefore the fluctuations of the results might be due to combined effects.

The thin sections of the metalimestones shows secondary effects such as variable grain sizes, recrystallized beds and stylolites. During formation of stylolites there might be some isotopic shift resulting in slight swing of the results. Interfingering of the metalimestones with the slates and phyllites is common. The interbedded terrigenous slates associated with the influx of fresh water from continents during deposition might result in lowering $\delta^{13}C$ values (Shao et al., 2000). In addition to this small level changes in the amount of primary organic carbon burial might also be a cause.

Jones et al. (2010) analyzed the relationship of isotopic covariations or $\delta^{13}C$ depletions to that of hydrothermal fluids accompanying intrusion of sills. The impact of 1m thick dike in the spotty phyllite unit (Fig. 3.1) on to the lower part of metalimestone is not significant. The $\delta^{13}C$ values are slightly depleted at the base but got more depleted going far from the dike at 150m level.

The $\delta^{13}C$ values doesn't show high variation compared to the thickness of the metalimestone unit (700m). This might be due to high levels of primary productivity and high rates of sedimentation as a result of increased rates of continental weathering ascribed to Pan African orogeny (Asmerom et al., 1991; Kaufman and Knoll, 1995).

5.8 Correlation

5.8.1 Local Correlation

Correlation of the units exposed in the study area to previously identified sequences is done based on stratigraphy and the carbonate isotope analysis. Slate units bounding the metalimestone are characteristics of the Tambien Group exposed elsewhere near the study area. However the thickness of the units in Koraro is higher and the variegated slate contains many intercalated metagraywacke layers compared to a similar sequence in the Tambien Group. Generally, the lithological units and stratigraphic relationships are comparable to Tambien Group exposures in other areas. The lower three formations are represented in the study area as in Tsedia and Chehmit synclines.

The carbon isotope analysis result shows only negative values. Such low $\delta^{13}C$ are commonly associated with glaciation (Hoffman et al., 1998) but the metalimestone didn't show any glacial feature. So far the negative carbon isotopic values recorded in the metamorphic rocks

in Tigrai are from Assem Limestone, top of Didikama Formation and some in Marian Bohkahko Formation. The Didikama Formation, which is the intercalations of dolomite and slate, is overlain by a black limestone unit, the Matheos Formation. On the other hand the Marian Bohkahko Formation is overlain by the Negash Diamictite (See chapter 2). This leads to the logical inference that the metalimestone unit is correlative to Assem limestone (Fig. 5.2). Furthermore the low values recorded above the metalimestone unit in the slate and phyllite intercalation is analogous to that of lower values recorded in Tsedia formations of Tsedia and Chehmit synclines (Data repository of Swanson-Hysell et al., 2015).

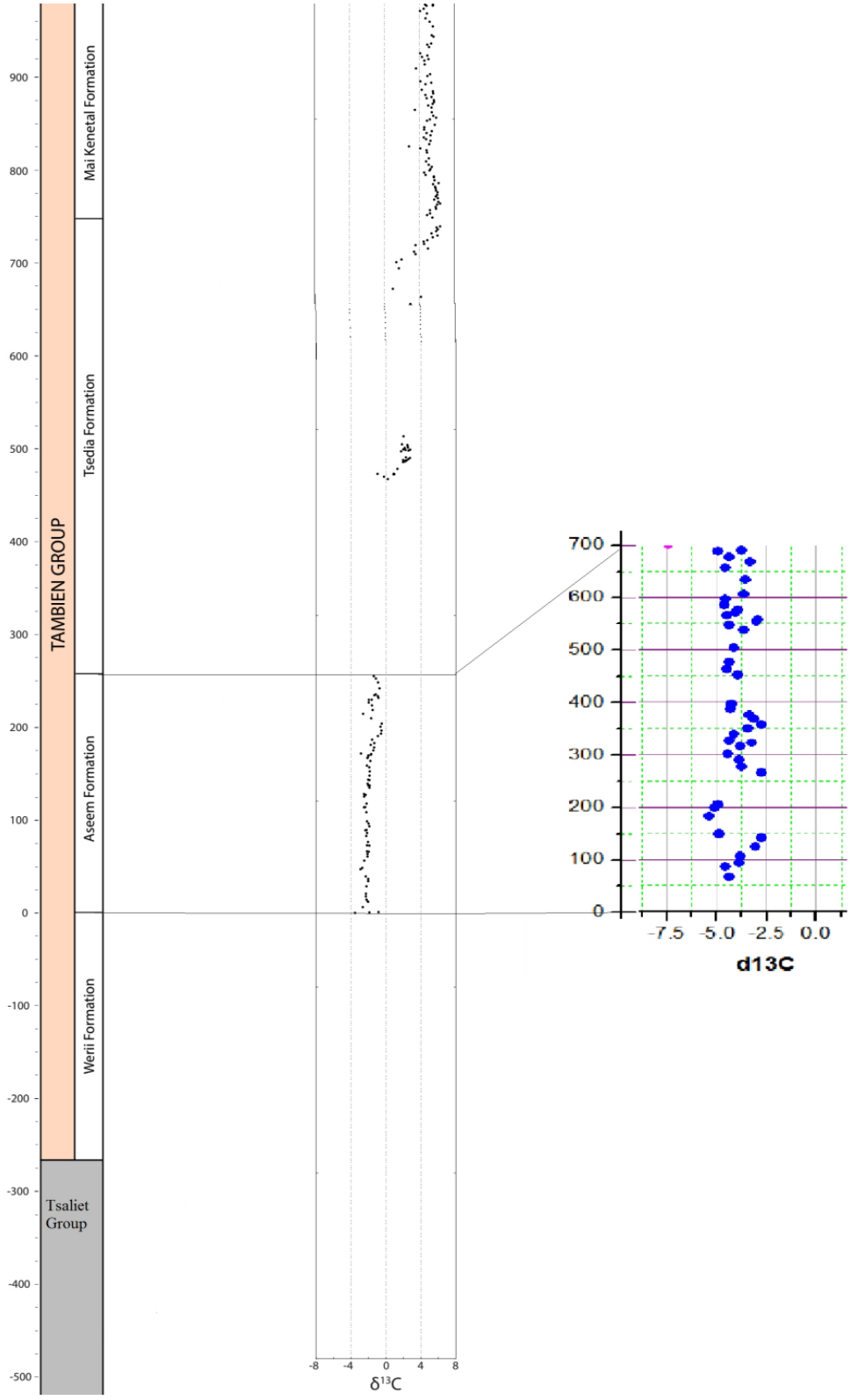

Fig. 5-2 Chemostratigraphic correlation of the study area to the west Mai Kenetal section (Data repository of Swanson-Hysell et al., 2015)

5.8.2 Global Correlation

The global correlation of Tambien Group to different lithological units in the world is done previously (e.g. Alene et al., 2006; Miller et al., 2009, 2011; Swanson-Hysell et al., 2015). The Tambien Group is a pre-Sturtian sequence extending through the Bitter Springs Stage (BSS) and represents one of the exceptional sequences exposed in Svalbard, Australia and Canada (Alene et al., 2006). Global synchronity of the BSS is supported by the U-Pb zircon dates from Tambien Group and integration of data from Fifteenmile Group. BSS is explained by the true polar wander (TPW) hypothesis. Fig. 5.3 shows composite of pre-Sturtian carbon isotope data comprising Little Dal/Coates Lake Groups and Fifteen Mile Group of Canada; Bitter Springs Formation of Australia and Hecla Hoek Group of Svalbard (Swanson-Hysell et al., 2015).

Lithologic wise, the sequences reported from the Akademikerbreen Group of Northeastern Svalbard show similarity with the ribbonite and grainstone metalimestone unit. According to Knoll and Swett (1990) the upper Grusdievbreen and lower Svanbergfjellet formations (negative $\delta^{13}C$) consists of green and red shale and siltstone with background stratigraphy consisting of pure and monotonous, mid- to proximal-shelf limestone ribbonite and intraclast breccias.

The dates from Ethiopia suggest deposition of the Tambien group was started ca. 820 Ma and spanned up to Sturtian Glaciation (ca. 717–662 Ma) (Swanson-Hysell et al., 2015).

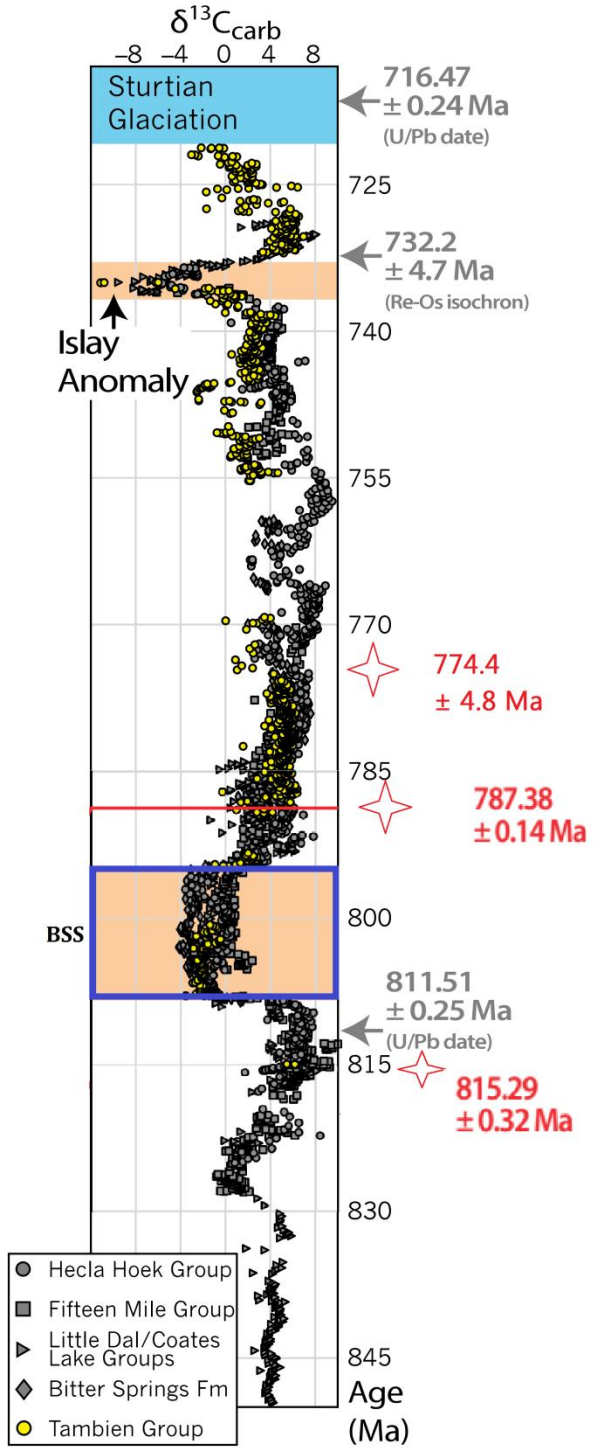

Fig. 5-3 Plot of composite pre-Sturtian carbon isotope data.

Dates shown in gray are from northwestern Canada. Those in red are from Ethiopia with the younger age dated in Negash below the Didikama Formation (Avigad et al., 2007). The remaining two are new zircon U-Pb dates from upper Tsedia formation and Werri formation (Swanson-Hysell et al., 2015). Blue rectangle shows the position of the metalimestone unit with the negative $\delta^{13}C$ values (Swanson-Hysell et al., 2015).

CHAPTER SIX

CONCLUSION AND RECOMMENDATIONS

6.1 Conclusion

The Koraro- Gelebeda metamorphic terrain is composed low grade metamorphic rocks intruded by aplite dikes and unconformably overlain by the Pebbly sandstone. The metamorphic rocks are slates and phyllites of different composition and texture, metavolcanics, metagraywackes, metalimestone, metasubvolcanics and psammites. The variation in degree of metamorphism of these rocks is due compositional heterogeneity, shear zones and fluids from dikes.

Microscopic study of the rocks shows the presence of newly formed metamorphic minerals (neocrystallized), recrystallized grains as well as features related to incomplete reaction between minerals. Furthermore, well developed metamorphic microstructures associated with pressure solution processes are also not uncommon. Protolith characteristics such relict primary bedding and uncompleted mineral reactions show a low grade of metamorphism.

Prograding metamorphism is seen from the fine sericite minerals to muscovite flakes of the pelitic rocks. A grade which can be classified in between slate and phyllite is even formed from these mineral associations. In general white micas from clay minerals and feldspars and quartz/feldspars dominate the composition the pelites/semepelites. Chlorites at the expense of the mafic minerals, plagioclases, calcite and the felsic minerals lead the composition of metasubvolcanics. The mineral assemblages indicate metamorphism up to lower green schist facies.

Structural analysis shows that the foliation almost parallel with bedding trends NNE to SSW and dips NW while most of the lineations are gently plunging towards north. Stereographic projection of the foliations, folds, kink bands and crenulations show a pattern which is related to deformation phases. The pelitic rocks which are grading to phyllites show S_0, S_1 and S_2 on the microscale. S_0 is bedding defined by the quartz-rich and quartz-poor layers, S_1 is phyllitic cleavage marked by sericites and muscovites and S_2 is discrete crenulation cleavage defined by sericites. Correlation is established between metamorphic and deformation events on the basis of porphyroblast - matrix relationships preserved in spotty phyllites and slates of the region. For example, pyrites and other related porphyroblasts show various relations with the main foliation: some are mantled without pressure shadow, others with pressure shadow as

well as fibrous quartz as fringe and others simply lay down on the foliation without any structure. These all evidences lead to the conclusion that the formation of the porphyroblasts is late to post tectonic of the main foliation.

The strain fringe structures and massive strain shadows are formed as result of inhomogeneous deformation of matrix adjacent to larger grains. These minerals are mantled and together with the sigmoidal tension gashes are used as shears sense indicators. Furthermore, the presence of many shear sense indicators in thin section and the variation in degree of foliation of the same rock units in outcrop level reveals the distribution of deformation was heterogeneous rather than homogenous.

Negative $\delta^{13}C$ values are obtained from analysis of the metalimestone samples. Together with the lithological and stratigraphical data, these values are used in correlation of the metalimestones regionally as well as globally. As a result the metalimestone unit is one of the rare non glacial lithological units having negative value during the Bitter Springs Stage (BSS). This is explained to be as a result of true polar wandering hypothesis (TPW) (Alene et al., 2006; Maloof et al., 2006; Swanson-Hysell et al., 2015). The fluctuations of the $\delta^{13}C$ values from the single measured section might be due to small level changes in the amount of primary organic carbon burial, interbedded siliciclastic materials associated with the influx of fresh water from continents during deposition or diagenetic effects.

6.2 Recommendations

It is highly recommended to analyze the insoluble residue content in the carbonates, because this would assist in interpretation of the $\delta^{13}C$ values. The type and concentration, correlation with the $\delta^{13}C$ values and relative proportion of the major and trace elements will resolve the effects of influx of external material and strong diagenetic influences.

The abundance of sulfide minerals in the rocks might affect the quality of water for drinking. Ground water acidity increases with the oxidation of sulfides. Since most of the sulfides including the pyrites are reddish in color due to oxidation, hydrogeochemical study in light of these minerals is recommended.

Panning for gold is a common task of the inhabitants. With the abundance of the sulfide pathfinders and quartz veins it is also recommended to study the genesis and economic value of gold in the study area.

References

Abdelsalam, M.G. and Stern, R.J. (1996). Sutures and shear zones in the Arabian-Nubian Shield. *Journal of African Earth Sciences*, **23**: 289–310.

Alene, M. (1998). Tectonomagmatic evolution of the Neoproterozoic rocks of the Mai Kenetal–Negash area, Tigrai, northern Ethiopia. Unpublished Ph.D. Thesis, University of Turin, Italy.

Alene, M., Jenkin, G.R.T., Leng, M.J. and Darbyshire, D.P.F. (2006). The Tambien Group, Ethiopia: An early Cryogenian (ca. 800–735 Ma) Neoproterozoic sequence in the Arabian-Nubian shield: *Precambrian Research*, **147**: 79–99.

Alene, M., Ruffini, R., Sacchi, R. (2000). Geochemistry and geotectonic setting of Neoproterozoic rocks from northern Ethiopia (Arabian–Nubian Shield). *Gondwana Res.* **3**: 333–347.

Allen, A. and Tadesse, G. (2003). Geological setting and tectonic subdivision of the Neoproterozoic orogenic belt of Tuludimtu, western Ethiopia. *Journal of African Earth Sciences*, **36**: 329–343.

Anderson T.F. and Arthur M.A. (1983). Stable isotopes of oxygen and carbon and their application to sedimentological and paleoenvironmental problems. In SEPM Short Course: Stable Isoto pes in Sedimentary Petrology, ed. MA Arthur, TF Anderson, IR Kaplan, J Veizer, LS Land, **10**.

Arkin, Y., Beyth, M., Dow, D. B., Levitte, D., Temesgen Haile and Tsegaye Hailu, (1971). Geological Map of Mekele Sheet (ND37-11), E.I.G.S, AddisAbaba, Ethiopia.

Asmerom, Y., Jacobsen, S.B., Knoll, A.H., Butterfield, N.J. and Swett, K. (1991). Strontium isotopic variations of Neoproterozoic seawater: Implications for crustal evolution. *Geochimica et Cosmochimica Acta*, **55**: 2883–2894.

Asrat, A., Barbey, P. and Gleizes, G., (2001). The Precambrian geology of Ethiopia: a review. *Africa Geoscience Review*, **18**: 271–288.

Asrat, A., Barbey, P., Ludden, J.N., Reisberg, L., Gleizes, G., Ayalew, D. (2004). Petrology and isotope geochemistry of the Pan-African Negash Pluton, Northern Ethiopia: Mafic-Felsic Magma Interactions during the Construction of Shallow-level Calc-alkaline Plutons. *J. Petrol*. **45**: 1147–1179.

Asrat, A. Gleizes, G., Barbey, P. Ayalew, D. (2003). Magma emplacement and mafic---felsic magma hybridisation: structural evidence from the Pan-African Negash pluton, Northern Ethiopia. *Journal of Structural Geology*, **25**: 1451-1469.

Avigad, D., Kolodner, K., McWilliams, M., Persing, H., Weissbrod, T. (2003). Origin of northern Gondwana Cambrian sandstone revealed by detrital zircon SHRIMP dating. *Geology*, **31** (3): 227–230.

Avigad, D., Stern, R. J., Beyth, M., Miller, N. and McWilliams, M. (2007). Detrital zircon U–Pb geochronology of Cryogenian diamictites and Lower Palaeozoic sandstone in Ethiopia (Tigrai): age constraints on Neoproterozoic glaciation and crustal evolution of the southern Arabian– Nubian Shield. *Precambrian Research*, **154**: 88– 106.

Barker, A. J. (1998). *Introduction to metamorphic textures and microstructures*. Stanley Thomes, Cheltenham, United Kingdom, 263 pp.

Beyth, M., (1971). The geology of central and western Tigre. Min. Mines, Addis Ababa, unpublished report.

Beyth, M., (1972). The geology of central and western Tigre, Ethiopia. Unpublished Ph.D. Dissertation, University of Bonn, Germany, 155 pp.

Beyth, M., Avigad, D., Wetzel, H.-U., Matthews, A., Berhe, S.M. (2003). Crustal exhumation and indications for snowball Earth in the East African Orogen: north Ethiopia and east Eritrea. *Precambrian Res*. **123**: 187–201.

Bingen, B., Jacobs, J., Viola, G., Henderson, I.H.C., Skara, O., Boyd, R., Thomas, R.J., Solli, A., Key, R.M., Daudi, E.X.F. (2009). Geochronology of the Precambrian crust in the Mozambique belt in NE Mozambique and implications for Gondwana assembly. *Precambrian Research*, **170**: 231–255.

Blanford, W.T. (1870). Report on the Geology of Portion of Abyssinia. Assoc. Roy. School of Mines. London, 487 pp.

Blenkinsop, Tom G. (2002). *Deformation microstructures and mechanisms in minerals and rocks*. Kluwer Academic Publishers. New York, 150 pp.

Bogliotti, C. (1989). A reinterpretation of the large-scale structure of Precambrian rocks in the Adola goldfield (Ethiopia) based on two generations of interference pattern. *Precambrian Research*, **44**: 289–304.

Bonavia, F.F. and Chorowicz, F. (1993). Neoproterozoic structures in the Mozambique orogenic belt of southern Ethiopia. *Precambrian Research*, **62**: 307–322.

Bons, P. D., Elburg, M. A. and Gomez-Rivas, E. (2012). A review of the formation of tectonic veins and their microstructures. *Journal of Structural Geology*, **43**: 33-62.

Calver, C. R. (1996). Reconnaissance isotope chemostratigraphy of Neoproterozoic carbonates rocks in western Tasmania. *Tasmanian Geological Survey Record*, *10*(1996), 19.

Collins, A.S. (2006). Madagascar and the amalgamation of Central Gondwana. *Gondwana Research*, **9**: 3–16.

Dalziel, I.W.D. (1992). On the organization of American plates in the Neoproterozoic and the breakout of Laurentia. *GSA Today*, **2**: 240-241.

Danelli, G., 1943. Geologia dell'Africa Oriental (3 vol. text and 1vol. maps). R. Acc. Italia, Rome.

Davis, G. and Reynolds, S. (1996). *Structural geology of rocks and regions*, Jhon Wiley & Sons. New York, 776 pp.

Derry, L.A., Kaufman, A.J. and Jacobsen, S.B. (1992). Sedimentary cycling and environmental change in the Late Proterozoic: evidence from stable and radiogenic isotopes. *Geochim. Cosmochim. Acta*, **56**:1317-1329.

De Waele, B., Kampunzu, A.B., Mapani, B.S.E., Tembo, F. (2006). The Mesoproterozoic Irumide belt of Zambia. *Journal of African Earth Sciences*, **46**, 36–70.

Dow, D.B, Beyth, M. and Tsegaye, H. (1971). Paleozoic glacial rocks recently discovered in Northern Ethiopia. *Geol. Mag*. **108**: 53-60.

Fossen, H. (2010). *Structural geology*. Cambridge University Press, New York, USA, 463 pp.

Fritz, H., Abdelsalam, M., Ali, K.A., Bingen, B., Collins, A.S., Fowler, A.R., Ghebreab, W., Hauzenberger, C.A., Johnson, P.R., Kusky, T.M., Macey, P., Muhongo, S., Stern, R.J. and Viola, G. (2013). Orogen styles in the East African Orogen: A review of the Neoproterozoic to Cambrian tectonic evolution. *Journal of African Earth Sciences*. **86**:65–106.

Fritz, H., Tenczer, V., Wallbrecher, C.A., Hauzenberger, E., Hoinkes, G., Muhongo, S., Mogessie, A. (2005). Central Tanzanian tectonic map: a step forward to decipher Proterozoic structural events in the East African Orogen. Tectonics 24, TC6013.

Garland, C.R. (1972). Geological Map of Adigrat Area. 1:250,000(ND 37-7). E.I.G.S, Addis Ababa, Ethiopia.

Garland, C.R. (1980). Geology of Adigrat Area: Ministry of Mines Energy and Water Resources. Memoir no.l, 51 pp.

Gaucher, C., Sial, A. N., Halverson, G. P., and Frimmel, H. E. (2009). The Neoproterozoic and Cambrian: a time of upheavals, extremes and innovations. *Developments in Precambrian Geology*, **16**: 3-11.

Ghebreab, W. (1992). The geological evolution of the Adola Precambrian greenstone belt, southern Ethiopia. *Journal of African Earth Sciences,* **14**: 457–469.

Ghebreab, W. (1996). An outline of major Pan-African lithologic assemblages and shear zones in Eritrea: implications for mineral exploration. *Africa Geosciences Review,* **3**: 355–366.

Ghebreab, W. (1999). Tectono-metamorphic history of Neoproterozoic rocks in eastern Eritrea. *Precambrian Research,* **98**: 83–105.

Ghebreab, W., Talbot, C.J. and Page, L. (2005). Time constraints on exhumation of the East African Orogen from field observations and 40Ar/39Ar cooling ages of low-angle mylonites in Eritrea, NE Africa. *Precambrian Research,* **139**: 20–41.

Halverson, G. P. (2006). A Neoproterozoic chronology. In *Neoproterozoic geobiology and paleobiology* (pp. 231-271). Springer Netherlands.

Halverson, G.P., Hoffman, P.F., Schrag, D.P., Kaufman, A.J. (2002). A major perturbation of the carbon cycle before the Ghaub glaciation (Neoproterozoic) in Namibia: Prelude to snowball Earth? *Geochemistry, Geophysics, Geosystems,* **3**(6): 1-24.

Halverson, G.P., Hoffman, P.F., Schrag, D.P., Maloof, A.C., Rice, A.H. (2005). Towards a Neoproterozoic composite carbon isotopic record. *Geol. Soc. Amer. Bull.* **117**: 1181–1207.

Halverson, G.P., Maloof, A.C. and Hoffman, P.F. (2004). The Marinoan glaciation (Neoproterozoic) in Svalbard. *Basin Research,* **16**: 297–324.

Halverson, G.P., Wade, B.P., Hurtgen, M.T., Barovich, K.M. (2010). Neoproterozoic chemostratigraphy. *Precambrian Research*, **182**: 239–412.

Hanson, R.E., Wilson,T.J. and Munyanyiwa, H. (1993). Geologic evolution of the Late Proterozoic Zambezi Belt in Zambia. *Journal of African Earth Sciences*, in press.

Hanson, R.E., Wilson, T.J. and Munyanyiwa, H. (1994). Geological evolution of the Neoproterozoic Zambezi orogenic belt in Zambia. *Journal of African Earth Sciences*, **18**: 135-150.

Hargrove, U., Martin, M.W., Hanson, R.E., Singletary, S., Bowring, S., Munyanyiwa, H. (1998). Tectonic inversion of the Paleo- and Neoproterozoic metamorphic rocks in the Zambezi belt, Mt. Darwin area, NE Zimbabwe. Geological Society America Abstracts Programs 30, A-292.

Hepworth, J.V. (1972). The Mozambique Orogenic Belt and its foreland in northeast Tanzania: a photogeologically-based study. *Journal of the Geological Society, London*, **128**: 461–500.

Hoefs, J. (2009). *Stable isotope geochemistry*. Springer-Verlag Berlin Heidelberg, 285 pp.

Hoffman, P.F. (1999). The break-up of Rodinia, birth of Gondwana, true polar wander and the snowball Earth. *Journal of American Earth Science*, **28**: 17-33.

Hoffman, P.F., Kaufman A., Halverson G. and Schrag D. (1998). A Neoproterozoic snowball Earth. *Science*, **281**: 1342–1346.

Holmes, A. (1951). The sequence of Precambrian orogenic belts in south and central Africa. In: 18th International Geological Congress, Great Britain 1948, part 14, 254–269.

Holness, M. B. and Graham, C. M. (1995). PTX effects on equilibrium carbonate-H2O-CO2-NaCl dihedral angles: constraints on carbonate permeability and the role of deformation during fluid infiltration. *Contributions to Mineralogy and Petrology*, **119**(2-3): 301-313.

Jacobsen, S.B. and Kaufman, A.J. (1999). The Sr, C and O isotopic evolution of Neoproterozoic seawater. *Chemical Geology*, **161**: 37–57.

Johnson, P.R., Andresen, A., Collins, A.S., Fowler, A.R., Fritz, H., Ghebreab, W., Kusky, T., Stern, R.J. (2011). Late Cryogenian-Ediacaran history of the Arabian-Nubian Shield: a review of depositional, plutonic, structural, and tectonic events in the closing stages of the northern East African Orogen. *Journal of African Earth Sciences*, **61**: 167–232.

Johnson, P.R. and Woldehaimanot, B. (2003). Development of the Arabian-Nubian Shield. Perspectives on accretion and deformation in the northern East African Orogen and the assembly of Gondwana. In. Yoshida, M., Windley, B.F., Dasgupta, S. (Eds.). Proterozoic East Gondwana, Supercontinent Assembly and Breakup. *Geological Society, London, Special Publication,* **206**: 290–325.

Johnson, S.P. and Oliver, G.J.H. (2004). Tectonothermal history of the Kaourera Arc, northern Zimbabwe: implications for the tectonic evolution of the Irumide and Zambezi Belts of south central Africa. *Precambrian Research,* **130**: 71–97.

Jones, D.S., Maloof, A.C., Hurtgen, M.T., Rainbird, R.H., Schrag, D.P. (2010). Regional and global chemostratigraphic correlation of the early Neoproterozoic Shaler Supergroup, Victoria Island, northwestern Canada. *Precambrian Research,* **181**: 43–63.

Kaufman, A.J., Hayes, J.M., Knoll, A.H. and Germs, G.J.B. (1991). Isotopic compositions of carbonates and organic carbon from upper Proterozoic successions in Namibia: stratigraphic variation and the effects of diagenesis and metamorphism. *Precambrian Res.* **49**: 301-327.

Kaufman, A.J. and Knoll, A.H. (1995). Neoproterozoic variations in the C-isotope composition of sea water: stratigraphic and biogeochemical implications. *Precambrian Res.* **73**: 27–49.

Kaufman, A. J., Knoll, A. H., and Narbonne, G. M. (1997). Isotopes, ice ages, and terminal Proterozoic Earth history. *Proc. Nat. Acad. Sci. USA,* **95**: 6600–6605.

Kazmin, V. (1971). Precambrian of Ethiopia. *Nature, Physical Science,* 230 (16): 176-177.

Knoll, A. H., Hayes, J.M., Kaufman, A. J., Swett, K., and Lambert, I. B. (1986). Secular variation in carbon isotope ratios from Upper Proterozoic successions of Svalbard and East Greenland. *Nature*, ***321***(6073): 832-838.

Knoll, A.H. and Walter, M.R. (1992). Latest Proterozoic stratigraphy and Earth history: *Nature,* **356**: 673–677.

Knoll, A.H. and Swett, K. (1990). Carbonate deposition during the late Proterozoic era: An example from Spitsbergen. *American Journal of Science,* **290-A**: 104–132.

Kröner, A., Linnebacher, P., Stern, R.J., Reischmann, T., Manton, W., Hussein, I.M. (1991). Evolution of Pan-African island arc assemblages in the southern Red Sea Hills, Sudan,

and in southwestern Arabia as exemplified by geochemistry and geochronology. *Precambrian Research*, **53**: 99–118.

Levitte, D. (1970). The geology of Central part of Mekele sheet (ND 37-11). Ethiopian Institute of Geological Surveys, Note No. 821-201-12. 66 pp.

Libes, S. (2011). *Introduction to marine biogeochemistry*. Academic Press.

Maboko, M.A.H. and Nakamura, E. (2002). Isotopic dating of Neoproterozoic crustal growth in the Usambara Mountains of Northeastern Tanzania: evidence for coeval crust formation in the Mozambique Belt and the Arabian–Nubian Shield. *Precambrian Research*, **113**: 227–242.

Maloof, A. C., Halverson, G. P., Kirschvink, J. L., Schrag, D. P., Weiss, B. P., and Hoffman, P. F. (2006). Combined paleomagnetic, isotopic, and stratigraphic evidence for true polar wander from the Neoproterozoic Akademikerbreen Group, Svalbard, Norway. *Geological Society of America Bulletin*, ***118***(9-10): 1099-1124.

Mariga, J., Hanson, R.E., Martin, M.W., Singletary, S.J., Bowring, S.A. (1998). Timing of polyphase ductile deformation at deep to mid-crustal levels in the Neoproterozoic Zambezi belt, NE Zimbabwe. Geological Society America Abstracts Programs 30, A-292.

McMenamin, M.A.S. and McMenamin, D.L.S. (1990). The emergence of animals: the Cambrian breakthrough. *Columbia University Press*, New York, 217 pp.

Meert, J.G. and van der Voo, R. (1996). Paleomagnetic and $^{40}Ar/\ ^{39}Ar$ study of the Sinyai dolerite, Kenya: implications for Gondwana assembly. *Journal Geology*, **104**: 131-142.

Meert, J.G. and van der Voo, R. (1997). The assembly of Gondwana 800-550 Ma. *Journal Geodynamics*, **23**: 223-235.

Meert, J.G., van der Voo, R. and Ayub, S. (1995). Paleomagnetic investigation of the Neoproterozoic Gagwe lavas and Mbozi complex, Tanzania and the assembly of Gondwana. *Precambrian Research*, **74**: 225-244.

Miller, C. B. and Wheeler, P. A. (2012). *Biological oceanography*. John Wiley & Sons.

Miller, N.R., Alene, M., Sacchi, R., Stern, R.J., Conti, A., Kroner, A., Zuppi, G. (2003). Significance of the Tambien Group (Tigrai, N. Ethiopia) for snowball Earth events in the Arabian–Nubian Shield. *Precambrian Res*. **121**: 263–283.

Miller, N. R., Avigad, D., Stern, R. J. and Beyth, M. (2011). The Tambien Group, Northern Ethiopia (Tigre). *Geological Society, London, Memoirs*, **36**(1): 263-276.

Miller, N. R., Stern, R. J., Avigad, D., Beyth, M. and Schilman, B. (2009). Neoproterozoic carbonate-slate sequences of the Tambien Group, N. Ethiopia (I): pre-'Sturtian' chemostratigraphy and regional correlation. *Precambrian Research*, **170**: 129– 156.

Misi, A., Kaufman, A. J., Veizer, J., Powis, K., Azmy, K., Boggiani, P. C., and Iyer, S. S. (2007). Chemostratigraphic correlation of Neoproterozoic successions in South America. *Chemical Geology*, **237**(1): 143-167.

Mohr, P.A. (1962). The Geology of Ethiopia. Univ. Coil. of Addis Ababa press (reprinted in 1971 by the Hail Selassie University Press), Asmara, 268 pp.

Nedaw, D. (2010). Water Balance and Groundwater Quality of Koraro Area, Tigray, Northern Ethiopia. *Momona Ethiopian Journal of Science*, *2*(2): 110-127.

Passchier, C. W. and Trouw, R. A. (1996). *Microtectonics* (Vol. 2). Berlin: Springer, Germany, 366 pp.

Rey, J. and Galeotti, S. (2008). *Stratigraphy: terminology and practice*. Editions Technip.

Rino, S., Kon, Y., Sato, W., Maruyama, S., Santosh, M. and Zhao, D. (2008). The Grenvillian and Pan-African orogens: world's largest orogenies through geologic time, and their implications on the origin of super plume. *Gondwana Research*, **14**: 51-72.

Ripperdan, R. L. (1994). Global variations in carbon isotope composition during the latest Neoproterozoic and earliest Cambrian. *Annual Review of Earth and Planetary Sciences*, ***22***: 385-417.

Seilacher, A. (1999). Biomat-related lifestyles in the Precambrian. PALAIOS, 14: 86293.

Shao, L., Zhang, P., Dou, J., and Shen, S. (2000). Carbon isotope compositions of the Late Permian carbonate rocks in southern China: their variations between the Wujiaping and Changxing formations. *Palaeogeography, Palaeoclimatology, Palaeoecology*, ***161***(1): 179-192.

Sial, A. N., Ferreira, V. P., Dealmeida, A. R., Romano, A. W., Parente, C. V., DACOSTA, M. L., and Santos, V. H. (2000). Carbon isotope fluctuations in Precambrian carbonate sequences of several localities in Brazil. *Anais da Academia Brasileira de Ciências*, ***72***(4): 539-558.

Sifeta, K., Roser, B.P. and Kimura, J.I. (2005). Geochemistry, provenance, and tectonic setting of Neoproterozoic metavolcanic and metasedimentary units, Werri area, Northern Ethiopia. *Journal of African Earth Sciences,* **41**: 212–234.

Stanistreet, I.G., Kukla, P.A. and Henry, G. (1991). Sedimentary response to a Late Proterozoic Wilson Cycle: the Damara Orogen and Nama Foreland, Namibia. *Journal African Earth Sciences,* **13**: 141-156.

Stern, R.J. (1994). Arc assembly and continental collision in the Neoproterozoic East African Orogen: implications for the consolidation of Gondwanaland. *Ann. Rev. Earth Planet. Sci.* **22**: 319–351.

Stern, R.J. (2002). Crustal evolution in the East African Orogen: a neodymium isotopic perspective. *Journal of African Earth Sciences,* **34**: 109–117.

Stern, R.J. (2008) Neoproterozoic crustal growth: the solid earth system during a critical time of earth history. *Gondwana Res,* **14**:33–50.

Stern, R.J., Ali, K.A., Abdelsalam, M.G., Wilde, S.A., Zhou, Q. (2012). U-Pb Zircon geochronology of the eastern part of the Southern Ethiopian Shield. *Precambrian Research,* **206–207**: 159–167.

Swanson-Hysell, N. L., Maloof, A. C., Condon, D. J., Jenkin, G. R., Alene, M., Tremblay, M. M., Tesema, T., Rooney, A.D. and Haileab, B. (2015). Stratigraphy and geochronology of the Tambien Group, Ethiopia: Evidence for globally synchronous carbon isotope change in the Neoproterozoic. *Geology*, **43**(4): 323-326.

Tadesse, T. (1997). The Geology of Axum Area (ND 37-6). Ethiopian Institute of Geological Surveys, Addis Ababa. (Memoir No. 9), 184 pp.

Tefera, M., Chernet, T. and Haro, W. (1996). Geological Map of Ethiopia, second edition. Regional Mapping Department of the Ethiopian Geological Survey.

Tolessa, S., Bonavia, F.F., Solomon, M., Haile-Meskel, A., Teferra, E. (1991). Structural pattern of Pan-African rocks around Moyale, southern Ethiopia. *Precambrian Research,* **52**: 179–186.

Tsige, L. (2006). Metamorphism and gold mineralization of the Kenticha–Katawicha area: Adola belt, southern Ethiopia. *Journal of African Earth Sciences,* **45**: 16–32.

Tsige, L. and Abdelsalam, M.G. (2005). Neoproterozoic–Early Paleozoic gravitational tectonic collapse in the southern part of the Arabian-Nubian Shield: the Bulbul Belt of southern Ethiopia. *Precambrian Research,* **138**: 297–318.

Van der Pluijm, B. A. and Kaars-Sijpesteijn, C. H. (1984). Chlorite-mica aggregates: morphology, orientation, development and bearing on cleavage formation in very-low-grade rocks. *Journal of structural geology*, **6**(4), 399-407.

Viola, G., Henderson, I. H. C., Bingen, B., Thomas, R. J., Smethurst, M. A., and De Azavedo, S. (2008). Growth and collapse of a deeply eroded orogen: Insights from structural, geophysical, and geochronological constraints on the Pan-African evolution of NE Mozambique. *Tectonics*, ***27***(5).

Wilson, T.J., Grunow, A.M. and Hanson, R.E. (1997). Gondwana assembly: the view from southern Africa and East Gondwana. *Journal Geodynamics,* **23:** 263-286.

Woldemichael, B.W., Kimura, J.I., Dunkley, D.J., Kenichiro, T., Ohira, H. (2010). SHRIMP U-Pb zircon geochronology and Sr–Nd isotopic systematic of the Neoproterozoic Ghimbi-Nedjo mafic to intermediate intrusions of Western Ethiopia: a record of passive margin magmatism at 855 Ma? *International Journal of Earth Sciences*, **99**: 1773–1790.

Xiao, S. and Kaufman, A.J. (2006). Neoproterozoic Geobiology and Paleobiology. Springer, 314 pp.

Yibas, B., Reimold, W.U., Armstrong, R., Koeberl, C., Anhaeusser, C.R., Phillips, D. (2002). The tectonostratigraphy, granitoid geochronology and geological evolution of the Precambrian of southern Ethiopia. *Journal of African Earth Sciences*, **34**: 57–84.

Yihunie, T., Adachi, M. and Yamamoto, K. (2006). Geochemistry of the Neoproterozoic metabasic rocks from the Negele area, southern Ethiopia: tectonomagmatic implications. *Journal of African Earth Sciences,* **44**: 255–269.

Yihunie, T. and Hailu, F. (2007). Possible eastward tectonic transport and northward gravitational tectonic collapse in the Arabian–Nubian shield of western Ethiopia. *Journal of African Earth Sciences*, **49**: 1–11.

Yihunie, T. and Tesfaye, M. (2002). Structural evidence for the allochthonous nature of the Bulbul terrane in southern Ethiopia: a west-verging thrust nappe. *Journal of African Earth Sciences*, **34**: 85–93.

List of Appendix

Appendix One: Carbon Isotopic Value

Section- 1

d13C-values	Stratigraphic Level
-4.378132388	67
-4.576590784	85
-3.891127607	92
-3.788238704	106
-3.043246792	124
-2.758127649	141
-4.865874741	149
-5.379779889	181
-5.084856311	199
-4.916313381	204
-2.766475344	266
-3.730297195	276
-3.844721662	289
-4.436441807	300
-3.820901505	315
-3.265151406	322
-4.392898623	326
-4.1219554	338
-3.463774061	349
-2.726080459	356
-3.119893697	368
-3.383964348	376
-4.322980306	386
-4.256479542	395
-3.903406614	452
-4.518861064	462
-4.384119349	476
-4.094619966	503
-3.624333911	536
-3.027911237	553
-2.948214923	557
-4.4672754	562
-4.057155972	570
-4.337157099	574
-3.935464067	576
-4.594386493	586
-4.55035318	596
-3.641010408	605
-3.559711489	634
-4.545325167	656
-3.283366088	666
-4.377196644	676
-4.933815288	688
-3.720718586	689

Section- 2

d13C-values	Stratigraphic level
-7.38983	1
-7.01321	10
-7.62745	24
-5.28716	34
-5.63312	37
-6.0868	43
-5.60038	65
-6.1447	68
-6.70616	82

Appendix Two: Structural Data

Foliation Orientation				
No.	E	N	Dip	Dip direc.
1	526160	1532617	82	306
2	525907	1532365	57	291
3	525734	1532640	50	278
4	525750	1532647	46	300
5	525819	1530620	52	294
6	525592	1530273	44	318
7	524598	1529845	42	290
8	523851	1528735	47	300
9	521370	1528872	67	315
10	521313	1529036	63	301
11	524588	1529159	31	300
12	523495	1529056	54	303
13	522152	1528689	31	297
14	524773	1531693	42	295
15	524248	1532024	86	254
16	523741	1532472	72	317
17	524699	1531490	58	235
18	524625	1532356	65	294
19	524590	1531286	48	309
20	523652	1531780	40	300
21	522645	1531250	32	291
22	521221	1530562	50	320
23	520767	1530106	80	309
24	524314	1531417	52	276
25	523962	1528697	84	303

No.	E	N	Dip	Dip direc.
27	522563	1528412	60	291
28	521789	1528865	27	30
29	521070	1528315	32	298
30	520658	1528627	67	315
31	524321	1532781	63	301
32	523890	1532899	74	315
33	523746	1532678	54	301
34	522325	1532953	42	278
35	521855	1533022	31	288
36	520685	1533596	36	285
37	520523	1532251	75	293
38	52096	1531995	41	287
39	521856	1530987	29	356
40	523161	1532804	69	298
41	522312	1529580	47	305
42	521256	1532952	54	294
43	520690	1532665	69	301
44	520697	1532674	75	273
45	520702	1532680	72	317
46	521005	1532650	34	290
47	521212	1532671	52	318
48	521525	1533005	58	302
49	521890	1532965	36	302
50	523156	1532500	45	299
51	523252	1529512	45	289
52	525215	1528582	60	277

Type	No.	E	N	Trend	Plunge
Kink Bands	1	524591	1529794	176	29
	2	520593	1531463	350	10
	3	520735	1531824	15	20
	4	520710	1530271	214	16
	5	520610	1529890	5	18
	6	520690	1531521	2	25
	7	521557	1533058	28	33
Fold Axis	8	523192	1529937	23	12
	9	520860	1530266	23	20
	10	524780	1531451	179	18
	11	523592	1528562	15	3
	12	522452	1531988	15	13
	13	525741	1529785	8	32
	14	524851	1531698	11	2
	15	523363	1532920	188	25
Crenulation Lineation	16	524603	1530657	200	17
	17	523890	1532900	179	18
	18	524625	1530632	11	10
	19	523879	1532901	2	23
	20	524650	1530652	9	10

DECLARATION OF ORIGINALITY

I hereby declare that this thesis entitled " Deformation, metamorphism and chemical stratigraphy of Neoproterozoic rocks in Koraro-Gelebeda area, Northern Ethiopia" is my original work and has not been presented for a degree in any other University, and that all source of material used for the thesis have been duly acknowledged.

Mulubrhan Gebreslassie (Candidate) …….. …….

Signature Date

This is to certify that the above declaration made by the candidate is correct to the best of my knowledge.

Dr. Mulugeta Alene (Advisor) …….. …….

Signature Date